2012

The Role of Calcineurin in Dendritic Remodeling and Epileptogenesis in a Rat Model of Traumatic Brain Injury

John Campbell
Virginia Commonwealth University

THE ROLE OF CALCINEURIN IN DENDRITIC REMODELING AND EPILEPTOGENESIS IN A RAT MODEL OF TRAUMATIC BRAIN INJURY

A dissertation submitted in partial fulfillment of the requirements for the degree of Doctor of Philosophy at Virginia Commonwealth University

by

John Nelson Campbell
Bachelor of Science
The College of William & Mary
May 2002

Director: Severn B. Churn, Ph.D.
Associate Professor, Departments of Neurology,
Anatomy & Neurobiology, Pharmacology & Toxicology,
and Physiology & Biophysics

Virginia Commonwealth University
Richmond, Virginia
February 2012

ACKNOWLEDGMENT

I wish to thank several people for their support and guidance. I am especially indebted to my advisor, Dr. Churn, not only for mentoring me, but for giving me every possible opportunity to develop as a scientist and as a teacher. I am also very grateful to Dr. Povlishock, whose financial support through the training grant allowed me to continue my research in the Churn Lab, and whose encouragement has sustained me as well. I would like to thank the other members of my graduate committee: Dr. Hamm, for his invaluable advice on statistics and for allowing me to use his fluid percussion injury device; Dr. Meredith, for his thought-provoking conversations on structural plasticity and for allowing me to use his Neurolucida system; and Dr. Delorenzo and his lab members for giving generously of their time and expertise. The Director of the VCU Neuroscience Ph.D. Program, Dr. Bigbee, has also helped me greatly through his advice and encouragement, and by providing me opportunities to stay involved with the program.

Of course, I could not have come so far without my wife, Annie, and my family, who have patiently supported and lovingly inspired me throughout my graduate school career and for as long as I can remember.

TABLE OF CONTENTS

[a,b] Text adapted from research manuscript in press, with written permission of publisher

LIST OF FIGURES

LIST OF TABLES

ABSTRACT

THE ROLE OF CALCINEURIN IN DENDRITIC REMODELING AND EPILEPTOGENESIS IN A RAT MODEL OF TRAUMATIC BRAIN INJURY

By John N. Campbell

A dissertation submitted in partial fulfillment of the requirements for the degree of Doctor of Philosophy at Virginia Commonwealth University

Virginia Commonwealth University, 2012

Director: Severn B. Churn, Ph.D.
Associate Professor, Departments of Neurology,
Anatomy & Neurobiology, Pharmacology & Toxicology,
and Physiology & Biophysics

Traumatic brain injury (TBI), a leading cause of death and disability in the United States, causes potentially preventable damage in part through the dysregulation of neural calcium levels. This dysregulation likely affects the activity of the calcium-sensitive phosphatase, calcineurin, with serious implications for neural function. To test this possibility, the present study characterized the role of calcineurin in a rat model of brain trauma, the lateral fluid percussion injury model. Golgi-Cox histochemistry revealed an acute post-TBI loss and delayed overgrowth of dendritic spines on principal cortical cells. The spine loss appeared to require calcineurin activity, since administering a calcineurin inhibitor, FK506, 1 hour after TBI prevented the spine loss.

Additional experiments showed how calcineurin activity might be related to the spine loss. Specifically, Western blots and enzyme activity assays revealed an acute increase in the cortical activity of calcineurin and its downstream effector, the actin-depolymerizing protein, cofilin. The cofilin activation was blocked by the same FK506 treatment that prevented spine loss, suggesting a relationship between cofilin activation and spine loss. To investigate long-term consequences of calcineurin activation after TBI, rats were administered FK506 (Tacrolimus) 1 hour after TBI and then monitored for spontaneous seizure activity months later. Acute post-TBI treatment with FK506 reduced the frequency of late non-convulsive seizures but did not prevent late convulsive seizures, cortical atrophy, or thalamic damage. The results of the present study implicate calcineurin in the acute dendritic remodeling and late non-convulsive seizures that occur after TBI. Importantly, these findings reveal calcineurin as a potential therapeutic target in the treatment of TBI and its sequalae.

INTRODUCTION

The Exciting but Risky Lives of Dendritic Spines

Experience leaves a trace in the adult brain through the formation and elimination, strengthening and weakening of individual synapses [1,2]. In vertebrates this plasticity depends largely on tiny protuberances of neuronal membrane, known as dendritic spines [3]. Dendritic spines abound in forebrain regions where memories are formed and stored [4], regions in which nearly all excitatory synapses are formed on dendritic spines [5] and in which nearly all spines bear at least one excitatory synapse [6]. The importance of these spines to synaptic plasticity is further evidenced by their composition: each spine is equipped with a diverse complement of signaling proteins which work together to not only transduce synaptic communication, but to regulate synaptic efficacy in an activity-dependent and synapse-specific manner [7,8,9]. Such plasticity may, however, be risky business for the dendritic spine. Excitatory signaling can occur to toxic excess in many forms of brain injury and disease [10]. This excitotoxicity can trigger the rapid retraction of spines into the parent dendrite [11], potentially coinciding with a breakdown of the post-synaptic machinery [12,13] and separating the pre- and post-synaptic membranes. The collapse of a spine could therefore mean the loss of its synapse. However, this may be neuroprotective under certain circumstances. For example, by weakening or disconnecting an overactive

synapse, the collapse of a dendritic spine may help to prevent further excitotoxic damage to the parent neuron. Spine collapse could therefore act like a circuit-breaker. On the other hand, the collapse of a dendritic spine may entail risks for neuronal networks, especially if spine collapse disconnects synaptic partners or impairs synaptic communication. The resulting decrease in network activity may be temporary if the synaptic partners are able to re-connect. Still, a decrease in network activity lasting a day or longer can trigger homeostatic increases in the sensitivity of remaining excitatory synapses [14], or provoke the formation of new excitatory synapses [15]. Dendritic spines are a therefore a likely substrate for injury-induced and potentially pathological changes in brain circuitry. A better understanding of the mechanisms of dendritic spine collapse may reveal therapeutic targets for the treatment of brain injury and its sequelae.

This introduction considers potential mechanisms of dendritic spine collapse. The terms “spine loss” and “spine collapse” are used interchangeably herein to describe the retraction of a spine into the parent dendrite. Many mechanisms of spine loss have been demonstrated experimentally, including some which are pre-synaptic (*e.g.,* [16]), and others which are extra-synaptic, such as the removal of synapses by microglia [17,18,19,20]. Other studies have identified mechanisms which appear to be contained within the post-synaptic neuron. These post-synaptic mechanisms of spine loss are the focus of this introduction.

Since much of spine plasticity depends on intracellular Ca^{2+} ions, the first part of this introduction considers Ca^{2+} signaling within the dendritic spine and how this signaling affects spine structure and function.

Calcium in Dendritic Spine Plasticity

Intracellular Ca^{2+} signaling is integral to many cellular functions, including synaptic plasticity. Normally, excitatory signaling at the spine synapse causes an accumulation of Ca^{2+} ions within the dendritic spine. These ions relay the excitatory signal from the synaptic surface to Ca^{2+}-sensitive proteins within the dendritic spine. The Ca^{2+}-sensitive proteins then act on divergent biochemical pathways which ultimately determine post-synaptic structure and function. Some pathways alter the number or sensitivity of receptors at the spine synapse, thereby adjusting its response to subsequent signals [21,22]. Other pathways expand, lengthen, or shrink the spine by remodeling its cytoskeleton [23,24], morphological changes which can influence the spread of electrical and molecular signals [25,26,27]. Because antagonistic pathways compete for Ca^{2+} binding, the outcome of this competition depends on their relative Ca^{2+} sensitivity as well as on the magnitude and duration of the Ca^{2+} signal [28]. Likely for this reason, Ca^{2+} dynamics are tightly controlled in the dendritic spine. Indeed, Ca^{2+} dynamics are subject to a host of locally-regulated processes, including Ca^{2+} influx through gated channels and efflux through ion pumps, Ca^{2+} sequestration in organelles and binding of proteins, even the geometry of the dendritic spine [29,30,31]. However, many of these regulatory processes can be disrupted or over-activated by brain injury [32,33,34,35]. The resulting dysregulation of Ca^{2+}-sensitive pathways may have substantial consequences for the structure and function of the dendritic spine.

A major trigger for Ca^{2+} accumulation in the dendritic spine is glutamate. Glutamate, the predominant excitatory neurotransmitter in the mammalian brain, binds

metabotropic and ionotropic glutamate receptors expressed on the surface of the dendritic spine [30]. The interaction of glutamate with any type of glutamate receptor can affect the Ca^{2+} content of a dendritic spine. For example, metabotropic glutamate receptors (mGluRs) are coupled to G proteins that mediate, among other things, the release of intracellular stores of Ca^{2+} [36]. But while mGluRs do mediate some forms of spine plasticity [37,38,39], the role of these receptors under pathological conditions is not well understood. Some *in vitro* studies suggest that mGluR activation during excitotoxicity limits the post-synaptic influx of Ca^{2+} and the related neuronal degeneration [40,41]; other studies report evidence to the contrary [42]. A more recent *in vivo* study found that the truncation of mGluRs by calpain is a critical step in neuronal excitotoxicity [43]. Still, it is unclear to what extent mGluRs participate in Ca^{2+}-dependent mechanisms of dendritic spine collapse.

Ionotropic glutamate receptors open channels which make the cell membrane permeable to cations. All three known subtypes of ionotropic glutamate receptors can be expressed by dendritic spines: the 2-amino-3-(3-hydroxy-5-methylisoxazol-4-yl) proprionate (AMPA) receptor, the kainate receptor, and the N-methyl-D-aspartate (NMDA) receptor. These receptor subtypes differentially affect the Ca^{2+} content of a dendritic spine and so are described separately below.

AMPA Receptors

The AMPA receptor (AMPAR) is the primary route of fast synaptic input at the dendritic spine. The expression of AMPARs at the spine synapse is activity-dependent, which is integral to long-term plasticity of the post-synapse [44]. Upon binding

glutamate, the AMPAR opens a pore in the spine membrane through which ions travel along their concentration gradient. Due to the charge profile of this pore [45], AMPARs mostly conduct Na^+ and K^+, resulting in the rapid depolarization of the dendritic spine membrane. However, the ion permeability of the AMPAR is a function of its subunit composition. One subunit in particular, GluR2, confers impermeability to divalent cations, due to the presence of a polar arginine residue at a key site along the GluR2 pore-forming domain [46]. Therefore, AMPARs can be permeable to divalent cations such as Ca^{2+} and Zn^{2+} when formed without a GluR2 subunit, or when formed with a GluR2 in which a non-polar glutamine was substituted for the key arginine [47]. Normally in the adult brain, GluR2-lacking, Ca^{2+}-permeable AMPARs are expressed stably by interneurons but only transiently by principal cells of the neocortex and hippocampus [47,48]. The transient expression of Ca^{2+}-permeable AMPARs by principal cells is thought to be a mechanism of synaptic scaling – in this case, a sensitization of the post-synapse in response to a loss of synaptic activity [47].

Synaptic scaling by Ca^{2+}-permeable AMPARs can also occur pathologically. For example, hippocampal pyramidal neurons that are vulnerable to either ischemic or epileptogenic injury show an increased proportion of GluR2-lacking AMPARs in response to that particular injury [49]. This change in AMPAR composition may help to explain the pattern of neuronal death following ischemia [48]. However, it is unclear to what extent the cell death involves Ca^{2+} permeability, Zn^{2+} permeability, or other GluR2-related issues [50,51]. In fact, studies of transgenic mice have suggested that the Ca^{2+} conducted by Ca^{2+}-permeable AMPARs may not be directly toxic [52,53]. Instead, Ca^{2+}-permeable AMPARs may cause problems by facilitating the long-term potentiation

(LTP) of excitatory synapses [52]. Such synaptic scaling could promote hyperexcitability in neuronal networks and so indirectly contribute to pathology [54].

Kainate Receptors

Similar to the AMPAR, the post-synaptic kainate receptor contributes to membrane depolarization and exhibits subunit-dependent Ca^{2+} permeability [55]. However, at least in the hippocampus, the composition and function of post-synaptic kainate receptors appear to be region-specific [55,56]. Furthermore, kainate receptors appear to be expressed at specific types of synapses within these regions. For example, pyramidal neurons in hippocampal CA3 express post-synaptic kainate receptors almost exclusively on thorny excrescences [56], multi-lobed spines found at the synapses between mossy fibers and CA3 pyramidals [57].

Both kainate receptors and AMPARs can indirectly generate an influx of Ca^{2+} into the dendritic spine in a number of ways. First, membrane depolarization by AMPARs and/or kainate receptors is essential to the activation of NMDA receptors, a principal source of spine Ca^{2+} (see below). This depolarization may also open local voltage-sensitive Ca^{2+} channels (VSCCs) [58]. These VSCCs appear to enhance or support plasticity at hippocampal synapses [58], though the role of VSCCs in the pathological plasticity of dendritic spines is not yet known. Finally, kainate receptors and AMPARs may conduct enough Na^{+} to reverse the flow of local Na^{+}/Ca^{2+} transporters, resulting in an inward Ca^{2+} current across those transporters [59]. However, there is conflicting evidence over the role of Na^{+}/Ca^{2+} transporters in neuronal excitotoxicity [59,60].

NMDA Receptors

The NMDA receptor (NMDAR) is a major conduit of Ca^{2+} into dendritic spines throughout the neocortex and hippocampus [30]. Like the AMPAR and the kainate receptor, the NMDAR exhibits activity-dependent permeability to Na^+ and K^+ and subunit-dependent permeability to Ca^{2+} [61]. However, the Ca^{2+} permeability of the NMDAR can be 20 times greater than that of the other ionotropic glutamate receptors [62] and is far less dependent on subunit composition [63]. The subunit composition of the NMDAR does, however, determine its inactivation time and other functional properties that affect the size of its Ca^{2+} current [63,64]. Also unique among the ionotropic glutamate receptors, activation of the NMDAR requires the co-incidence of multiple events: binding of glutamate; binding of a co-agonist, such as glycine or D-serine; and a depolarization of the local membrane sufficient to dislodge the Mg^{2+} ion which normally occludes the NMDAR ion channel.

NMDARs play a central, well-characterized role in neuronal excitotoxicity [65]. Selective agonists of NMDARs can cause excitotoxicity *in vitro*, and glutamate-induced excitotoxicity is mostly blocked by NMDAR-selective antagonists (e.g., [66]). Similarly, NMDAR antagonists have proven to be neuroprotective in models of stroke and traumatic brain injury *in vivo* [67,68], suggesting that NMDAR activity can be neurotoxic. This NMDAR toxicity appears to be largely Ca^{2+}-dependent, as cell-permeable Ca^{2+} chelators are neuroprotective during excitotoxicity *in vitro* and *in vivo* [69].

Many studies have demonstrated that high intracellular Ca^{2+} concentrations are neurotoxic [32,70]. Yet, the amount of Ca^{2+} does not solely determine its toxicity. For instance, excitotoxic NMDAR activity can generate high intracellular concentrations of

Ca^{2+}, but an equivalent concentration of Ca^{2+} achieved with ionophores is not toxic to neurons *in vitro* [71]. The particular toxicity of NMDAR-mediated Ca^{2+} may be explained in a number of ways. One possibility is that NMDARs conduct Ca^{2+} into a diffusion-limited space, the head of the dendritic spine, thereby creating toxic foci of highly concentrated Ca^{2+}. However, this seems unlikely to explain the toxicity of NMDAR-mediated Ca^{2+}: excitotoxicity can still occur by NMDA receptors expressed on the dendritic shaft, a space which is less diffusion-limited [72]. Another, more likely possibility is that the toxicity relates to the special environment of the NMDAR, *e.g*., its neighboring clusters of Ca^{2+}-sensitive proteins and their effector pathways.

Calcium Nanodomains

The NMDAR-mediated Ca^{2+} current is a principal determinant of dendritic spine plasticity. This Ca^{2+} activates pathways which antagonistically control the size and shape of the dendritic spine as well as the expression and sensitivity of post-synaptic glutamate receptors [28]. The underlying pathways are mediated by Ca^{2+}-sensitive proteins anchored near NMDARs at the post-synaptic density [73], which suggests a competition among these pathways for the Ca^{2+} signal [7]. Yet, the size of the Ca^{2+} influx does not alone determine which Ca^{2+} sensitive proteins are activated [39]. Other important variables may be involved, including the Ca^{2+} sensitivity of the protein, its proximity to the Ca^{2+} signal, and any post-translational modifications of the protein due to cross-talk with other pathways. These variables are part of the “nanodomain,” the nano-scale environment in which a Ca^{2+} influx becomes an intracellular signaling event. In the dendritic spine, Ca^{2+} nanodomains may decide the outcome in the competition

between Ca^{2+}-sensitive pathways [74], ultimately determining whether LTP or LTD occurs, whether the spine grows or shrinks, and so on.

Ca^{2+} nanodomains may also influence the neuronal response to excitotoxicity [75]. For example, *in vitro* studies have demonstrated that toxicity of Ca^{2+} depends more on the source than on the amount of Ca^{2+} [71,76]. This "source specificity" of Ca^{2+} toxicity [75] may be related to proximity of Ca^{2+}-sensitive elements, such as mitochondria and apoptotic signaling pathways [77].

Other Ca^{2+}-sensitive elements of the nanodomain may determine different neuronal responses to excitotoxicity. One response in particular, the collapse of dendritic spines, is associated with a variety of excitotoxic brain injuries in humans and the relevant animal models [78,79]. But the collapse of dendritic spines may be more than a symptom of neuronal excitotoxicity; spine collapse potentially could contribute to injury-related pathology, such as cognitive impairment or epilepsy [78]. For this reason, a better understanding of dendritic spine collapse can be instructive in the treatment of brain injury. Research over the past decade has revealed a variety of biochemical mechanisms to explain dendritic spine collapse following brain injury. The following section is a review of four such mechanisms.

Post-Synaptic Mechanisms of Dendritic Spine Collapse

Dendritic Beading

In the late 1970's, James Olney and colleagues reported kainic acid caused spherical swellings in neuronal dendrites [80]. Similar swellings had been described by Santiago Ramon y Cajal in 1909, but their etiology remained unknown for nearly a

century. The formation of these varicosities, known as dendritic beading [78], is now generally regarded as an early and reversible sign of neuronal excitotoxicity [81]. Dendritic beading is commonly observed following brain injuries, especially those in which excitotoxicity is involved, such as epilepsy [78,82], stroke [83,84], and traumatic brain injury [85,86,87]. Dendritic beading can be induced by a variety of experimental conditions, including treatment with ionotropic glutamate receptor agonists [84,88,89,90], ischemia [91,92,93,94], activation of microglia [95], or by cooling [96,97]. Interestingly, neuronal degeneration is worsened when experimental conditions prevent dendritic beading, suggesting that the beading may be a neuroprotective response [90] (but see also [98]).

Two mechanisms are independently sufficient to induce dendritic beading: an osmotic shift involving ligand-gated and voltage-sensitive ion channels, and a Ca^{2+}-dependent disruption of dendritic cytoskeleton. The osmotic shift begins with an influx of ions into the dendrite, first through ionotropic glutamate receptors [80,84,89,90,94] and then through voltage-sensitive sodium [99,100,101] and chloride channels [98]. Eventually, the influx of ions outstrips their efflux through the Na^+/K^+ pump [102] and other means of extrusion, resulting in hyperosmotic foci within the dendrite. These foci draw fluid from neighboring segments of dendrite and/or from the extracellular environment [93], producing the characteristic appearance of spherical swellings separated by narrowed segments of dendrite [96,102].

Interestingly, the NMDAR-mediated Ca^{2+} current does not contribute substantially to the osmotic shift [89,99,102]. This may be due to Ca^{2+} uptake and buffering within the dendrite, which would minimize the effect of Ca^{2+} on osmolarity. However, the Ca^{2+}

influx does induce a different mechanism of dendritic beading, one in which Ca^{2+}-sensitive enzymes lead to the disruption the dendrite cytoskeleton. Evidence for this mechanism comes from reports of fragmented microtubules in electron micrographs of dendritic beads [96] and in neurons during excitotoxicity [103]. These microtubules are normally stabilized by the binding of microtubule associated protein 2 (MAP2) [104,105]. However, a dramatic loss of MAP2 occurs with excitotoxicity *in vivo* [106] and is attributed to Ca^{2+} signaling [103,107]. The loss of MAP2 and dendritic beading can both be prevented by the microtubule-stabilizing drug, taxol, in an acute hippocampal slice model of excitotoxicity [103]. Conversely, beading is induced when microtubules are destabilized by various agents, including nocodazole, platelet activating factor, or methyl-carbamyl platelet activating factor [108].

Microtubule disruption may explain the Ca^{2+}-dependent form of dendritic beading observed in the literature [96,103,107,109]. Unlike the beading induced by the osmotic shift, these Ca^{2+}-dependent beads are smaller in diameter [96] and more irregular in form [107]. Since Ca^{2+}-dependent and -independent (i.e., osmotic shift) forms have both been reported, the literature contains some disagreement over the etiology of dendritic beading. However, at least some conflicting reports may be explained by differences in experimental design. For example, dendritic beading tends to be Ca^{2+}-dependent when induced by NMDAR agonists [96,103,107] and Ca^{2+}-independent when induced by agonists of other, less Ca^{2+}-permeable glutamate receptors [80,89,99,101,106]. The Ca^{2+}-dependent form of dendritic beading has also been observed in kainic acid-treated Purkinje neurons [109]. Because mature Purkinje cells

lack NMDARs [110], this beading likely involves voltage-sensitive Ca^{2+} channels opened upon membrane depolarization by kainate receptors/AMPARs.

Though both Ca^{2+}-dependent and -independent mechanisms can be induced experimentally, both likely contribute to the dendritic beading observed in injured brains. In fact, their effects appear to be complementary: Ca^{2+}-dependent dendritic beads have an irregular, oblong shape [96,107], similar to Ca^{2+}-independent beads induced in the presence of a voltage-gated calcium channel blocker [101]. Therefore, the spherical shape of dendritic beads observed *in vivo* seems to require both Ca^{2+}-dependent and -independent mechanisms.

Dendritic beading is associated with a significant loss of dendritic spines, up to 50% on affected segments of dendrite [88]. Yet, most of this spine loss is only an apparent loss. Just as the fingers of a rubber glove are absorbed upon its inflation, dendritic spines may be engulfed by the swelling dendrite. However, within a few hours of a brief excitotoxic challenge, the dendritic beads gradually resolve and most of their spines re-emerge [84,88,97]. Importantly, this temporary spine loss does not appear to disrupt spine synapses. *In vitro* and slice culture studies have found that, while some synapses are lost in the process, most retracted spines re-emerge at their original sites [88,97]. Time-lapse imaging of mouse cortical neurons *in vitro* shows that pre- and post-synaptic components remain apposed during NMDA-induced spine collapse [88]. Therefore, synapses on collapsed spines may remain intact during brief excitotoxic challenges.

While the loss of dendritic spines during beading may be superficial and temporary, other mechanisms underlie more chronic spine loss as well as the

elimination of spine synapses. These mechanisms are all Ca^{2+}-dependent and their actions may be complementary. Interestingly, at least two of these mechanisms are mediated by the Ca^{2+}-sensitive phosphatase, calcineurin.

Calcineurin-Mediated Cofilin Activation

Calcineurin is a neurally-enriched, serine/threonine phosphatase which is stimulated upon its binding Ca^{2+}/calmodulin [111,112,113]. Calcineurin is expressed by every cell type in the brain, though its role in neurons has been particularly well-characterized. In fact, neuronal calcineurin appears to play a variety of roles in synaptic plasticity [114]. Notably, calcineurin is essential for the induction of long-term depression (LTD) at synapses in some hippocampal regions [115,116], where it regulates functional aspects of LTD, including the desensitization and endocytosis of post-synaptic AMPA receptors [21,117]. Furthermore, calcineurin is involved in the structural plasticity of dendritic spines: it is responsible for the shrinkage of dendritic spines associated with the induction of LTD [23], and for the collapse of dendritic spines following excitotoxic injury [11,118]. Though many details are still under investigation, a number of candidate pathways linking calcineurin activity to dendritic spine collapse have been identified. One such pathway involves proteins of the actin depolymerizing factor (ADF)/cofilin family (cofilin).

Cofilin binds and severs actin filaments (F-actin) and accelerates their depolymerization [119]. Since actin filaments are the major cytoskeletal element in the dendritic spine [120,121], actin breakdown by cofilin can destabilize the spine cytoskeleton, resulting in spine shrinkage [23] or even collapse. Indeed, the distribution

of cofilin fits with its role in the remodeling of dendritic spines. Cofilin is distributed heterogeneously in the dendritic spine, found abundantly in the PSD and the spine periphery but is mostly absent from the spine core [122]. This distribution overlaps the outer edges of the spine's more dynamic actin network, a pool of F-actin that rapidly responds to glutamate stimulation [123]. Therefore, the co-localization of cofilin with this dynamic pool of actin is consistent with the role of cofilin in spine remodeling.

Like many proteins in the dendritic spine, the activity of cofilin is regulated by phosphorylation. In the case of cofilin, its activity depends on the phosphorylation state of a key amino acid residue, serine 3 (ser3). Phosphorylation of ser3 decreases the ability of cofilin to bind (and therefore sever) actin filaments [119]. Ser3 phosphorylation is catalyzed by LIM kinases [124,125,126,127,128]. In turn, LIM kinase activity depends on the signaling cascades of the Rho, Rac and Cdc42 family of small GTPases [129,130], some of which are influenced by Ca^{2+}-sensitive pathways that begin at the NMDA receptors. Therefore, NMDA receptors may be linked to cofilin inactivation by Ca^{2+}-dependent pathways involving the small GTPases (*e.g.,* Rac1 and Ras) and LIM kinase.

NMDA receptors are also linked to cofilin activation by a different Ca^{2+}-sensitive pathway, one mediated by calcineurin. This is because calcineurin dephosphorylates and thereby activates Slingshot [131], a family of cofilin phosphatases [132,133] which are enriched in neurons [134] and which localize to dendritic spines [135]. Slingshot then dephosphorylates the cofilin ser3 residue [132], which increases the binding and breakdown of F-actin by cofilin [119]. Thus, NMDA receptor activity can stimulate cofilin

via a calcineurin-Slingshot pathway, or inactivate cofilin *via* a small GTPase-LIMK pathway.

The calcineurin-Slingshot pathway is one mechanism which couples NMDAR activity with cofilin activity. Indeed, cofilin activation is associated with spine shrinkage following low frequency stimulation of NMDARs (i.e., LTD) [23] and with spine collapse following excessive stimulation of NMDARs (i.e., excitotoxicity) [118]. Yet, frequencies of NMDAR activation that induce long-term potentiation (LTP) also cause cofilin inactivation and spine growth [24,136]. So, how could LTP-inducing frequencies inactivate cofilin, while lower and higher frequencies have just the opposite effect? One possibility is that there are multiple, cofilin-activating pathways which differ in Ca^{2+} sensitivity. For example, cofilin activating pathways may be either very sensitive or very insensitive to Ca^{2+}, such that only excitotoxic levels of Ca^{2+} could induce both types of pathways, which together overwhelm the opposing pathways, resulting in cofilin activation.

An alternative but not exclusive possibility is that cofilin does not work alone in the collapse of dendritic spines. In fact, the effect of cofilin on F-actin can be simulated with latrunculin A, a drug which inhibits actin polymerization [137]. Yet, treating cultured neurons with latrunculin A does not entirely reproduce the spine collapse associated with NMDA excitotoxicity [72,138]. Wispy, filopodia-like structures remain. These structures, termed “spine remnants” [138,139,140], have been offered as evidence that the dendritic spine is bolstered by the proteins contained within, not just by the spine’s cytoskeleton [140]. Indeed, each dendritic spine contains a dense network of proteins [9] which may suffice to stabilize the spine *in vitro*. However, it remains to be seen

whether this protein netowrk is enough to prevent collapse in the more densely packed *in vivo* environment, where the spine is likely subject to greater external pressures. Nonetheless, recently published *in vitro* studies have demonstrated the critical role of two proteins in dendritic spine stability, and in doing so, identified novel mechanisms of dendritic spine collapse. These mechanisms involve intracellular pathways that extend far beyond the dendritic spine, even one that reaches to the cell nucleus and back.

Snk-Mediated SPAR Proteolysis

Another intracellular event associated with spine collapse is the proteolysis of SPAR, the spine-associated Rap guanosine triphosphatase activating protein [12,141,142]. SPAR is a 190kDa protein with separate binding sites for actin and post-synaptic density (PSD) proteins, and a guanosine triphosphatase activating protein (GAP)-like domain [12]. SPAR is localized to the dendritic spine, where the binding and catalytic domains of SPAR suggest its involvement in cytoskeletal regulation. For example, its binding domains may allow SPAR to physically bridge the post-synaptic density to the spine cytoskeleton [141], which could stabilize the spine. Additionally, its catalytic domain allows SPAR to inactivate two functionally distinct [143] cytoskeletal regulating members of the Ras family of small GTPases [144]: Rap2 and, to a lesser extent, Rap1 [141].

Clues to the role of SPAR in the dendritic spine have emerged from experiments which altered SPAR protein expression. One study found that SPAR re-organizes cytoskeletal actin when expressed in COS-7 cells, and that SPAR over-expression induces spine growth in cultured hippocampal neurons [141]. Another study reported

that RNAi knockdown of SPAR weakened post-synaptic responsiveness to glutamate in cultured hippocampal neurons [145]. These studies suggest that SPAR stabilizes both structural and functional aspects of the dendritic spine.

Excitotoxic insult causes a loss of SPAR *in vitro*, which correlates with a loss of dendritic spines and of the major PSD scaffold protein, PSD-95 [12,142]. This excitotoxic depletion of SPAR requires the following: a Ca^{2+} influx mediated by NMDA receptors and/or voltage gated Ca^{2+} channels; the activation of calcineurin; and a downstream increase in the transcription of serum inducible kinase, Snk (also known as polo-like kinase 2) which upregulates Snk protein expression [12]. Snk then phosphorylates SPAR, targeting it for ubiquitination and subsequent proteolysis [12,145,146]; the proteolysis likely occurs by proteosomes transported into the spine in response to NMDA receptor activity [147]. Despite its dependence on nuclear events, SPAR depletion can be detected within a few hours of excitotoxic insult. For example, in cultured hippocampal neurons, a significant loss of SPAR protein is observed from 3 hours to over 72 hours after exposure to glutamate [142]. This degradation of SPAR is matched in timing and magnitude by an increase in Snk protein levels [142].

Loss of SPAR also corresponds to a decrease in miniature excitatory post-synaptic currents (mEPSCs) [145]. This post-synaptic desensitization has led to the hypothesis that SPAR proteolysis is a mechanism of synaptic scaling (for review, see [148]) – in this case, a homeostatic reduction of synaptic activity in response to excessive synaptic activity [145]. This synaptic scaling may be a neuroprotective mechanism deployed in response to excitotoxicity. However, it is not yet understood how SPAR proteolysis is able to downscale post-synaptic activity. One possibility is that

the related loss of PSD-95, an important scaffold protein of the post-synaptic density, disrupts the clustering of NMDA receptors at the post-synaptic density. The dispersal of synaptic NMDARs does correspond to increased resistance to excitotoxicity in another *in vitro* model [72].

Another possibility is that the collapse of the dendritic spine physically separates the pre- and post-synaptic components. This spine collapse may be due to the loss of SPAR as either a structural protein or as a negative regulator of the GTPase Rap2. Constitutively active Rap2 causes a loss of dendritic spines and spine synapses in cultured neurons [143]; a similar outcome may occur when proteolysis of SPAR releases Rap2 from negative regulation. Future studies could test this hypothesis by transfecting neurons with a mutant SPAR lacking an inactive RapGAP domain. More investigation is needed to appreciate the relationship between the Snk-SPAR pathway and excitotoxic spine collapse.

MARCKS Proteolysis

SPAR degradation is not the only proteolytic event associated with the excitotoxic collapse of dendritic spines. The targeted degradation of another spine protein, myristoylated alanine-rich C-kinase substrate (MARCKS), is also activity-dependent and linked to dendritic spine collapse [138]. MARCKS is expressed heterogeneously across the neocortex and subcortical structures, and enriched in neuronal processes [149]. MARCKS is also found in some dendritic spines [149], though its function there is not completely understood. Yet, recent evidence implicates MARCKS in the activity-dependent plasticity of dendritic spines [150,151,152,153],

where it is thought to integrate converging signals from protein kinase C (PKC) and Ca^{2+}/calmodulin [154]. When neither phosphorylated by PKC nor bound by calmodulin, MARCKS adheres to the cell membrane and promotes the growth of the actin network, potentially by sequestering phospholipids which affect actin dynamics [155]. Furthermore, by physically anchoring the cytoskeleton to the cell membrane, MARCKS may stabilize dendritic structure [156]. Therefore, the loss of MARCKS can limit the growth and anchorage of the actin cytoskeleton, which may destabilize dendritic spines.

Experimental depletion of MARCKS *in vitro* has revealed its importance to the stability of dendritic spines. For example, spine density and size are significantly decreased following RNA interference of MARCKS protein expression in cultured hippocampal cells [150]. MARCKS protein levels and spine density are also reduced following exogenous activation of PKC [150], suggesting that PKC phosphorylation may target MARCKS for proteolysis. PKC is active during NMDA-induced excitotoxicity [157,158], which may explain the extensive proteolysis of MARCKS under those conditions. Indeed, within 10 minutes of a 30 second treatment with 50μM NMDA, MARCKS protein is reduced by nearly 50% and spine density by roughly 75% in cultured hippocampal neurons [138]. Strikingly, all of the MARCKS proteolysis and nearly half of the spine loss were blocked by inhibitors of cathepsin B/L [138], cysteine proteases for which MARCKS is a known substrate [159]. Considered together, these observations support a mechanism of dendritic spine collapse as follows: excessive NMDA receptor activity leads to MARCKS phosphorylation by PKC and subsequent proteolysis by cathepsin B/L; the loss of MARCKS protein inhibits actin growth and/or

disconnects the cytoskeleton from the plasma membrane, which progressively destabilizes and ultimately collapses the dendritic spine.

The Snk-SPAR pathway is one putative mechanism of synaptic scaling, could MARCKS proteolysis be another? One recent publication found that MARCKS proteolysis is associated with the post-ischemic development of NMDA tolerance. In this study, cultured neocortical neurons were deprived of glucose and oxygen for 30 minutes. One hour later, these neurons showed a 23% loss of MARCKS protein, a transient, 75% reduction in dendritic spine density, and a similarly transient tolerance to NMDA-induced excitotoxicity [151]. Treatment with the actin-stabilizing compound, jasplakinolide, blocked both the dendritic spine loss and NMDA tolerance, as did treatment with proteosome inhibitors that preserved MARCKS protein levels[*] [151]. Therefore, the spine loss and NMDA tolerance required both proteolysis and the breakdown of the actin cytoskeleton. Yet, it is unclear just how NMDA tolerance is related to these other phenomena. One possibility is that proteolytic events (e.g., MARCKS) drive the breakdown of the spine cytoskeleton, which destabilizes the spine and disperses glutamate receptors and/or related signaling proteins from the post-synaptic region. If the dispersal of signaling proteins affected signal reception or processing, this could explain the decreased response of these post-ischemic neurons to NMDA treatment. Consistent with this scenario, the authors reported that brief ischemia decreased the actin binding of two important post-synaptic proteins, the NMDA receptor subunit NR2B, and PSD-95, but did not affect their protein expression

[*]Curiously, one of the proteosome inhibitors, MG132, was ineffective in blocking MARCKS proteolysis in the study by Graber *et al.* (2004). However, the Graber study induced excitotoxicity with NMDA, not ischemia. Therefore, the discrepancy between the two studies may be explained by differences in experimental design.

[151]. These observations suggest that post-synaptic proteins detach from the spine cytoskeleton following brief ischemia, which could disperse the signaling proteins and reduce their responsiveness to subsequent signals.

Dendritic spine collapse may protect the parent neuron at the expense of the neuronal network. The resulting disruptions in network activity or connectivity could contribute to the cognitive impairment which follows injury, and may even facilitate the development of epilepsy . The next section considers traumatic brain injury, a common form of brain injury which is associated with both dendritic spine loss and epilepsy.

Traumatic Brain Injury and Post-Traumatic Epilepsy

Traumatic brain injury (TBI) occurs when the brain is damaged by external forces, such as impact, penetration, blast, or a sudden change in velocity. TBI occurs approximately every 19 seconds in the United States and is a leading cause of morbidity and mortality, resulting in more than 1.3 million hospitalizations and more than 50,000 deaths in the U.S. each year [160]. Those that survive TBI often face lifelong impairments and other complications [161] which incur lifelong costs in quality of life, productivity, and medical care. Indeed, the personal, financial, and societal costs of a single TBI can last for decades, since TBI predominantly affects children and young adults [160]. The high incidence and chronic costs make TBI one of the most expensive diseases in the U.S., estimated at $60 billion dollars in the year 2000 alone [162].

One significant complication of TBI is post-traumatic epilepsy. This form of acquired epilepsy is characterized by spontaneous, recurrent seizures which begin weeks to years after TBI. Epilepsy is a common consequence of TBI, diagnosed in 2-

25% of TBI survivors [163,164]. Conversely, TBI is a common cause of epilepsy, accounting for about 5% of all cases of epilepsy in the general population [165]. Most post-traumatic epileptics exhibit partial seizures as the dominant seizure type (91% cases), originating in either the temporal lobe (54% cases) or in the frontal neocortex (33% cases) [166,167]. Though conventional anti-seizure drugs are indicated for its treatment, post-traumatic epilepsy is often refractory to drugs and surgery [168,169]. Though difficult to treat, post-traumatic epilepsy may be preventable, as the latency between TBI and seizure onset suggests a wide window for therapeutic intervention. While efforts to prevent human post-traumatic epilepsy have so far been disappointing [170], hope has emerged from research in rodent models of the disease [171].

Several models of closed-head injury, the predominant form of human TBI, have been adapted for studying post-traumatic epilepsy. In two of these models, the cortical contusion model and the fluid percussion model, rats and mice subjected to a laterally-placed TBI develop spontaneous, recurrent seizures within weeks to months [172,173,174,175]. However, the mechanisms which lead from TBI to seizures in these models have not been identified. Nor is it known when these mechanisms are initiated, though some studies of humans and rodent models suggest that epileptogenesis begins within minutes of TBI [176,177]. A better understanding of the mechanisms and timing of epileptogenesis are essential to developing prophylactic treatments for post-traumatic epilepsy.

CHAPTER I

TRAUMATIC BRAIN INJURY CAUSES AN FK506-SENSITIVE LOSS AND AN OVERGROWTH OF DENDRITIC SPINES

INTRODUCTION

Survivors of traumatic brain injury (TBI), most of whom are young adults, often suffer lifelong disabilities. The devastating consequences of TBI derive in part from its progressive nature: the immediate, mechanical destruction of tissue can be followed by days to weeks of excitotoxic and inflammatory damage [178,179]. This cumulative injury can alter neural function well beyond the focally-damaged tissue and so may contribute to TBI-induced neuropathologies, such as cognitive impairment and post-traumatic epilepsy. Animal modeling of TBI has revealed that cognitive impairment can occur in the absence of cell death (*e.g.*, [180]) and that the onset of PTE can be many months after TBI [181]. It is therefore likely that cognitive impairment and PTE develop from disruptions in neural circuitry beyond the acute loss of cells. A better understanding of how TBI disrupts neural circuitry should uncover novel therapeutic targets for treating TBI-induced neuropathologies.

One potential mechanism of disrupted neural circuitry may be the loss of dendritic spines. Dendritic spines are specialized protuberances of dendritic membrane which form the post-synaptic component of most excitatory synapses in the brain [5].

The stability of the dendritic spine depends on synaptic activity [182]. Indeed, the loss of its pre-synaptic partner can cause the spine to retract into the dendritic shaft [16], and spine collapse due to deafferentation is a well-characterized phenomenon. However, an excess of synaptic activity can also cause spine collapse, through the toxic excitation of glutamate receptors [84]. Multiple post-synaptic mechanisms linking excitotoxicity to dendritic spine loss have been proposed and demonstrated *in vitro* (reviewed in [183]). Interestingly, at least two of these mechanisms are mediated by the calcium-sensitive phosphatase, calcineurin (CaN) [11,12]. Since CaN is activated by glutamate signaling [184] and glutamate signaling occurs to excess after TBI [185], it is plausible that an increase in CaN activity leads to dendritic spine loss after TBI.

Here we report an extensive analysis of dendritic spine density in the laterally injured brain. In addition, this study and its companion [186] present evidence of CaN-dependent mechanisms by which TBI results in dendritic spine loss. In particular, this study describes a region-specific loss of dendritic spines which can be blocked by a single, post-injury injection of FK506, a pharmacological inhibitor of CaN. This spine loss coincides, temporally and regionally, with changes in cofilin activity observed by our companion study [186]. In addition, the spine loss is followed by an apparent overgrowth of dendritic spines in both hemispheres of hippocampus. Overall, these findings suggest that the rat forebrain undergoes an extensive turnover of dendritic spines during recovery from lateral brain injury, which may participate in the development of cognitive impairment and post-traumatic epilepsy. Furthermore, these findings identify CaN as a potential therapeutic target in the treatment of TBI.

MATERIALS AND METHODS

Animal Use and Care

Use of animal subjects was performed in strict accordance with the *Guide for the Care and Use of Laboratory Animals*, provided by the National Institutes of Health, and approved in advance by the Virginia Commonwealth University Institutional Animal Care and Use Committee. Animal subjects received *ad libitum* access to food and water and were maintained on 12hr light/dark cycles throughout the experiment.

Surgical preparation and fluid percussion injury

Adult male Sprague-Dawley rats (90 day old; 350-400g; n=21) were anesthetized with sodium pentobarbital (54 mg/kg intraperitoneally; i.p.) and placed into a stereotactic frame. A 4.8-mm hole was made over the left hemisphere using a trephine centered 4mm caudal to bregma and -3mm lateral to the sagittal suture. A screw was inserted over the opposite hemisphere to anchor the skull attachments. A modified female Luer-Loc syringe hub (2.6mm inside diameter) was placed over the exposed dura, affixed with a cyanoacrylate adhesive, and then secured with dental acrylic. On the following day, subjects were anesthetized (4% isoflurane in a carrier gas mixture of 26% N_2O and 70% O_2) in a chamber, then removed from the chamber and immediately subjected to fluid percussion of the intact dura over their left parietal cortex. The fluid percussion device used in these experiments is identical to that described by Dixon and colleagues [187]. The Luer-Loc fitting, screw, and dental cement were removed from the skull immediately following injury. Subjects were then placed in a supine position and the time at which they righted themselves was recorded. Upon recovery of righting reflexes,

subjects were placed on a heating pad for at least 30 minutes (and up to 1 hour) until ambulatory, then returned to home cages and monitored daily. At 1hr post-injury, some subjects received a single intraperitoneal injection of FK506 (5mg/kg; Fujisawa Chemical Company, Osaka, Japan).

Golgi-Cox histology and light microscopy

At 1hr, 24hr, and 1wk after lateral fluid percussion injury, subjects were injected with a lethal dose of pentobarbital, perfused intracardially with saline (0.9%, 120mL, room temperature), and decapitated. Brains were quickly extracted and immersed into a Golgi-Cox staining solution prepared from a commercially-available kit (FD Rapid Golgistain Kit, FD Neurotechnologies, Inc., Baltimore, MD, U.S.A.). After 24hr of staining, brains were blocked to remove tissue rostral and caudal to the hippocampus, immersed in fresh staining solution, and stored at room temperature in the dark for a total of 2 weeks. The remainder of the staining procedure was performed according to the kit instructions.

Following the staining procedure, brains were cut into 200μm thick coronal sections using a vibratome (Leica, Wetzler, Germany). Sections were mounted onto 2%-gelatin coated slides and air-dried at room temperature in the dark overnight. Slide-mounted sections were developed and dehydrated according to the kit instructions, and coverslipped with Permount.

Three brain sections nearest the injury site were selected for further analysis. Golgi-impregnated principal cells from the following regions were assessed for dendritic spine density: layers II and III of parietal neocortex penumbral to the site of injury

("ipsilateral neocortex$_{II,III}$") and an analogous area of the contralateral hemisphere ("contralateral neocortex$_{II,III}$"); the pyramidal cell layer of the hippocampal subfields CA1 and CA3 in each hemisphere; and the granule cell layer of the dorsal leaf of the dentate gyrus (dDG; Figure 1) in each hemisphere. Brain region identification was aided by a standard atlas of the rat brain [188]. Golgi-stained principal cells were then visualized by light microscope (Nikon Optiphot-2, Nikon Optiphot, Melville, NY, U.S.A.). Under a 40x objective lens, pyramidal and granule neurons were identified by their location within cell layers and by the shape of their soma and dendritic arbor. Dendrites were visualized using a 100x/oil-immersion lens for manual tracing and dendritic spine quantification.

Dendrite tracing and dendritic spine quantification

To ensure consistency of sampling, the following inclusion criteria were applied. The dendrite sampled had to be (1) a second- or third-order branch, (2) within 30μm-150μm of the parent cell soma (as measured along the dendrite; "proximal") (3) not obscured by other Golgi-stained tissue, (4) showing no signs of degeneration which would interfere with spine quantification (*i.e.*, blebbing or beading of the proximal dendrite), and (5) connected to a soma which did not appear swollen or necrotic.

For each group of animals, at least 10 neurons per brain region per hemisphere were included in the analysis (for *n* values, see Table 1). Fully-stained principal neurons within each region of interest were first selected under minimal magnification (4x objective). Under high magnification (100x oil-immersion objective), selected neurons were then screened according to the inclusion criteria described above. For each

neuron, one proximal branch of dendrite was traced to a minimum length of 20μm. With regard to granule cells of the dDG, only dendrites oriented dorsolaterally were analyzed. Dendrites were traced through the x-, y-, and z-planes using a digitizing microscope stage under control of Neurolucida (MicroBrightField, Inc., Williston, VT, U.S.A.). The lengths of tracings were computed by Neurolucida Explorer software (MicroBrightField, Inc.). Along each traced segment of dendrite, dendritic spines were counted according to their morphology [189,190]: thin spines and mushroom-shaped spines were counted together as "pedunculated spines," whereas spines lacking a neck constriction (*e.g.*, stubby spines and filopodia-like spines) were counted as "non-pedunculated spines" (Figure 2). Spine density was calculated as the number of spines visible along a traced segment of dendrite, divided by the length of the traced segment. No correction was made for spines not seen due to the angle or plane of section.

Statistical analyses

Mean spine densities in injured brains were statistically compared to those from the corresponding dendritic arbor and brain region of age- and drug treatment-matched control brains. Each mean was derived from a pool of spine densities obtained from 3 identically-treated rats. Student's t-tests were used to compare the FK506-treated injured group to the FK506-treated uninjured group, while one-way analysis of variance (ANOVA) with Tukey post hoc test was used for all other comparisons. Statistical analyses were performed with GraphPad Prism, version 5.0 (GraphPad Software, Inc., La Jolla, CA, U.S.A.). Comparisons generating *p* values less than 0.05 were considered

statistically significant. Data are presented as group mean ± standard error of the mean (SEM).

RESULTS

Lateral fluid percussion injury

Adult male rats received a traumatic brain injury by fluid percussion of the dura overlying their left parietal cortex (mean pressure, 2.22 ± 0.02atm; between groups, $p > 0.05$). A common correlate of injury severity is the length of time between injury and the recovery of righting reflexes ("righting time") [191]. In the present study, the mean righting time was 8min 52sec ± 1min 31sec ($n = 12$) and was not significantly different between groups ($p > 0.05$). Some subjects exhibited apnea immediately following injury (5 out of 12 subjects) and were mechanically ventilated as needed (mean duration of ventilation, 1min 32sec ± 52sec). All subjects survived the injury.

Dendritic spine quantification in injured and uninjured forebrain

To determine the effect of TBI on dendritic structure, brains were recovered 1hr, 24hr, and 1wk after lateral fluid percussion injury (LFPI) and subjected to a modified Golgi-Cox procedure (see Materials and Methods). Proximal dendrites (within 30-150μm of soma) of Golgi-stained principal cells were manually traced (mean length of tracing ± standard deviation, 33.90 ± 9.43μm) and spine density was quantified, in the following forebrain regions: neocortex$_{II,III}$ penumbral to the LFPI site ("ipsilateral neocortex$_{II,III}$") and in an analogous region of the contralateral hemisphere ("contralateral neocortex$_{II,III}$"); the hippocampal subfields, CA1 and CA3; and the dorsal leaf of the

dentate gyrus (dDG; Figure 1). Mean densities of pedunculated spines (thin spines and mushroom-shaped spines; Figure 2) and non-pedunculated spines (stubby spines and filopodia-like spines; Figure 2) are provided in a supplementary table (Table 1). Overall, 1,264 dendrites were traced and 57,372 dendritic spines were counted.

On apical dendrites in neocortex$_{II,III}$, lateral fluid percussion injury caused a transient decrease in spine density

Pyramidal cells in neocortex$_{II,III}$ receive excitatory synapses on spines throughout their apical and basilar dendritic arbors. To investigate the effect of traumatic brain injury on these dendritic spines, we began by assessing spine density on the apical dendrites of neocortex$_{II,III}$ pyramidal cells in control and laterally injured brains (Figure 3). In control brains, neocortex$_{II,III}$ pyramidal cells (n=14) displayed an average of 1.20 ± 0.08 spines/μm on proximal apical dendrites, consistent with previously published data [192]. This spine density included an average of 0.74 ± 0.05 pedunculated spines/μm and an average of 0.46 ± 0.04 non-pedunculated spines/μm. At 1hr post-LFPI, the total spine density of these dendrites did not differ significantly from that of controls, in ipsilateral or contralateral neocortex$_{II,III}$ (each *vs.* control, $p > 0.05$; Figure 4a). Nor was the pedunculated or non-pedunculated spine density of these dendrites appreciably different from control values, in ipsilateral or contralateral neocortex$_{II,III}$ (each *vs*. control, $p > 0.05$; Figure 4b,c).

By 24hr post-LFPI however, apical dendrites in neocortex$_{II,III}$ showed a significant loss of spine density. Specifically, in ipsilateral neocortex$_{II,III}$, the total spine density of these dendrites decreased by 21% relative to controls (*vs*. control, $p < 0.05$; Figure 4a).

Further analysis revealed an underlying change in the density of pedunculated spines: pedunculated spine density decreased 30% from control values (*vs*. control, $p < 0.01$; Figure 4b). Since the non-pedunculated spine density of these dendrites was relatively unchanged at this time (*vs*. control, $p > 0.05$; Figure 4c), it is likely that the loss of pedunculated spine density involved more than just a change in spine phenotype (*i.e.*, from pedunculated to non-pedunculated). Furthermore, the effect on spine density appeared to be greater in the ipsilateral hemisphere. In contralateral neocortex$_{II,III}$, the pedunculated spine density of apical dendrites decreased 14% relative to controls, a change which was not statistically significant (*vs*. control, $p > 0.05$; Figure 4b). Thus, the data indicate that by 24hr post-LFPI there is a selective loss of pedunculated spine density from apical dendrites in ipsilateral neocortex$_{II,III}$. Because pedunculated spines are associated with stable synapses [193], a decrease in their density could indicate synaptic re-modeling in the injured brain.

The decrease in pedunculated spine density was not permanent. By 1wk post-LFPI in ipsilateral neocortex$_{II,III}$, the pedunculated spine density of apical dendrites recovered to control levels (*vs.* control, $p > 0.05$; Figure 4b). Likewise in contralateral neocortex$_{II,III}$, the pedunculated spine density of these dendrites did not differ significantly from control values (*vs*. control, $p > 0.05$; Figure 4b). Nor was the non-pedunculated spine density altered relative to controls, in either hemisphere of neocortex$_{II,III}$ (*vs*. control, $p > 0.05$; Figure 4c). The data therefore describe a recovery in the pedunculated spine density of apical dendrites in neocortex$_{II,III}$ by 1wk post-LFPI.

Overall, these results suggest that lateral TBI transiently decreased the pedunculated spine density of apical dendrites in ipsilateral neocortex$_{II,III}$. This decrease

is not likely due to acute mechanical trauma, as it occurred by 24hr but not by 1hr post-LFPI. The timing is more consistent with a secondary injury process, such as excitotoxicity. Importantly, these changes in post-synaptic structure could indicate extensive alterations of neocortex$_{II,III}$ circuitry in the injured brain.

On basilar dendrites in neocortex$_{II,III}$, spine density fluctuated during recovery from lateral fluid percussion injury

Basilar dendrites in neocortex$_{II,III}$ were also studied in control and laterally injured brains. In control brains, the proximal basilar dendrites of neocortex$_{II,III}$ pyramidals (n=13) displayed 1.07 ± 0.04 spines/μm; a similar value has been reported previously [192]. This spine density included 0.65 ± 0.03 pedunculated spines/μm and 0.43 ± 0.02 non-pedunculated spines/μm. Following LFPI, the spine density of these dendrites did not differ significantly from controls ($p > 0.05$). However, basilar spine density did change significantly across time points after LFPI, as summarized below. Micrographs of representative dendrites from ipsilateral neocortex$_{II,III}$ are also provided (Supplementary Figure 1).

From 1hr to 24hr post-LFPI in ipsilateral neocortex$_{II,III}$ the total spine density of basilar dendrites decreased by 27% (1hr post-LFPI *vs*. 24hr post-LFPI, $p < 0.001$; Figure 5a). Further analysis revealed an underlying, 35% decrease in pedunculated spine density (1hr post-LFPI *vs*. 24hr post-LFPI, $p < 0.01$; Figure 5b) but no change in non-pedunculated spine density (1hr post-LFPI *vs*. 24hr post-LFPI, $p > 0.05$; Figure 5c), across these time points. In the contralateral hemisphere, a similar pattern was observed. From 1hr to 24hr post-LFPI in contralateral neocortex$_{II,III}$, basilar dendrites

showed a 26% decrease in pedunculated spine density (1hr post-LFPI *vs*. 24hr post-LFPI, $p < 0.001$; Figure 5b) while non-pedunculated spine density was relatively unchanged (*vs*. control, $p > 0.05$; Figure 5c). Thus, the data demonstrate that from 1hr to 24hr post-LFPI basilar dendrites undergo a selective loss of pedunculated spine density in the bilateral neocortex$_{II,III}$.

The decrease in basilar spine density was followed by an increase. From 24hr to 1wk post-LFPI, basilar spine density increased by 35% in the ipsilateral neocortex$_{II,III}$ and by 26% in the contralateral neocortex$_{II,III}$ (24hr post-LFPI *vs*. 1wk post-LFPI, $p < 0.01$; Figure 5a). Again, the underlying change was in pedunculated spine density, which increased by 46% in the ipsilateral neocortex$_{II,III}$ and by 32% in the contralateral neocortex$_{II,III}$ across these time points (24hr post-LFPI *vs*. 1wk post-LFPI, $p < 0.001$ and $p < 0.01$, respectively; Figure 5b). The non-pedunculated spine density of basilar dendrites did not change from 24hr to 1wk post-LFPI, however, but did increase significantly from 1hr to 1wk post-LFPI in the contralateral neocortex$_{II,III}$ (1hr post-LFPI *vs*. 1wk post-LFPI, $p < 0.05$; Figure 5c). The data suggest extensive remodeling of basilar dendritic structure in the bilateral neocortex$_{II,III}$ during recovery from LFPI.

On apical dendrites in hippocampal CA1, lateral fluid percussion injury caused a delayed increase in spine density

CA1 pyramidal cells have proximal dendrites which form spine synapses primarily with Shaffer collateral and commissural axons [194]. In the rat brain, these synapses occur throughout the proximal apical and basilar dendritic arbors of CA1 pyramidal cells [194]. We investigated the effect of TBI on the spine density of these

dendrites, beginning with the apical dendrites. In control brains, the proximal apical dendrites of CA1 pyramidals (n=15) exhibited 1.56 ± 0.08 dendritic spines/μm, consistent with previously published studies [195,196]. This spine density consisted of 0.83 ± 0.04 pedunculated spines/μm and 0.52 ± 0.05 non-pedunculated spines/μm. Similar to dendrites in neocortex$_{II,III}$, apical dendritic spine density was not affected at 1hr post-LFPI, in either hemisphere of CA1 (*vs*. control, $p > 0.05$; Figure 6a-c). Nor was there any appreciable change in spine density by 24hr post-LFPI (*vs*. control, $p > 0.05$; Figure 6a-c), in contrast to what was observed in neocortex$_{II,III}$. However, there was a delayed increase in the spine density of CA1 apical dendrites, as described below. Micrographs of representative dendrites from ipsilateral CA1 are provided as a supplementary figure (Supplementary Figure 2).

By 1wk post-LFPI, the spine density of proximal apical dendrites increased dramatically in both hemispheres of CA1. In ipsilateral CA1, for instance, the spine density of these dendrites rose by 32% relative to controls (*vs*. control, $p < 0.001$; Figure 4a). Further analysis revealed underlying changes in pedunculated and non-pedunculated spine density, which increased by 31% and 33% respectively, compared to controls (*vs*. control, $p < 0.001$ and 0.01, respectively; Figure 6b,c). Meanwhile, in the contralateral CA1, spine density increased by 22% relative to controls (*vs*. control, $p < 0.05$; Figure 6a), though pedunculated and non-pedunculated spine density did not differ significantly from that of controls (each *vs*. control, $p > 0.05$; Figure 6b,c). Overall, the data indicate that LFPI causes a delayed, but substantial increase in the spine density of proximal apical dendrites in bilateral CA1. These changes are consistent with an increased density of excitatory synapses on CA1 dendrites, *e.g.*, reactive

synaptogenesis [197,198], and so could have considerable implications for hippocampal circuitry in the injured brain.

On basilar dendrites in hippocampal CA1, lateral fluid percussion injury caused a delayed increase in spine density

Proximal basilar dendrites of CA1 pyramidals were also examined. In control brains, the proximal basilar dendrites of CA1 pyramidals (n=12) exhibited 1.48 ± 0.11 spines/μm, similar to previously published data [196]. This total spine density included 0.92 ± 0.08 pedunculated spines/μm and 0.56 ± 0.04 non-pedunculated spines/μm. As with CA1 apical dendrites, the spine density of CA1 basilar dendrites at 1hr or 24hr post-LFPI did not differ significantly from that of controls (ipsilateral or contralateral *vs*. control, $p > 0.05$; Figure 7a-c).

By 1wk post-LFPI however, basilar dendrites in both hemispheres of CA1 showed significant increases in spine density. In ipsilateral CA1 for example, spine density increased 23% relative to controls (1.82 ± 0.08 total spines/μm *vs.* control, $p < 0.01$; Figure 7a), though neither pedunculated nor non-pedunculated spine density at 1wk post-LFPI differed significantly from controls (each *vs*. control, $p > 0.05$; Figure 7b,c). However, the pedunculated spine density at this time point was increased when compared to earlier time points, by 33% relative to 1hr post-LFPI and by 49% relative to 24hr post-LFPI (1hr post-LFPI *vs*. 1wk post-LFPI, $p < 0.01$; 24hr post-LFPI *vs*. 1wk post-LFPI, $p < 0.001$; Figure 7b).

Meanwhile, in the contralateral CA1, a similar increase in spine density observed. Basilar dendrites in contralateral CA1 showed a 27% increase in total spine density (*vs*.

control, $p < 0.05$; Figure 7a), apparently driven by a 25% rise in pedunculated spine density (*vs.* control, $p < 0.05$; Figure 7b). Therefore, the data indicate that LFPI causes a delayed, but significant increase in basilar dendritic spine density bilaterally in CA1. As with the apical dendrites in CA1, this increase in spine density could signify the formation of novel excitatory circuits in the injured brain.

On apical dendrites in hippocampal CA3, lateral fluid percussion injury caused a delayed increase in spine density

Pyramidal cells of hippocampal CA3 form synapses with associational and commissural fibers on dendritic spines throughout their proximal apical and basilar arbors [194]. To understand the effect of LFPI on these spines, we compared apical dendritic spine density between control and laterally injured brains. In control brains, the proximal apical dendrites of CA3 pyramidals (n=10) averaged 1.24 ± 0.11 dendritic spines/μm, comprising 0.72 ± 0.08 pedunculated spines/μm and 0.52 ± 0.04 non-pedunculated spines/μm. Similar to what was observed in CA1, apical dendritic spine density at 1hr or 24hr post-LFPI did not differ significantly from that of controls, in either hemisphere of CA3 (*vs*. control, $p > 0.05$; Figure 8a-c).

As was also observed in CA1, however, LFPI caused a delayed increase in the spine density of apical CA3 dendrites. By 1wk post-LFPI in ipsilateral CA3, for instance, spine density increased 31% relative to controls (*vs*. control, $p < 0.01$; Figure 8a). Further analysis revealed an underlying, 33% increase in pedunculated spine density (*vs.* control, $p < 0.05$; Figure 8b) but no significant change in non-pedunculated spine density (*vs.* control, $p > 0.05$; Figure 8c), relative to controls. However, unlike what was

observed in CA1, the effect appeared to be limited to the ipsilateral hemisphere: in the contralateral CA3, spine density at 1wk post-LFPI did not differ significantly from that of controls (*vs*. control, $p > 0.05$; Figure 8a-c) though pedunculated spine density had increased 44% relative to the 24hr post-LFPI time point (24hr post-LFPI *vs*. 1wk post-LFPI, $p < 0.05$; Figure 8b). Therefore, LFPI caused a delayed increase in the spine density of CA3 apical dendrites, and to a greater extent in the ipsilateral hemisphere. As with the neocortex and CA1, this increase in spine density could have substantial implications for the excitatory circuitry of the injured forebrain.

On basilar dendrites in hippocampal CA3, lateral fluid percussion injury caused a delayed increase in spine density

Basilar dendrites of CA3 pyramidal cells were also examined in control and laterally injured brains. In control brains, the proximal basilar dendrites of CA3 pyramidals (n=12) exhibited 1.28 ± 0.09 dendritic spines/μm, which consisted of 0.73 ± 0.05 pedunculated spines/μm and 0.55 ± 0.04 non-pedunculated spines/μm. Consistent with the apical dendrites in this region, the spine density of basilar dendrites at 1hr or 24hr post-LFPI did not differ significantly from that of controls, in either hemisphere of CA3 (*vs*. control, $p > 0.05$; Figure 9a-c). However, these dendrites also showed a delayed increase in spine density, as described below. Micrographs of representative dendrites from ipsilateral CA3 are provided as a supplementary figure (Supplementary Figure 3).

By 1wk post-LFPI, the spine density of CA3 basilar dendrites increased significantly above control levels in both hemispheres. In the ipsilateral CA3, for

example, these dendrites showed a 34% increase in total spine density, driven by a 41% increase in pedunculated spine density (each *vs*. control, $p < 0.01$; Figure 9b). While non-pedunculated spine density at 1wk post-LFPI did not change significantly relative to controls, it did increase by 66% from 1hr post-LFPI and by 27% from 24hr post-LFPI (1hr post-LFPI *vs*. 1wk post-LFPI, $p < 0.001$; 24hr post-LFPI *vs*. 1wk post-LFPI, $p < 0.05$; Figure 9c). Meanwhile, in the contralateral CA3, similar changes in spine density were observed: total spine density increased by 25%, driven by a 36% increase in pedunculated spine density, compared to controls (*vs*. control, $p < 0.05$ and $p < 0.01$, respectively; Figure 9b).

In general, the data indicate that LFPI caused a delayed increase in basilar spine density in both hemispheres of CA3. As with $neocortex_{II,III}$ and CA1, this increase in spine density could indicate an increased density of excitatory synapses and therefore have considerable implications for hippocampal circuitry in the injured brain.

On dentate granule cell dendrites, lateral fluid percussion injury caused an acute decrease and a delayed increase in spine density

Granule cells, the principal cells of the dentate gyrus, receive mostly associational and commissural synapses on spines of their proximal dendrites [194]. The spine density of these dendrites in the dorsal dentate gyrus (dDG) was compared between control and laterally injured brains. In control brains, the proximal dendrites of dDG granule cells (n=27) displayed 1.43 ± 0.06 total spines/μm, as previously reported [199]. This spine density included 0.83 ± 0.04 pedunculated spines/μm and 0.60 ± 0.03 non-pedunculated spines/μm. At 1hr after LFPI, the spine density of these dendrites

was relatively unchanged in either hemisphere, relative to controls (*vs*. control, $p > 0.05$; Figure 10a-c). However, LFPI did cause a loss and subsequent gain of spine density in dDG at later time points, as described below. Micrographs of representative dendrites from ipsilateral dDG are provided as a supplementary figure (Supplementary Figure 4).

By 24hr post-LFPI, dDG showed a hemisphere-specific loss of spine density. Specifically, in the ipsilateral dDG, pedunculated spine density decreased 20% (*vs*. control, $p < 0.05$; Figure 10b) without any appreciable change in non-pedunculated spine density (*vs*. control, $p > 0.05$; Figure 10c), relative to controls. However, in the contralateral dDG, spine density at 24hr post-LFPI did not differ significantly from that of controls (*vs*. control, $p > 0.05$; Figure 10a-c).

As observed in neocortex$_{II/II}$, the loss of spine density in dDG was not permanent. In fact, by 1wk post-LFPI, spine density in the ipsilateral dDG had increased above control levels. In particular, total spine density increased 17% over control values (*vs*. control, $p < 0.05$; Figure 10a), apparently driven by an 18% rise in pedunculated spine density relative to controls (*vs*. control, $p < 0.05$; Figure 10b). While the non-pedunculated spine density of these dendrites did not change relative to controls (*vs*. control, $p > 0.05$; Figure 10c), it did increase 20% relative to the 1hr and 24hr post-LFPI time points (1hr post-LFPI *vs*. 1wk post-LFPI, $p < 0.05$; 24hr post-LFPI *vs*., 1wk post-LFPI; Figure 10c).

In the contralateral dDG, spine density also increased at 1wk post-LFPI, but only when compared to earlier post-LFPI time points. For example, total spine density in contralateral dDG increased 22% from 1hr post-LFPI and 23% from 24hr post-LFPI (1hr post-LFPI *vs*. 1wk post-LFPI, $p < 0.05$; 24hr post-LFPI *vs*. 1wk post-LFPI, $p < 0.05$;

Figure 10a). Likewise, pedunculated spine density in contralateral dDG increased 26% from 1hr post-LFPI and 43% from 24hr post-LFPI (1hr post-LFPI *vs*. 1wk post-LFPI, $p < 0.05$; 24hr post-LFPI *vs*. 1wk post-LFPI, $p < 0.001$; Figure 10b). However, non-pedunculated spine density at this time point did not differ significantly from controls nor from earlier post-LFPI time points (*vs*. control, 24hr post-LFPI, or 1hr post-LFPI; $p > 0.05$; Figure 10c). Overall, the data show that LFPI causes a delayed increase in the proximal dendritic spine density of granule cells in the ipsilateral dDG. This increase in spine density, like that observed in the other hippocampal subfields, may indicate substantial re-wiring of the hippocampus in response to lateral brain injury.

FK506 administration increased dendritic spine density in uninjured neocortex$_{II,III}$

In vivo imaging has revealed a daily turnover in dendritic spine populations of the adult rodent brain [200,201]. If this turnover of dendritic spines is mediated by CaN, then inhibiting CaN could increase the density of dendritic spines. To test this hypothesis and reduce a potential confound to the present study, uninjured subjects were administered the calcineurin inhibitor, FK506 (5mg/kg; i.p.) and their brains were recovered 2hr or 23hr later for Golgi-Cox analysis of spine density. The mean spine densities and ratio$_{P:N}$ are provided in Table 1.

FK506 administration caused significant increases in the pedunculated spine density of basilar dendrites in neocortex$_{II,III}$, relative to drug-naïve controls. Specifically, at 2hr post-injection, the pedunculated spine density of these dendrites increased 29% relative to drug-naïve controls (*vs*. drug-naïve control, $p < 0.05$; Figure 11b). This increase appeared to persist for many hours. By 23hr post-injection, pedunculated spine

density was increased 31% relative to drug-naïve controls, driving a significant 29% increase in the total spine density, relative to drug-naïve controls (*vs*. drug-naïve control, $p < 0.001$ and $p < 0.01$, respectively; Figure 11a,b). A similar effect was recently reported in adult mice given daily doses of FK506 [202], and another study found that CaN inhibition increases synaptogenesis [203]. However, these findings are beyond the scope of the present study. Still, to avoid a potential confound to our study, FK506-treated, injured subjects were compared only to FK506-treated, uninjured subjects.

FK506 administration prevented the loss of dendritic spine density at 24hr post-injury

CaN activity has been implicated in the injury-induced loss of dendritic spine density *in vitro* [11] and *in vivo* [118,204]. To determine whether CaN activity could explain the loss of spine density at 24hr post-LFPI, some experimental subjects (n=3) were administered the CaN inhibitor, FK506 (5mg/kg; i.p) 1hr after LFPI. The timing of this injection was based on evidence that CaN activity increases within hours of LFPI [186]. Furthermore, this dosage of FK506 has been shown to block dendritic spine loss in a different *in vivo* model of brain injury [118]. Brains of FK506-treated subjects were harvested 24hr after LFPI and subjected to Golgi-Cox histochemistry. Some uninjured subjects (n=3) were used as drug controls and received a single injection of FK506 (5mg/kg; i.p.) 23hr prior to sacrifice.

A single, post-injury injection of FK506 completely blocked the decreases in spine density otherwise observed at 24hr post-LFPI. Indeed, spine density was not statistically different between uninjured and injured subjects treated with FK506, in any region examined, on either apical or basilar dendrites (each *vs*. control, $p > 0.05$; Figure

12). This means that FK506 preserved spine density in those regions which otherwise lost roughly 20% of their spine density at this time point (*i.e.*, ipsilateral neocortex$_{II,III}$ and dDG). The data thus strongly suggest that CaN activity is necessary for the loss of spine density at 24hr post-LFPI.

DISCUSSION

This study demonstrates that LFPI can cause significant changes in dendritic spine density and that these changes are time- and brain region-specific. One major finding is that LFPI caused a loss of spine density on proximal dendrites in ipsilateral neocortex$_{II,III}$ and dDG. This loss of spine density was prevented by administration of FK506, a pharmacological inhibitor of CaN, which represents a second major finding in this study. Indeed, a single, post-injury dose of FK506 preserved spine density at 24hr post-LFPI. A third major finding is that LFPI causes a delayed, regional increases in spine density in both hemispheres of rat hippocampus, which is consistent with reactive synaptogenesis (*e.g.*, [197,198]). Specifically, within 1wk of LFPI, spine density increased in CA1 and CA3 bilaterally, and in dDG ipsilaterally. The implications of each of these major findings are considered below.

Lateral fluid percussion injury decreased spine density in neocortex and dentate gyrus

In theory, a reduction in dendritic spine density could be due to a loss of spines or to a lengthening of the dendrite. Though the latter possibility cannot be excluded by this study, it seems unlikely for three reasons: first, a shortening, rather than a lengthening, of pyramidal dendrites has been reported in a lateral TBI model [205];

second, *in vitro* imaging of developing neurons suggests that dendrites grow from the terminal tip or branch point [206], which would not affect the medial portion that we sampled for spine density; third, our data indicate that LFPI differentially affects pedunculated and non-pedunculated spine densities. For these reasons, a loss of spines most likely explains the reduction in spine density we observed. Interestingly, this spine loss corresponds in time, region, and magnitude with a loss of synaptic proteins reported in a different TBI model [207]. Taken together, these findings suggest that lateral TBI causes synapse degeneration near the site of focal injury.

Interestingly, the apparent loss of pedunculated spines we observed at 24hr post-LFPI occurred independent of any change in non-pedunculated spine density. There are a number of possible explanations for this phenotype-specific effect. One possibility relates to the mechanism of spine loss: if an excess (or lack) of synaptic activity caused the spine loss, only spines with synapses would be directly affected. Since the pedunculated phenotype is typical of synapse-bearing spines [193], this can explain why only pedunculated spines were lost after LFPI.

An alternative explanation is that both spine populations decrease after LFPI, but only non-pedunculated spines are replenished by 24hr post-LFPI. Non-pedunculated spines could replenish in response to a decrease in synaptic activity after LFPI. Indeed, immature spines are formed in response to a pharmacological blockade of synaptic transmission in the hippocampus *in vitro* [208]; a similar effect could occur with a reduction in synaptic transmission, or with a loss of synapses, *e.g.*, the 60% loss that occurs within days of lateral cortical contusion [209].

A third possibility is that LFPI causes some pedunculated spines to shrink and assume a non-pedunculated morphology. Shrinkage of pedunculated spines could mask a loss of non-pedunculated spines. Indeed, spine shrinkage is associated with activation of the actin binding protein, cofilin [23]. Our companion study [186] reports that cofilin activation in the neocortex and hippocampus coincides with the spine loss we observed. For these reasons, spine shrinkage could explain why only pedunculated spines appeared to be affected by LFPI. Future studies using *in vivo* imaging and transgenic techniques are needed to better characterize the fate of pedunculated and non-pedunculated spines in this brain injury model.

Further study is also needed to determine whether the spine loss we observed corresponds to a loss of synapses. Studies in which cultured neurons were exposed to glutamate receptor agonists [11,88] or cold [97] suggest that collapsed dendritic spines can maintain synaptic contacts. However, other *in vitro* studies show that spine collapse can disrupt synapses: in hippocampal slices, excessive synaptic activity leads to an FK506-sensitive upregulation of Snk (serum-inducible kinase), resulting in proteolysis of the spine stabilizing protein, SPAR (spine-associated Rap guanosine triphosphatase activating protein) [12]. This Snk-SPAR pathway leads to spine loss as well as reductions in miniature post-synaptic potentials and in the immunoreactivity of the critical post-synaptic protein, PSD-95 [12,145]. Interestingly, the Snk-SPAR pathway primarily affects pedunculated spines on proximal dendrites [12] and requires hours to develop [142,210]. These *in vitro* findings are therefore consistent with our observation that spine loss occurred on proximal dendrites and can explain the delay in the onset of spine loss after brain injury. Furthermore, our companion study found a slight loss of

SPAR immunoreactivity in the ipsilateral hippocampus at 18hr post-LFPI [186]. This finding raises the possibility that SPAR proteolysis can explain the spine loss observed by the present study in the ipsilateral dentate gyrus. Therefore, the potential role of this FK506-sensitive signaling pathway in TBI-induced spine loss is an intriguing topic for further study.

Pharmacological inhibition of calcineurin prevented the decrease in spine density at 24hr post-injury

CaN is a calcium-stimulated phosphatase which mediates functional and structural plasticity on both sides of the synapse [23,114]. One mechanism by which CaN regulates post-synaptic structure involves the breakdown of the spine cytoskeleton. As demonstrated *in vitro*, CaN dephosphorylates and so activates Slingshot [131], a family of phosphatases which in turn activate proteins of the actin depolymerizing factor (ADF)/cofilin family (cofilin) [132]. Activated cofilin binds and breaks apart filaments of actin, enabling many forms of functional and structural plasticity in the neuron (for review, see [119]). For example, cofilin is responsible for the shrinkage of dendritic spines that accompanies the long-term depression of spine synapses [23].

Our companion study reports evidence that LFPI caused significant increases in cofilin activity [186]. In some cases, the cofilin activation observed in our companion study corresponds to spine loss observed in the present study. Specifically, our companion study reports that the ipsilateral neocortex and hippocampus each show increases in cofilin activity at 24hr post-LFPI (signified by decreases in the

phosphorylation of the cofilin serine 3 residue; [186]). At the same time point and in the same forebrain regions, the present study reports a significant loss of dendritic spines. These parallel findings raise the possibility that cofilin activation is responsible for spine loss after LFPI (but see also Discussion in [186]). Other brain injury models have also linked cofilin activation to spine loss [118,204,211].

Another parallel between the present study and its companion involves the CaN inhibitor, FK506. Our companion study found that a single, post-injury injection of FK506 blocked cofilin de-phosphorylation in the neocortex at 24hr post-LFPI [186]. At the same time point and in the same brain region, an identical treatment with FK506 prevented spine loss in the present study. Therefore, in the neocortex at least, the FK506-sensitive de-phosphorylation of cofilin corresponds to spine loss after LFPI. These findings agree with our previous research in a rat model of *status epilepticus*, in which FK506 treatment (5mg/kg) prevented cofilin de-phosphorylation and a coinciding loss of dendritic spines. Preventing spine loss in these different models of brain injury could maintain synaptic integrity and so reduce the risk of cognitive impairment and other sequelae. Therefore, these results emphasize the potential of CaN as a therapeutic target in treating brain injury.

Lateral fluid percussion injury caused a delayed overgrowth of dendritic spines in CA1, CA3, and dDG

Previously published studies do not predict an increase in dendritic spine density following lateral brain injury. For example, in a study by Schwarzbach and colleagues (2006), moderate (1.4-2.1atm) lateral fluid percussion injury had no effect on the apical

and basilar dendritic spine densities of mouse CA1 pyramidals at 1wk post-injury [195]. In addition, Scheff and colleagues (2005) found that lateral cortical contusion caused a loss of synapses in CA1 *stratum radiatum* which lasted at least 60 days post-injury [209]. Consequently, though using a different model of TBI, we were surprised to find an increase in the dendritic spine density of CA1 apical dendrites (as well as in other brain regions) at 1wk post-LFPI.

It is possible that the spine overgrowth we observed in CA1 occurred only on proximal dendrites. Unlike previously published studies, our study focused on second- or third-order dendrites within 30-150μm of the cell soma. Compared to distal dendrites, these proximal regions of CA1 pyramidal dendrites are less dense with synapses [212]. Proximal dendrites may therefore be a more accessible target for re-innervating axons following injury. Indeed, the apical dendritic field of CA1, the *stratum radiatum*, is re-innervated within a week or so of lateral cortical contusion in rat [209,213]. If re-innervating fibers connect with *de novo* dendritic spines, this could explain the increased spine density in CA1 at 1wk post-LFPI.

Delayed increases in spine density have also been associated with experimental denervation [214] and ischemia. Within days of ischemic injury, for example, CA1 apical dendrites show an increase in spine density [196,215]. Since moderate LFPI can depress cerebral blood flow [216], further investigation is needed to know whether there is a mechanistic relationship between spine overgrowth in the ischemia and LFPI models.

An overgrowth of dendritic spines may be a clue to understanding the altered electrophysiology of the hippocampus following lateral brain injury. An

electrophysiological study by Akasu and colleagues found an increase in the excitability of rat CA1 at 1wk after moderate LFPI (1.5-2.0atm) [217]. Other research suggests that this increased excitability is due to recurrent circuits formed by CA1 axon collaterals. Indeed, CA1 axons invade the *stratum radiatum* within weeks of epileptogenic brain injury in rat, and this corresponds to an increase in CA1 excitability [198]. It is likely that these CA1 axons form synapses on CA1 dendrites, since CA1 pyramidals become increasingly interconnected when brain injury leads to epilepsy [218]. Alternatively, the increased spine density in CA1 and CA3 may represent innervation by commissural or extra-hippocampal regions. In any case, further investigation is needed to determine whether reactive synaptogenesis can explain the spine overgrowth we observed. A better understanding of how the brain is re-wired after injury holds promise for the treatment of TBI-related pathologies such as cognitive impairment and post-traumatic epilepsy.

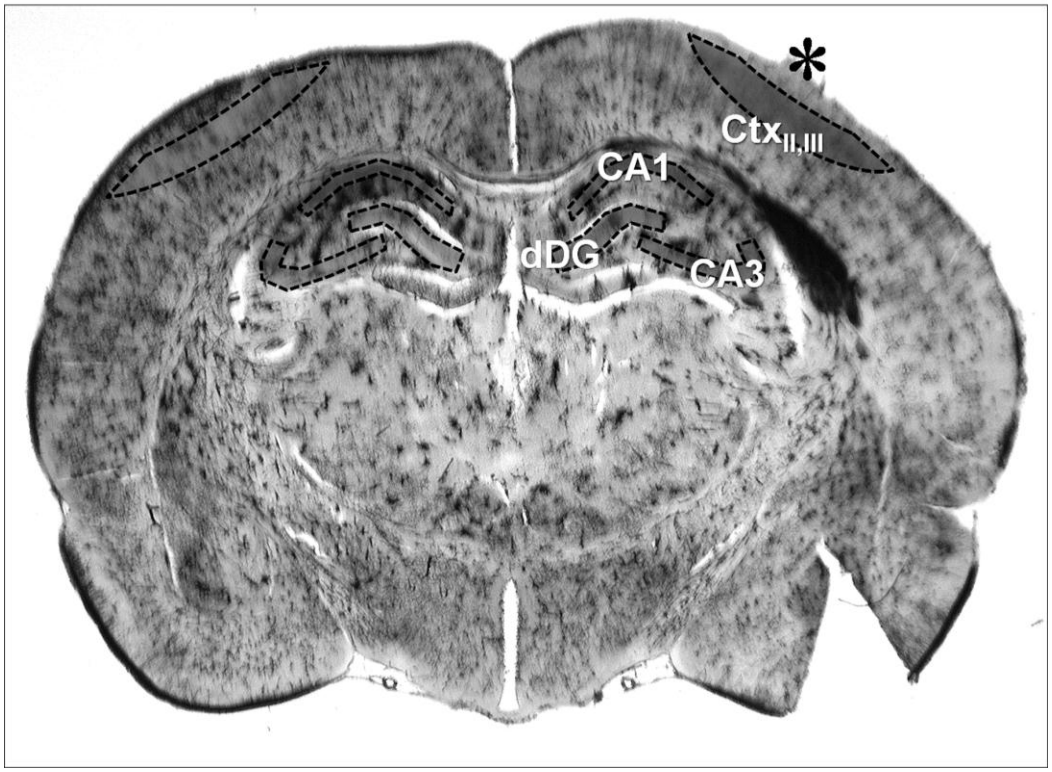

FIGURE 1 – **Forebrain regions sampled for dendritic spine density.** Shown is a micrograph of a Golgi-stained section of adult rat brain recovered 24hr after lateral fluid percussion injury of the left hemisphere. The approximate site of fluid percussion is indicated with an asterisk (*). Dendritic spine density was sampled in the shaded brain regions located ipsilateral and contralateral to the impact site, including layer II,III of the parietal neocortex ("Ctx"), the hippocampal subfields CA1 and CA3, and the dorsal leaf of the dentate gyrus ("dDG"). Analogous regions of uninjured brains were similarly assessed for spine density. Also visible in this image is where a wedge-shaped portion of ventral neocortex was excised prior to sectioning, to mark the ipsilateral hemisphere.

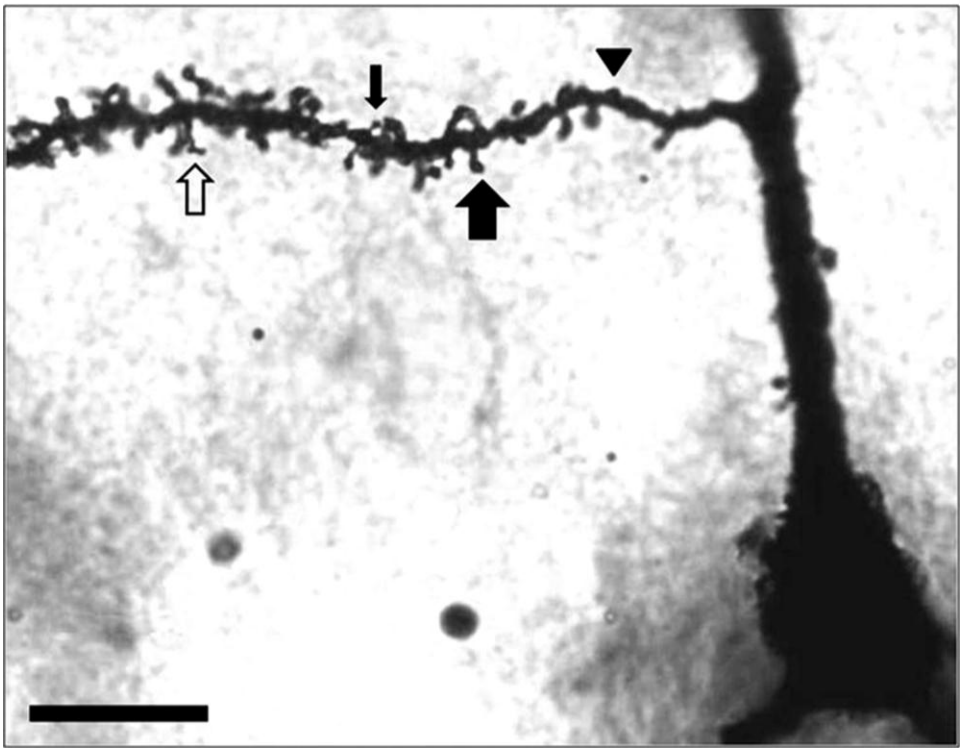

FIGURE 2 – **Dendritic spines on a Golgi-stained pyramidal neuron from layer II,III of rat neocortex**. A thin spine and a mushroom-shaped spine are marked, respectively, with a thin arrow and a thick arrow. A stubby spine and a filopodia-like spine are marked, respectively, with an arrowhead and a hollow arrow. Thin spines and mushroom-shaped spines were counted together as “pedunculated” spines, whereas stubby spines and filopodia-like spines were counted together as “non-pedunculated” spines. The arrowhead also approximates the minimum distance (30μm) from the cell soma beyond which dendrites were traced and spine density was sampled. Scale bar, 10μm.

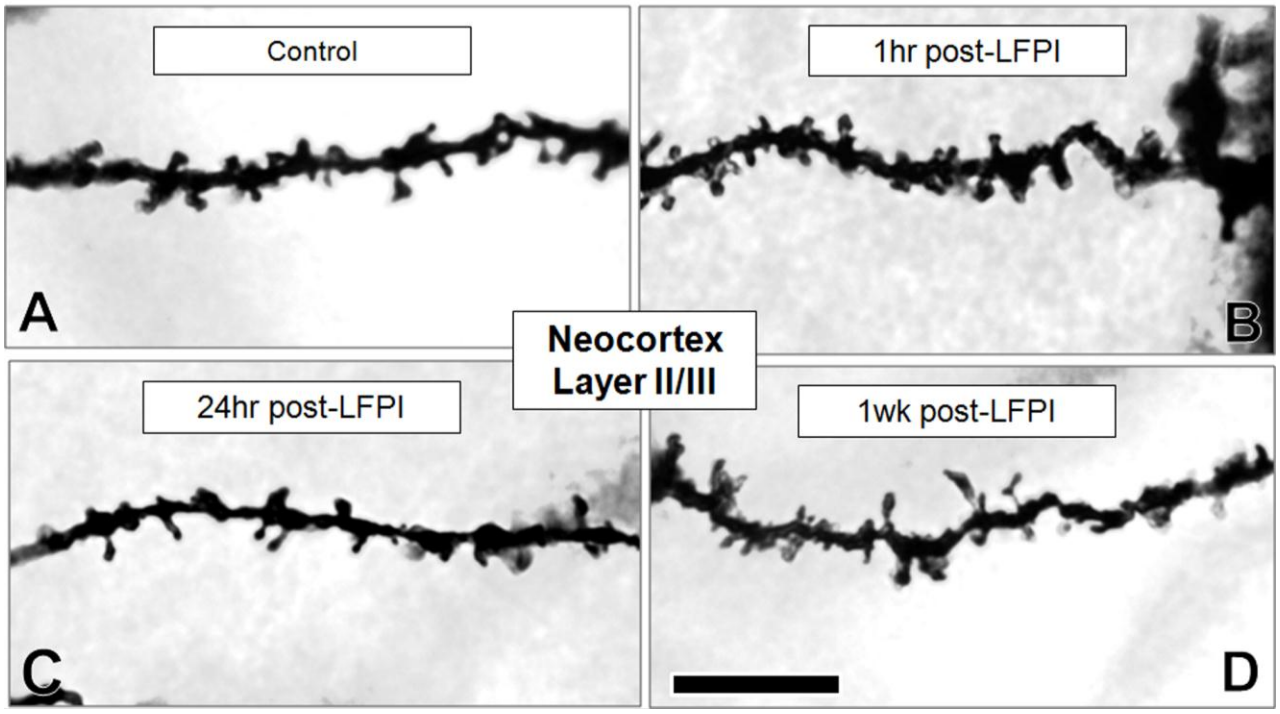

FIGURE 3 – **Representative apical dendrites from Golgi-stained pyramidal cells in layer II,III neocortex.** Shown are proximal dendrites (within 30-150μm of cell soma) from the apical arbors of Golgi-stained pyramidal cells in rat neocortex layer II,III. Panel A shows a control dendrite with 8.10 pedunculated spines/10μm (110% of group mean) and 4.05 non-pedunculated spines/10μm (88% of group mean). Panels B, C, and D show dendrites in the penumbral region of the focal injury. Panel B shows a dendrite at 1hr post-LFPI, with 7.09 pedunculated spines/10μm (102% of group mean) and 4.46 non-pedunculated spines/10μm (92% of group mean). Panel C shows a dendrite at 24hr post-LFPI, with 4.89 pedunculated spines/10μm (95% of group mean) and 4.14 non-pedunculated spines/10μm (98% of group mean). Panel D shows a dendrite at 1 week post-LFPI, with 8.05 pedunculated spines/10μm (119% of group mean) and 4.98 non-pedunculated spines/10μm (117% of group mean). Note that not all spines counted are in focus in these micrographs. Scale bar, 10μm.

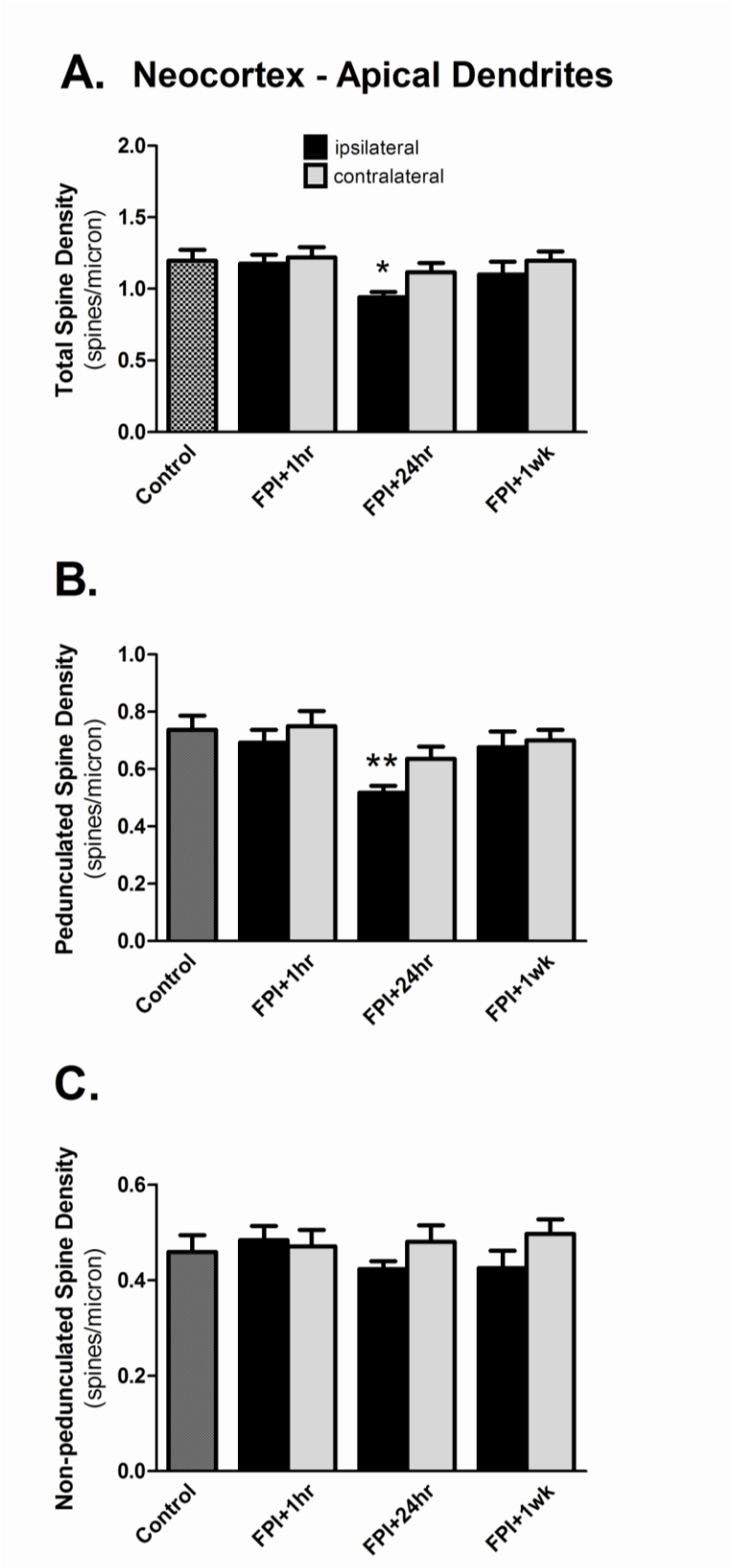
A. Neocortex - Apical Dendrites
ipsilateral
contralateral
Total Spine Density
(spines/micron)
2.0
1.5
1.0
0.5
0.0
*
Control
FPI+1hr
FPI+24hr
FPI+1wk
B.
Pedunculated Spine Density
(spines/micron)
1.0
0.8
0.6
0.4
0.2
0.0
**
Control
FPI+1hr
FPI+24hr
FPI+1wk
C.
Non-pedunculated Spine Density
(spines/micron)
0.6
0.4
0.2
0.0
Control
FPI+1hr
FPI+24hr
FPI+1wk

FIGURE 4 – On apical dendrites in neocortex$_{II,III}$, lateral fluid percussion injury caused a transient decrease in spine density. Rat brains were recovered 1hr, 24hr, or 1wk after moderate lateral fluid percussion injury, and subjected to Golgi-Cox histochemistry. Golgi-stained pyramidal neurons were selected at random from neocortex layer II,III ("neocortex$_{II,III}$"), either adjacent to the site of injury ("ipsilateral"; black bars) or in an analogous region of the contralateral hemisphere ("contralateral"; gray bars). The density of pedunculated spines (mushroom spines and thin spines) and the density of non-pedunculated spines (stubby spines and filopodia-like spines) were each quantified on traced segments of proximal apical dendrites ($n_{neurons} > 13$). In ipsilateral neocortex$_{II,III}$, apical dendritic spine density decreased significantly by 24hr post-LFPI, relative to controls (A). Further analysis revealed a phenotype-specific change in spine density, specifically, a decrease in the density of pedunculated spines (B) with no appreciable change in the density of non-pedunculated spines (C). Both total and pedunculated spine densities recovered by 1wk post-LFPI (A,B). Meanwhile, in contralateral neocortex$_{II,III}$, the spine density of apical dendrites did not differ significantly from that of controls, at any time point (B). * *vs*. control, $p < 0.05$; ** *vs*. control, $p < 0.01$

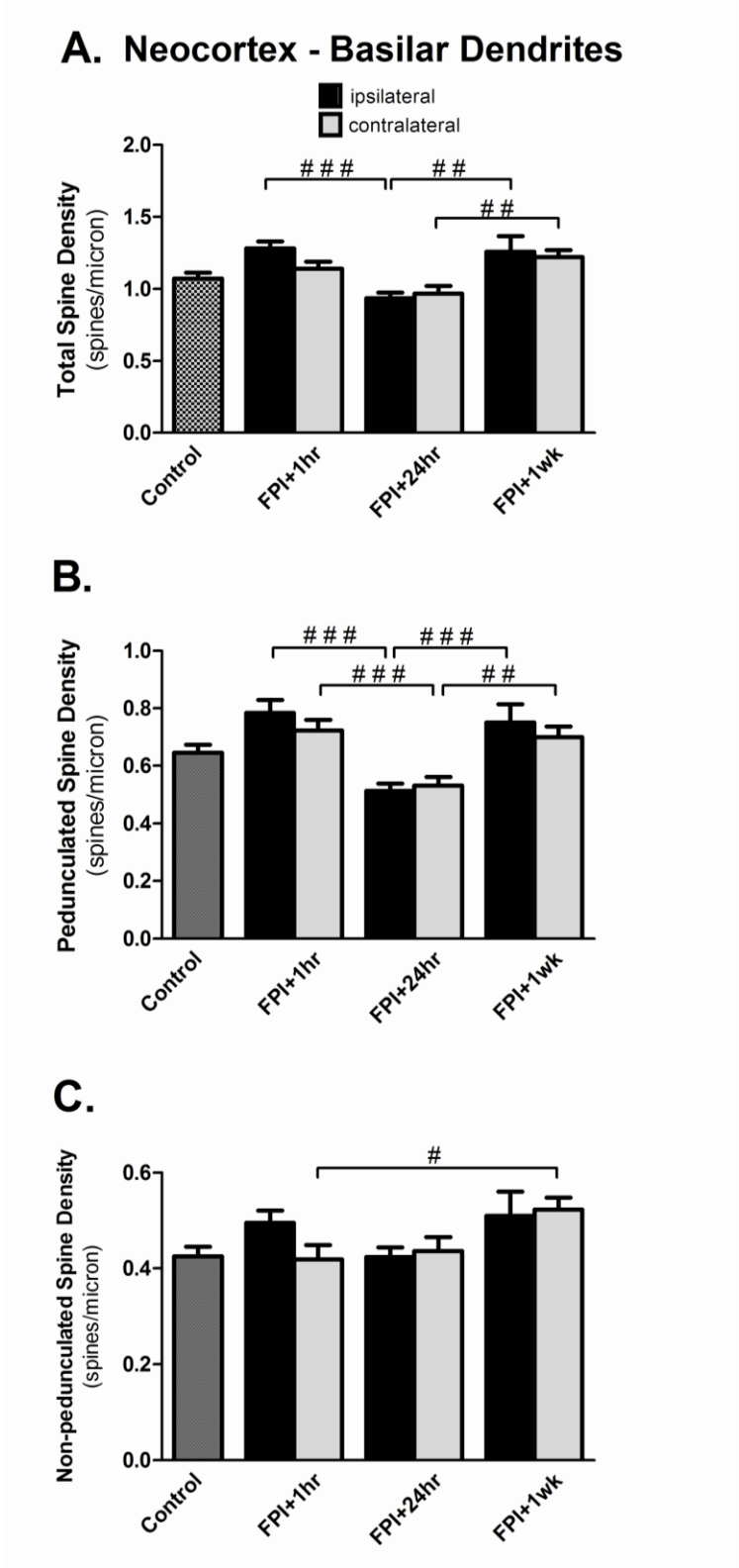
A. Neocortex - Basilar Dendrites
ipsilateral
contralateral
Total Spine Density
(spines/micron)
2.0
1.5
1.0
0.5
0.0
###
##
##
Control
FPI+1hr
FPI+24hr
FPI+1wk
B.
Pedunculated Spine Density
(spines/micron)
1.0
0.8
0.6
0.4
0.2
0.0
###
###
###
##
Control
FPI+1hr
FPI+24hr
FPI+1wk
C.
Non-pedunculated Spine Density
(spines/micron)
0.6
0.4
0.2
0.0
#
Control
FPI+1hr
FPI+24hr
FPI+1wk

FIGURE 5 – On basilar dendrites in neocortex$_{II,III}$, spine density fluctuated during recovery from lateral fluid percussion injury. Rat brains were recovered 1hr, 24hr, or 1wk after moderate lateral fluid percussion injury and stained using a Golgi-Cox procedure. Golgi-stained pyramidal neurons were selected at random from neocortex layer II,III ("neocortex$_{II,III}$") either adjacent to the site of injury ("ipsilateral"; black bars) or in an analogous region of the contralateral hemisphere ("contralateral"; gray bars). Pedunculated spine density (mushroom spines and thin spines) and non-pedunculated spine density (stubby spines and filopodia-like spines) were quantified on traced segments of proximal basilar dendrites ($n_{neurons} > 13$). The spine density of these dendrites did not change relative to controls, but showed significant changes across time points post-LFPI. For example, the total spine density of these dendrites decreased from 1hr to 24hr post-LFPI in ipsilateral neocortex$_{II,III}$, and increased from 24hr to 1wk post-LFPI in bilateral neocortex$_{II,III}$ (A). Further analysis revealed underlying changes in pedunculated spine density, which decreased from 1hr to 24hr post-LFPI and increased from 24hr to 1wk post-LFPI, in both hemispheres of neocortex$_{II,III}$ (B). However, there were no corresponding changes in non-pedunculated spine density, except an increase from 1hr to 1wk post-LFPI in the contralateral neocortex$_{II,III}$ (C). # *vs*. other bracketed group, $p < 0.05$; ## *vs*. other bracketed group, $p < 0.01$; ### *vs*. other bracketed group, $p < 0.001$

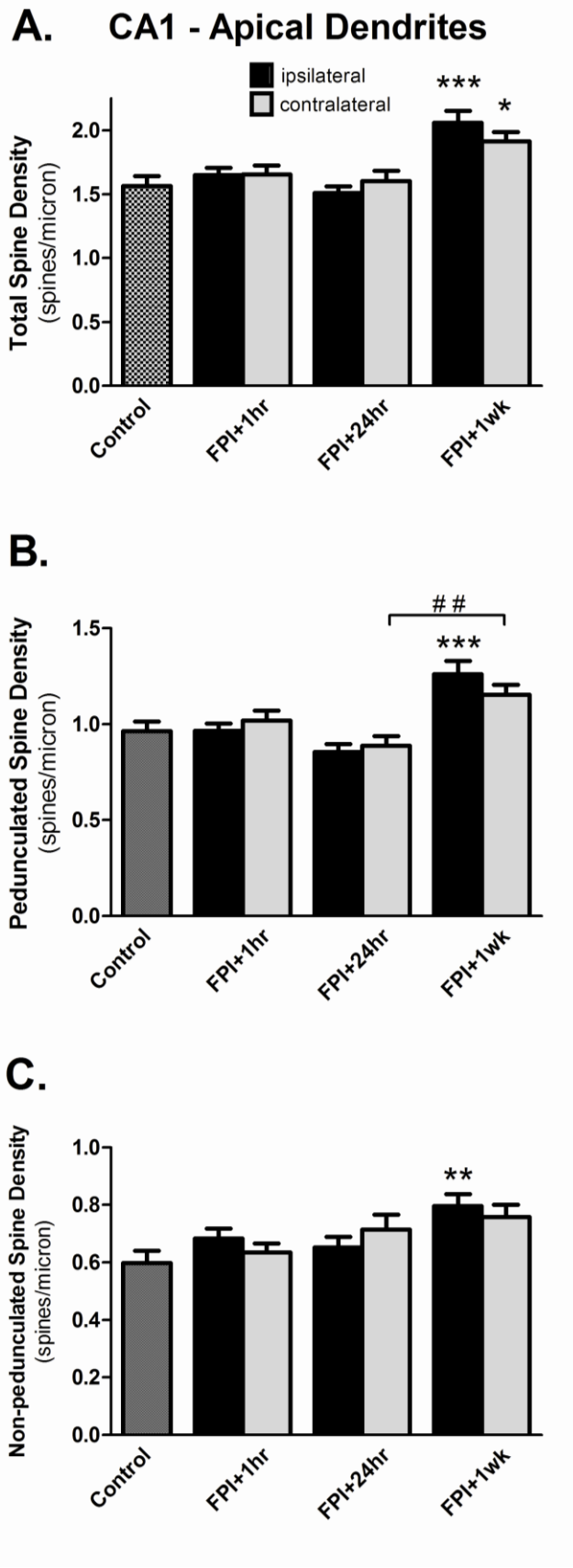
A.
CA1 - Apical Dendrites
ipsilateral
contralateral
***
*
Total Spine Density
(spines/micron)
2.0
1.5
1.0
0.5
0.0
Control
FPI+1hr
FPI+24hr
FPI+1wk
B.
##
***
Pedunculated Spine Density
(spines/micron)
1.5
1.0
0.5
0.0
Control
FPI+1hr
FPI+24hr
FPI+1wk
C.
**
Non-pedunculated Spine Density
(spines/micron)
1.0
0.8
0.6
0.4
0.2
0.0
Control
FPI+1hr
FPI+24hr
FPI+1wk

FIGURE 6 - On apical dendrites in hippocampal CA1, lateral fluid percussion injury caused a delayed increase in spine density. Rat brains were recovered 1hr, 24hr, or 1wk after moderate lateral fluid percussion injury and subjected to Golgi-Cox histochemistry. Golgi-stained pyramidal neurons were selected at random from ipsilateral CA1 (black bars) and from contralateral CA1 (gray bars). Pedunculated spine density (mushroom spines and thin spines) and non-pedunculated spine density (stubby spines and filopodia-like spines) were quantified on traced segments of proximal apical dendrites ($n_{neurons} > 13$). The total spine density of these dendrites increased significantly at 1wk post-LFPI relative to controls, in both hemispheres of CA1 (A). Pedunculated spine density increased significantly at 1wk post-LFPI relative to controls in ipsilateral CA1, and from 24hr to 1wk post-LFPI in contralateral CA1 (B). In addition, ipsilateral CA1 showed a corresponding increase in non-pedunculated spine density at 1wk post-LFPI (C). * *vs*. control, $p < 0.05$; ** *vs*. control, $p < 0.01$; *** *vs*. control, $p < 0.001$; ## *vs*. other bracketed group, $p < 0.01$

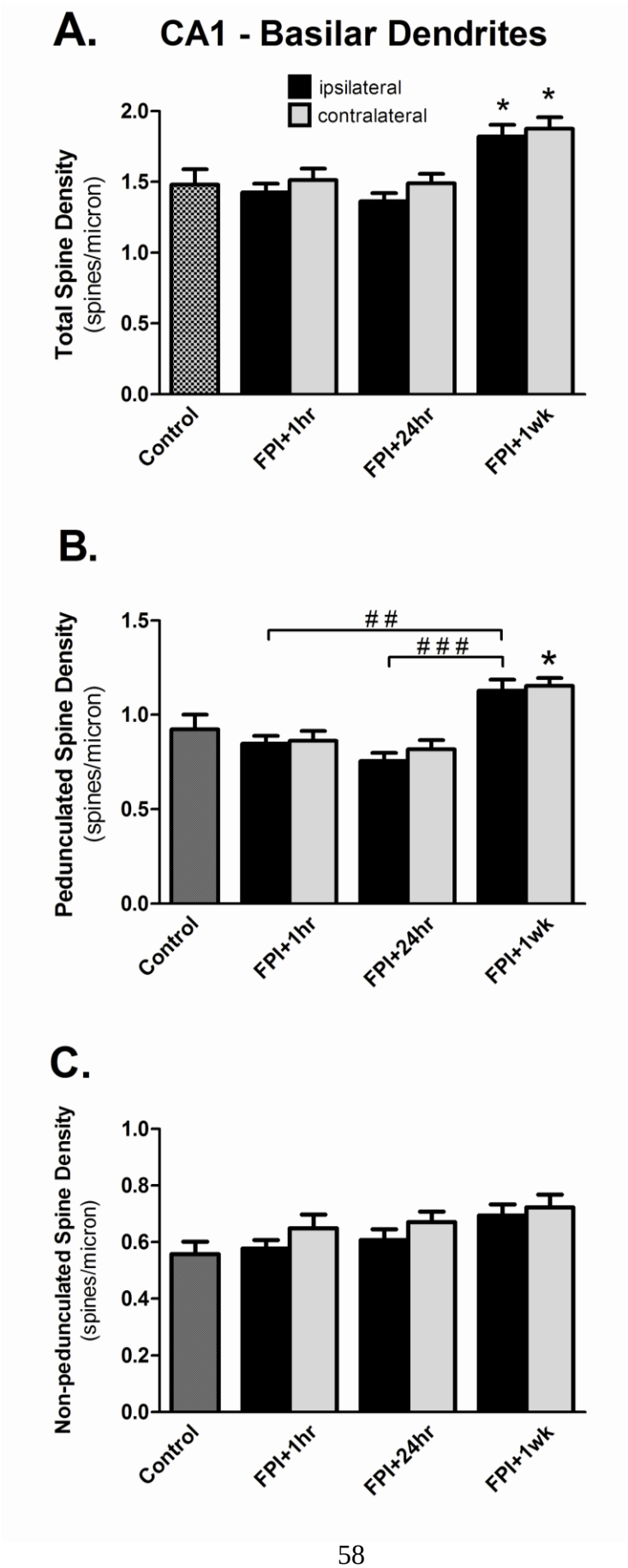
A.
CA1 - Basilar Dendrites
ipsilateral
contralateral
Total Spine Density
(spines/micron)
2.0
1.5
1.0
0.5
0.0
*
*
Control
FPI+1hr
FPI+24hr
FPI+1wk
B.
Pedunculated Spine Density
(spines/micron)
1.5
1.0
0.5
0.0
##
###
*
Control
FPI+1hr
FPI+24hr
FPI+1wk
C.
Non-pedunculated Spine Density
(spines/micron)
1.0
0.8
0.6
0.4
0.2
0.0
Control
FPI+1hr
FPI+24hr
FPI+1wk

FIGURE 7 – **On basilar dendrites in hippocampal CA1, lateral fluid percussion injury caused a delayed increase in spine density.** Rat brains were recovered 1hr, 24hr, or 1wk after moderate lateral fluid percussion injury and stained using a Golgi-Cox procedure. Golgi-stained pyramidal neurons were selected at random from ipsilateral CA1 (black bars) and from contralateral CA1 (gray bars). Pedunculated spine density (mushroom spines and thin spines) and non-pedunculated spine density (stubby spines and filopodia-like spines) were quantified on traced segments of proximal basilar dendrites ($n_{neurons} > 12$). The total spine density of these dendrites increased significantly at 1wk post-LFPI relative to controls, in both hemispheres of CA1 (A). Pedunculated spine density increased significantly from 1hr to 1wk post-LFPI and from 24hr to 1wk post-LFPI in ipsilateral CA1, and relative to controls in contralateral CA1 (B). However, there were no corresponding changes in the non-pedunculated spine density of these dendrites (C). * *vs*. control, $p < 0.05$; ## *vs*. other bracketed group, $p < 0.01$; ### *vs*. other bracketed group, $p < 0.001$

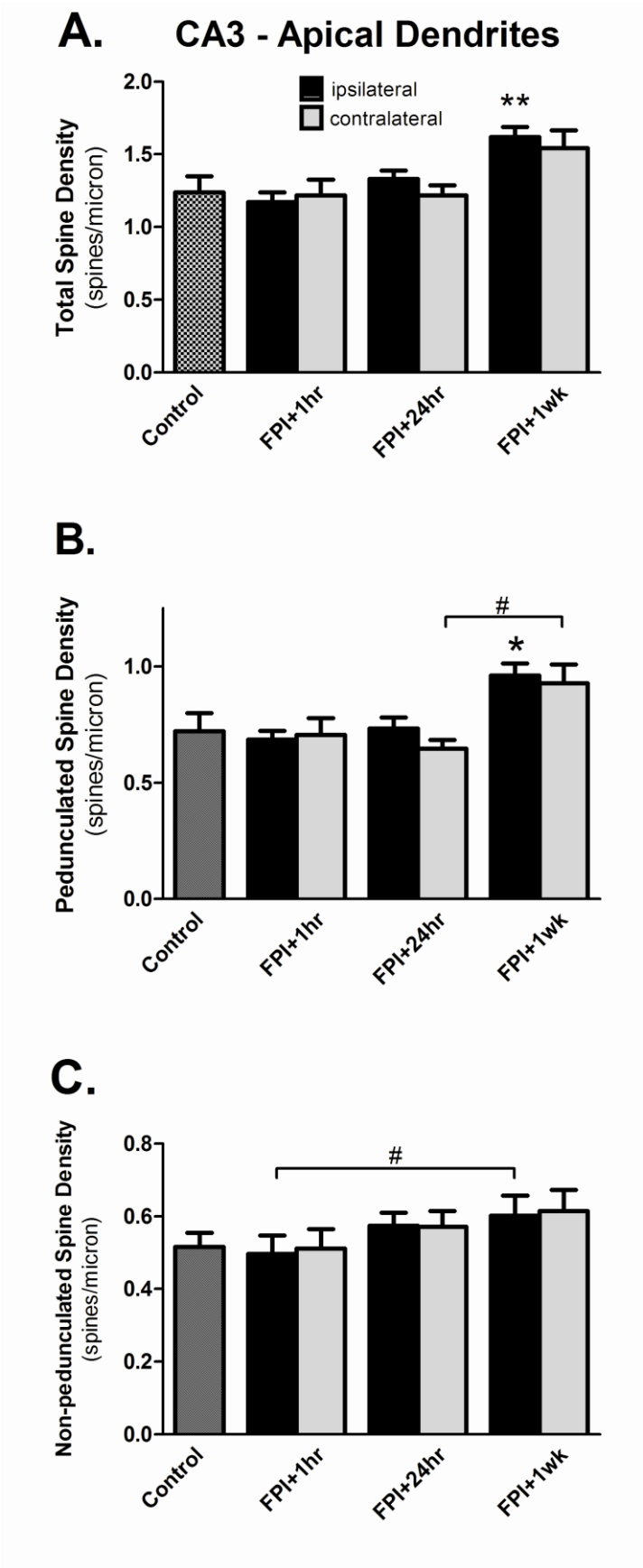
A.
CA3 - Apical Dendrites
ipsilateral
contralateral
**
Total Spine Density
(spines/micron)
2.0
1.5
1.0
0.5
0.0
Control
FPI+1hr
FPI+24hr
FPI+1wk
B.
#
*
Pedunculated Spine Density
(spines/micron)
1.0
0.5
0.0
Control
FPI+1hr
FPI+24hr
FPI+1wk
C.
#
Non-pedunculated Spine Density
(spines/micron)
0.8
0.6
0.4
0.2
0.0
Control
FPI+1hr
FPI+24hr
FPI+1wk

FIGURE 8 – **On apical dendrites in hippocampal CA3, lateral fluid percussion injury caused a delayed increase in spine density.** Rat brains were recovered 1hr, 24hr, or 1wk after moderate lateral fluid percussion injury and subjected to Golgi-Cox histochemistry. Golgi-stained pyramidal neurons were selected at random from ipsilateral CA3 (black bars) and from contralateral CA3 (gray bars). Pedunculated spine density (mushroom spines and thin spines) and non-pedunculated spine density (stubby spines and filopodia-like spines) were quantified on traced segments of proximal apical dendrites ($n_{neurons} > 10$). In ipsilateral CA3, the total spine density of these dendrites increased significantly at 1wk post-LFPI (A), driven by a rise in pedunculated spine density (B), relative to controls. In contrast, contralateral CA3 showed only an increase in pedunculated spine density from 24hr to 1wk post-LFPI (B). In terms of non-pedunculated spine density, the only significant change was an increase from 1hr to 1wk post-LFPI in ipsilateral CA3 (C). * *vs*. control, $p < 0.05$; ** *vs*. control, $p < 0.01$; # *vs*. other bracketed group, $p < 0.05$

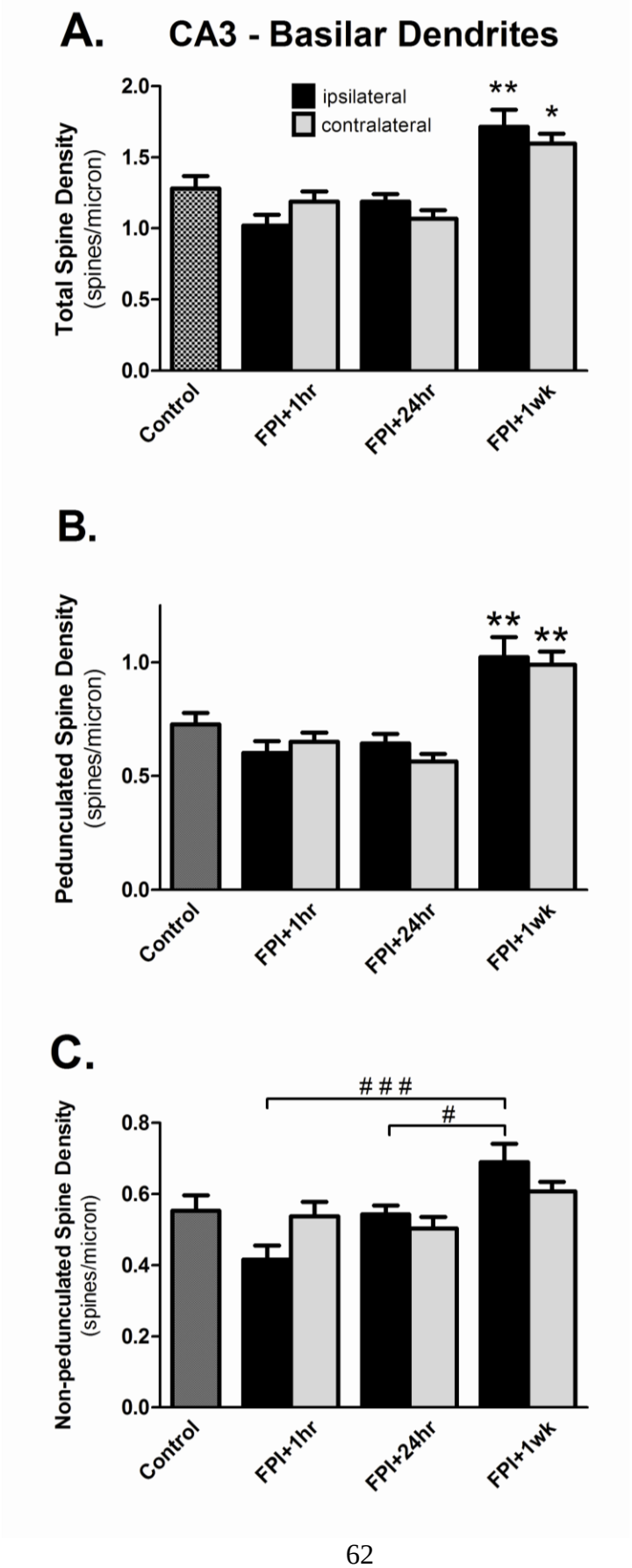
A.
CA3 - Basilar Dendrites
ipsilateral
contralateral
Total Spine Density
(spines/micron)
2.0
1.5
1.0
0.5
0.0
**
*
Control
FPI+1hr
FPI+24hr
FPI+1wk
B.
Pedunculated Spine Density
(spines/micron)
1.0
0.5
0.0
**
**
Control
FPI+1hr
FPI+24hr
FPI+1wk
C.
Non-pedunculated Spine Density
(spines/micron)
0.8
0.6
0.4
0.2
0.0
###
#
Control
FPI+1hr
FPI+24hr
FPI+1wk

FIGURE 9 – **On basilar dendrites in hippocampal CA3, lateral fluid percussion injury caused a delayed increase in spine density.** Rat brains were recovered 1hr, 24hr, or 1wk after moderate lateral fluid percussion injury and stained using a Golgi-Cox procedure. Golgi-stained pyramidal neurons were selected at random from ipsilateral CA3 (black bars) and from contralateral CA3 (gray bars). Pedunculated spine density (mushroom spines and thin spines) and non-pedunculated spine density (stubby spines and filopodia-like spines) were quantified on traced segments of proximal basilar dendrites ($n_{neurons} > 12$). The total spine density of these dendrites increased significantly by 1wk post-LFPI relative to controls, in both hemispheres of CA3 (A). Further analysis revealed underlying changes in pedunculated spine density, which increased significantly in both hemispheres of CA3 relative to controls (B). In contrast, non-pedunculated spine density did not change appreciably in either hemisphere of CA3 relative to controls, but did increase from 1hr to 1wk post-LFPI and from 1hr to 24hr post-LFPI in the ipsilateral CA3 (C). * *vs*. control, $p < 0.05$; ** *vs*. control, $p < 0.01$; # *vs*. other bracketed group, $p < 0.05$; ### *vs*. other bracketed group, $p < 0.001$

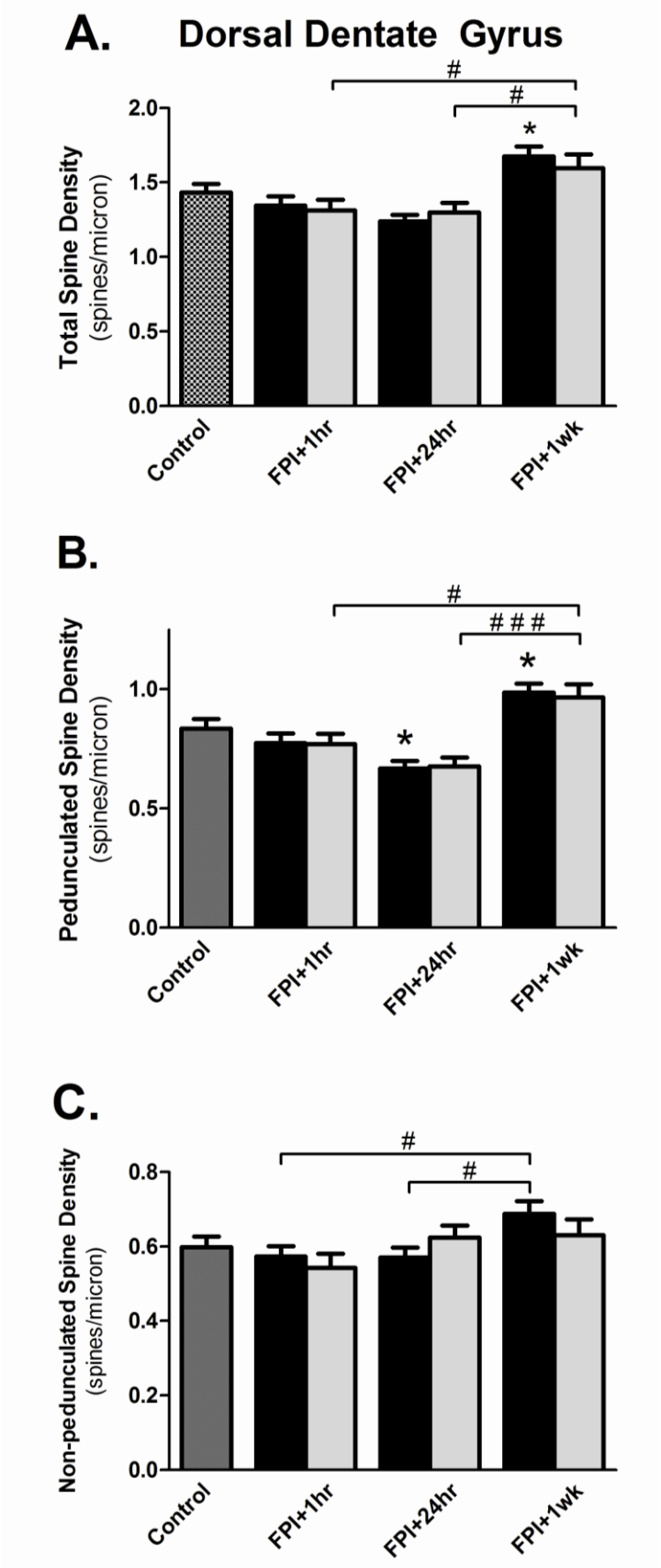
A.
Dorsal Dentate Gyrus
Total Spine Density
(spines/micron)
2.0
1.5
1.0
0.5
0.0
#
#
*
Control
FPI+1hr
FPI+24hr
FPI+1wk
B.
Pedunculated Spine Density
(spines/micron)
1.0
0.5
0.0
#
###
*
*
Control
FPI+1hr
FPI+24hr
FPI+1wk
C.
Non-pedunculated Spine Density
(spines/micron)
0.8
0.6
0.4
0.2
0.0
#
#
Control
FPI+1hr
FPI+24hr
FPI+1wk

FIGURE 10 – On dentate granule cell dendrites, lateral fluid percussion injury caused an acute decrease and a delayed increase in spine density. Rat brains were recovered 1hr, 24hr, or 1wk after moderate lateral fluid percussion injury and subjected to Golgi-Cox histochemistry. Golgi-stained granule cells were selected at random from the dorsal leaf of the dentate gyrus (dDG) in the ipsilateral (black bars) and the contralateral (gray bars) hemispheres. Pedunculated spine density (mushroom spines and thin spines) and non-pedunculated spine density (stubby spines and filopodia-like spines) were quantified on traced segments of proximal dendrites ($n_{neurons}$ > 12). The total spine density of these dendrites increased by 1wk post-LFPI relative to controls in ipsilateral dDG, as well as from 1hr to 1wk and from 24hr to 1wk in the contralateral dDG (A). In terms of pedunculated spine density, ipsilateral dDG showed a significant decrease at 24hr post-LFPI and a significant increase at 1wk post-LFPI, whereas contralateral dDG showed an increase from 1hr to 1wk post-LFPI and from 24hr to 1wk post-LFPI (B). The non-pedunculated spine density of these dendrites only changed appreciably in the ipsilateral dDG, where an increase was observed from 1hr to 1wk post-LFPI and from 24hr to 1wk post-LFPI (C). * *vs*. control, $p < 0.05$; # *vs*. other bracketed group, $p < 0.05$; ### *vs*. other bracketed group, $p < 0.001$

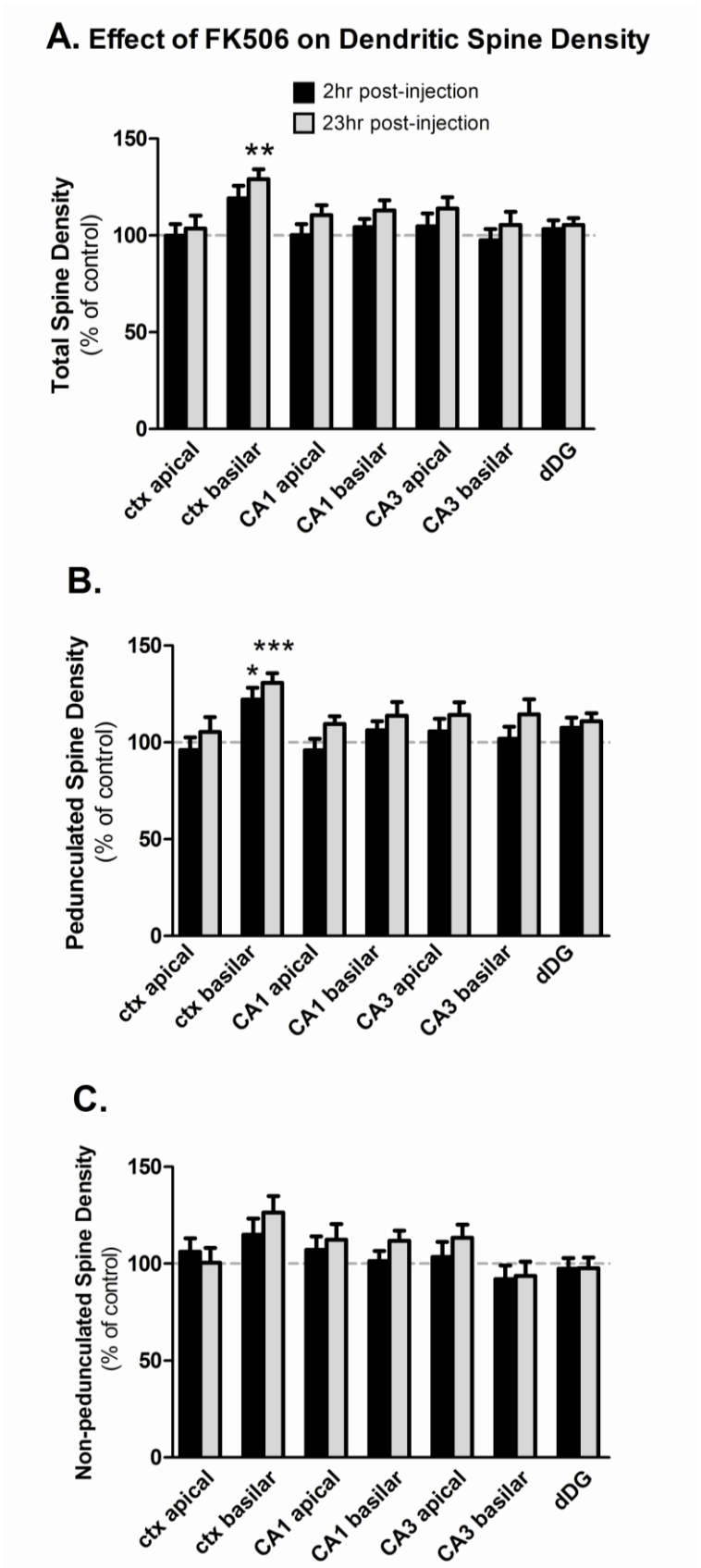
A. Effect of FK506 on Dendritic Spine Density
2hr post-injection
23hr post-injection
Total Spine Density
(% of control)
150
100
50
0
**
ctx apical
ctx basilar
CA1 apical
CA1 basilar
CA3 apical
CA3 basilar
dDG
B.
Pedunculated Spine Density
(% of control)
150
100
50
0
***
*
ctx apical
ctx basilar
CA1 apical
CA1 basilar
CA3 apical
CA3 basilar
dDG
C.
Non-pedunculated Spine Density
(% of control)
150
100
50
0
ctx apical
ctx basilar
CA1 apical
CA1 basilar
CA3 apical
CA3 basilar
dDG

FIGURE 11 – FK506 administration increased dendritic spine density in uninjured neocortex$_{II,III}$. Rat brains were recovered 2hr (black bars) or 23hr (gray bars) after FK506 administration (5mg/kg; i.p.), and subjected to Golgi-Cox histochemistry. Golgi-stained principal cells were selected at random and bilaterally from the following forebrain regions: neocortex$_{II,III}$, hippocampus CA1, hippocampal CA3, and the dorsal leaf of the dentate gyrus (*n* values are given in Table 1). Pedunculated spine density and non-pedunculated spine density were quantified on traced segments of proximal dendrites. By 2hr post-injection, FK506 administration did not significantly affect the total spine density of these dendrites (A) but caused a significant increase in the pedunculated spine density of basilar dendrites in neocortex$_{II,III}$ relative to controls (B). By 23hr post-injection, both the total spine density (A) and pedunculated spine density (B) of basilar dendrites in neocortex$_{II,III}$ were increased significantly relative to controls. ** *vs*. control, $p < 0.05$; ** *vs*. control, $p < 0.01$; *** *vs*. control, $p < 0.001$;

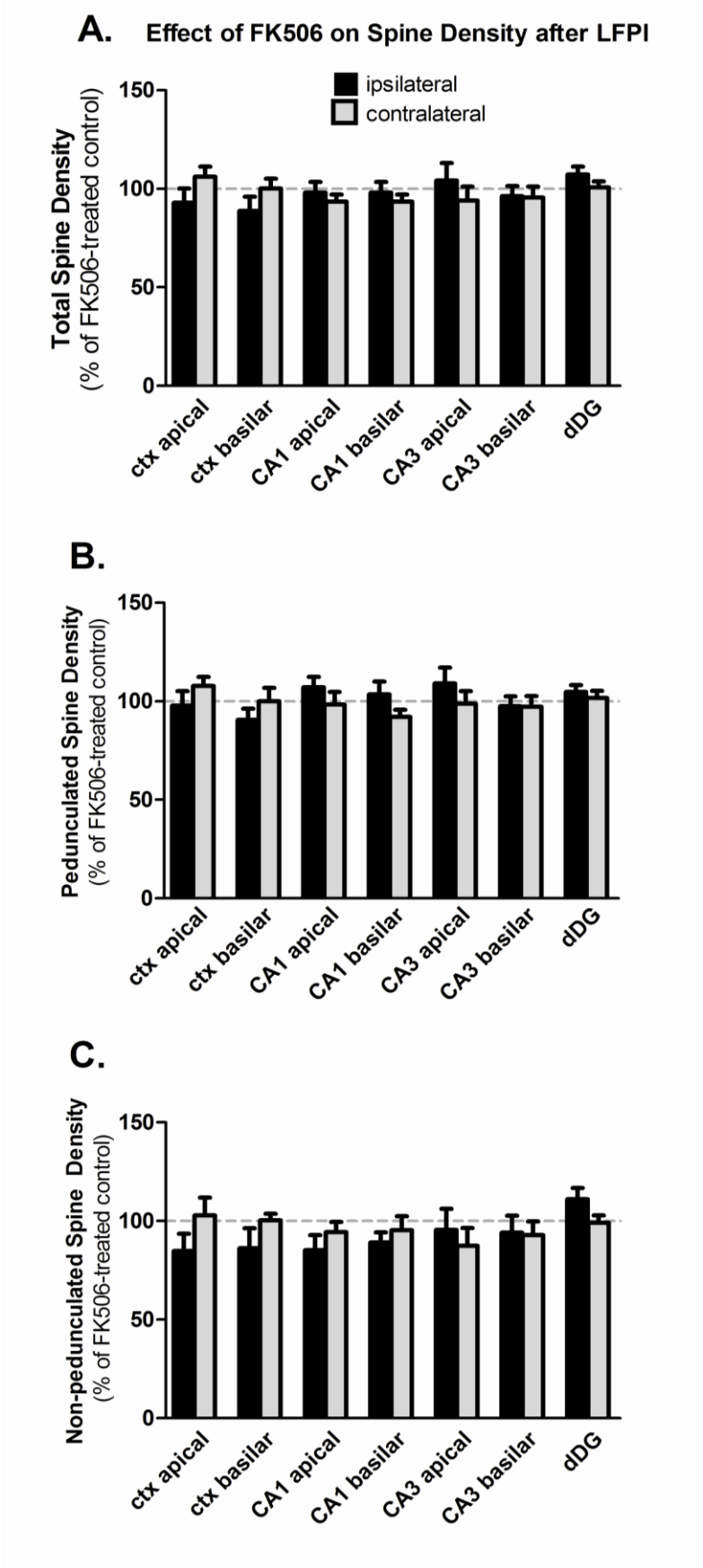
A.
Effect of FK506 on Spine Density after LFPI
ipsilateral
contralateral
Total Spine Density
(% of FK506-treated control)
150
100
50
0
ctx apical
ctx basilar
CA1 apical
CA1 basilar
CA3 apical
CA3 basilar
dDG
B.
Pedunculated Spine Density
(% of FK506-treated control)
150
100
50
0
ctx apical
ctx basilar
CA1 apical
CA1 basilar
CA3 apical
CA3 basilar
dDG
C.
Non-pedunculated Spine Density
(% of FK506-treated control)
150
100
50
0
ctx apical
ctx basilar
CA1 apical
CA1 basilar
CA3 apical
CA3 basilar
dDG

FIGURE 12 – **FK506 administration prevented a loss of dendritic spine density following lateral fluid percussion injury.** Rats received a lateral brain injury by fluid percussion and were administered FK506 (5mg/kg; i.p.) 1hr later. Rat brains were recovered 24hr after injury and subjected to Golgi-Cox histochemistry. Golgi-stained principal cells were selected at random from the ipsilateral (black bars) and contralateral (gray bars) hemispheres of neocortex$_{II,III}$ ("Ctx"), hippocampus CA1, hippocampal CA3, and the dorsal leaf of the dentate gyrus ("DG"; *n* values are provided in Table 1). Pedunculated spine density and non-pedunculated spine density were quantified on proximal dendrites in these regions. Administering FK506 at 1hr post-injury preserved pedunculated spine density at 24hr post-LFPI on apical dendrites in ipsilateral neocortex$_{II,III}$ and on granule cell dendrites in ipsilateral dDG (B), dendrites which otherwise showed significant spine loss at this time point (see Figures 4b and 10b). Data given as percent of FK506-treated, uninjured controls.

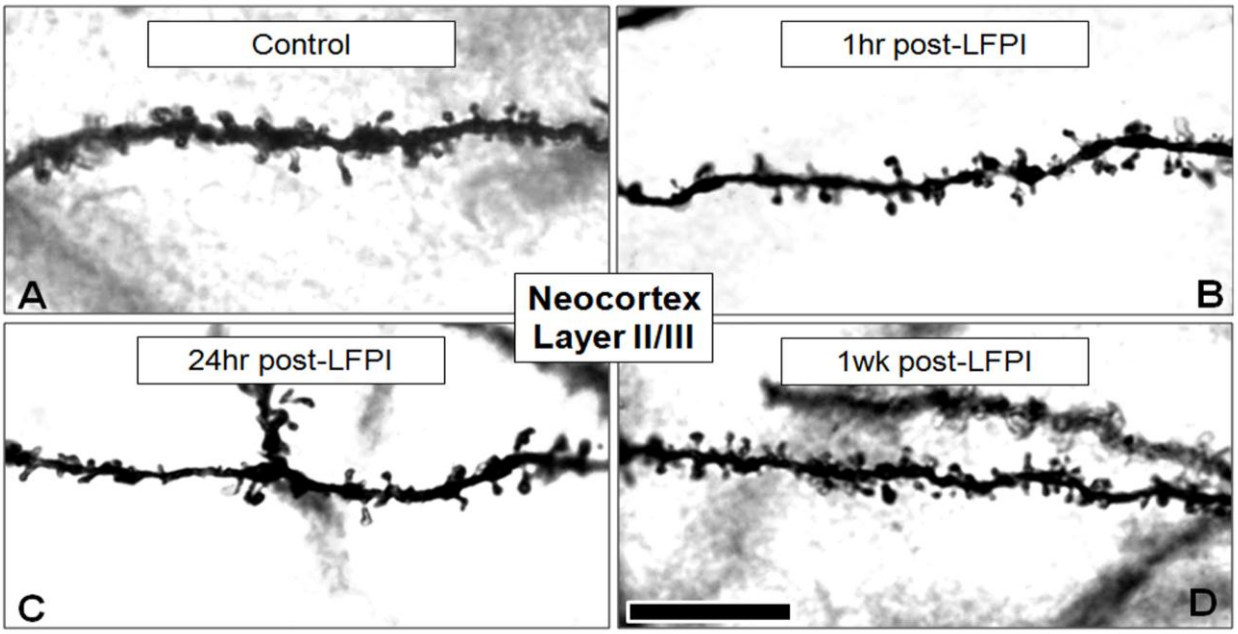

SUPPLEMENTARY FIGURE 1 – Basilar dendritic spine density in ipsilateral neocortex after lateral fluid percussion injury. Shown are proximal dendrites (within 30-150ìm of cell soma) from the basilar arbors of Golgi-stained pyramidal cells in rat neocortex$_{II,III}$. Panel A shows a control dendrite with 6.64 pedunculated spines/10ìm (103% of group mean) and 3.92 non-pedunculate spines/10ìm (92% of group mean). Panels B, C, and D show dendrites in the penumbral region of the focal injury. Panel B shows a dendrite at 1hr post-LFPI, with 7.59 pedunculated spines/10ìm (97% of group mean) and 5.77 non-pedunculated spines/10ìm (116% of group mean). Panel C shows a dendrite at 24hr post-LFPI, with 4.95 pedunculated spines/10ìm (97% of group mean) and 4.40 non-pedunculated spines/10ìm (104% of group mean). Panel D shows a dendrite at 1wk post-LFPI, with 9.69 pedunculated spines/10ìm (129% of group mean) and 5.09 non-pedunculated spines/10ìm (100% of group mean). Note that not all spines counted are in focus in the micrographs. Scale bar, 10ìm.

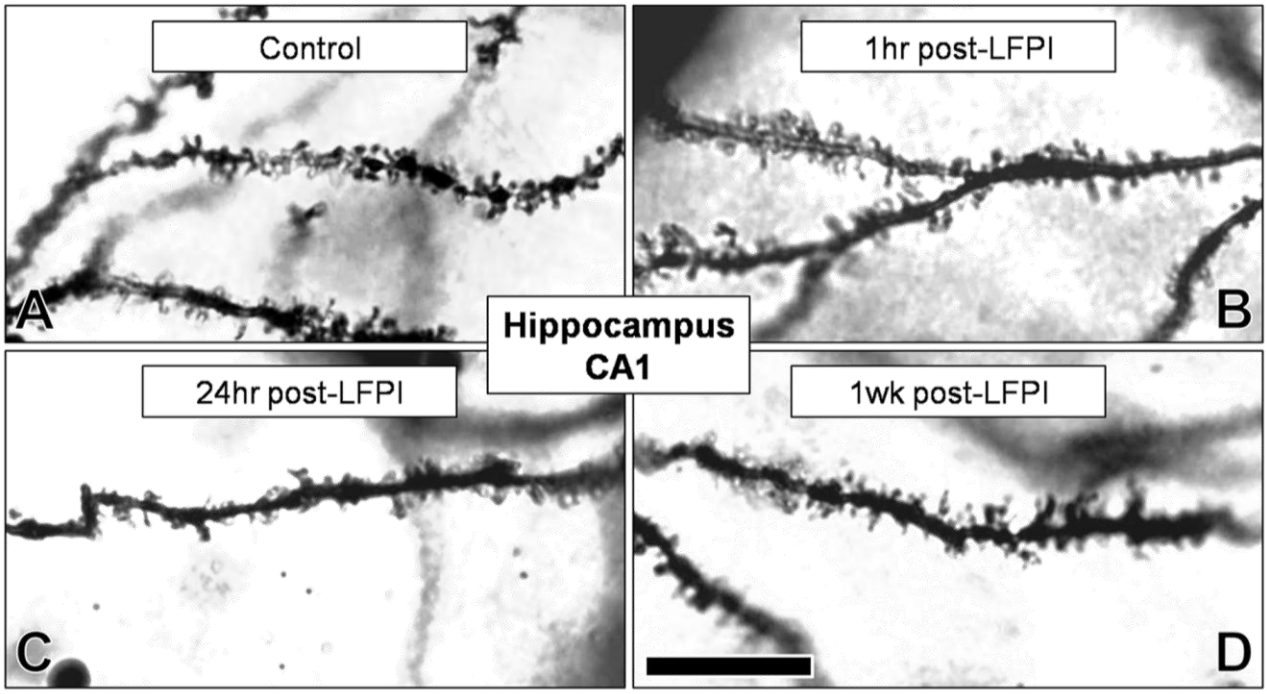

SUPPLEMENTARY FIGURE 2 – **Apical dendritic spine density in ipsilateral CA1 after lateral fluid percussion injury.** Shown are proximal dendrites (within 30-150μm of cell soma) from the apical arbors of Golgi-stained pyramidal cells in rat hippocampal CA1. Panel A shows a control dendrite with 10.00 pedunculated spines/10μm (109% of group mean) and 4.59 non-pedunculated spines/10μm (82% of group mean). Panel B shows a dendrite at 1hr post-LFPI, with 10.18 pedunculated spines/10μm (111% of group mean) and 5.60 non-pedunculated spines/10μm (100% of group mean). Panel C shows a dendrite at 24hr post-LFPI, with 7.74 pedunculated spines/10μm (84% of group mean) and 7.07 non-pedunculated spines/10μm (126% of group mean). Panel D shows a dendrite at 1wk post-LFPI, with 10.38 pedunculated spines/10μm (113% of group mean) and 7.55 non-pedunculated spines/10μm (135% of group mean). Note that not all spines counted are in focus in the micrographs. Scale bar, 10μm.

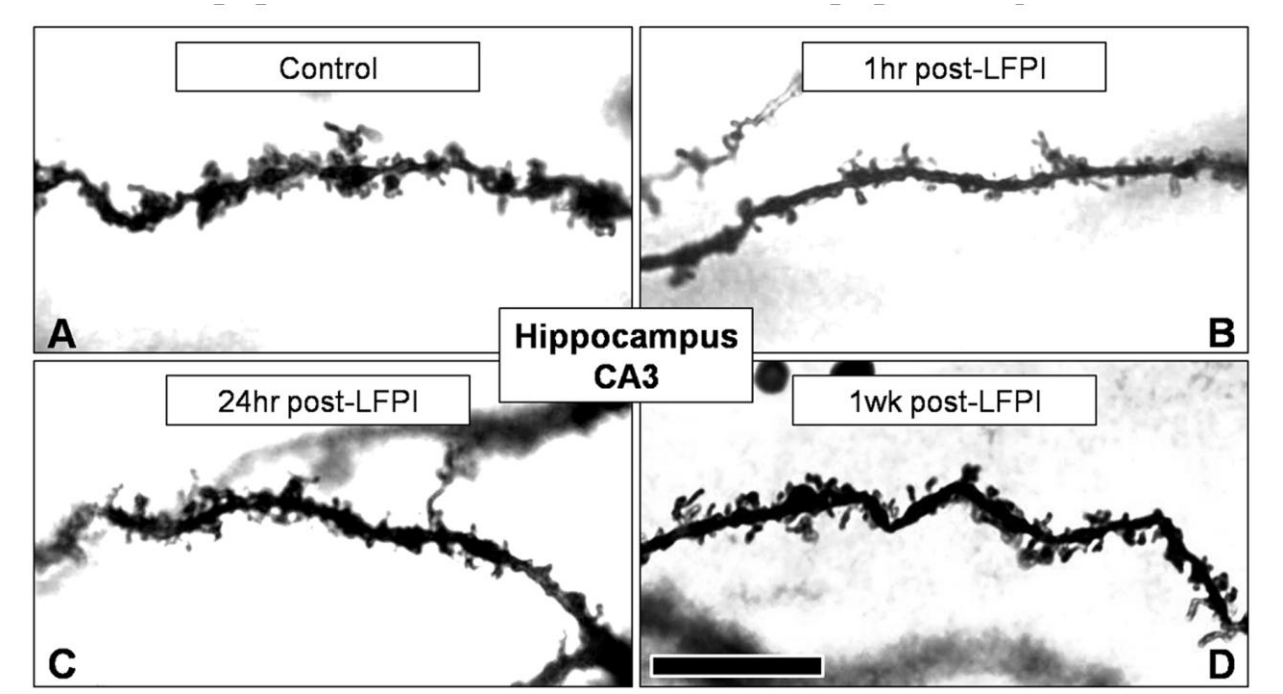

SUPPLEMENTARY FIGURE 3 – **Basilar dendritic spine density in ipsilateral CA3 after lateral fluid percussion injury.** Shown are proximal dendrites (within 30-150μm of cell soma) from the basilar arbors of Golgi-stained pyramidal cells in rat hippocampal CA3. Panel A shows a control dendrite with 8.56 pedunculated spines/10μm (118% of group mean) and 5.45 non-pedunculated spines/10μm (98% of group mean). Panel B shows a dendrite at 1hr post-LFPI, with 7.16 pedunculated spines/10μm (119% of group mean) and 3.12 non-pedunculated spines/10μm (75% of group mean). Panel C shows a dendrite at 24hr post-LFPI, with 8.93 pedunculated spines/10μm (139% of group mean) and 6.20 non-pedunculated spines/10μm (114% of group mean). Panel D shows a dendrite at 1wk post-LFPI, with 8.90 pedunculated spines/10μm (87% of group mean) and 5.93 non-pedunculated spines/10μm (86% of group mean). Note that not all spines counted are in focus in the micrographs. Scale bar, 10μm.

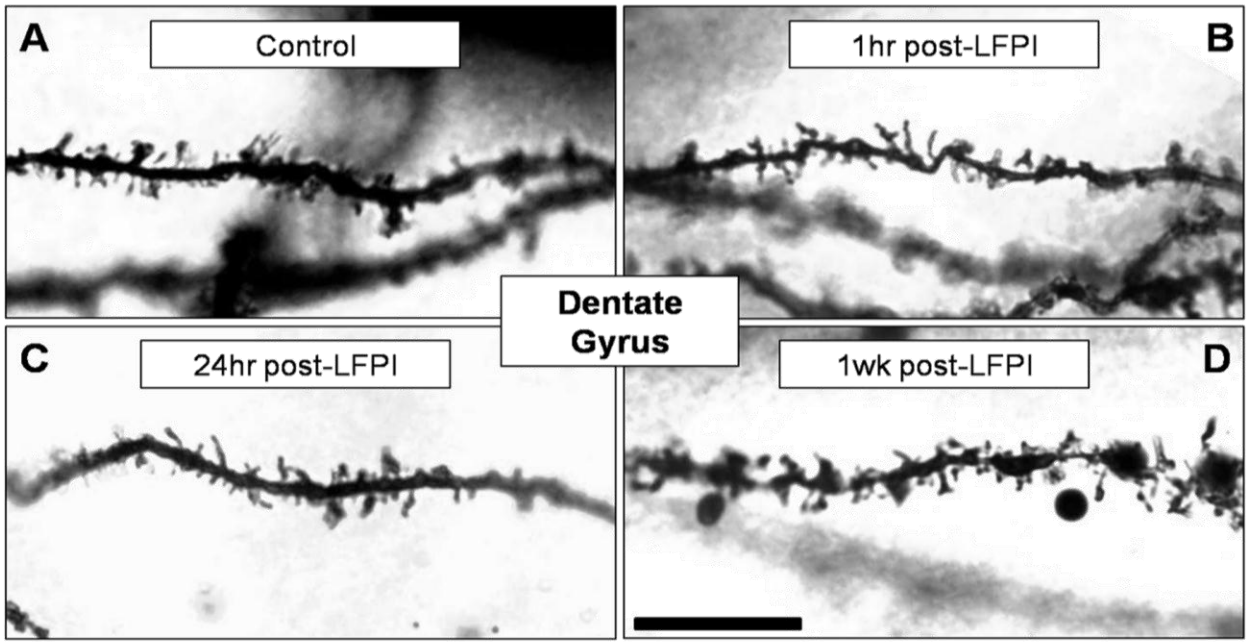

SUPPLEMENTARY FIGURE 4 – **Dendritic spine density in ipsilateral dentate gyrus after lateral fluid percussion injury.** Shown are proximal dendrites (within 30-150μm of cell soma) of Golgi-stained granule cells in the dorsal leaf of the rat dentate gyrus. Panel A shows a control dendrite with 10.32 pedunculated spines/10μm (124% of group mean) and 5.90 non-pedunculated spines/10μm (99% of group mean). Panel B shows a dendrite at 1hr post-LFPI, with 7.50 pedunculated spines/10μm (97% of group mean) and 5.28 non-pedunculated spines/10μm (92% of group mean). Panel C shows a dendrite at 24hr post-LFPI, with 5.96 pedunculated spines/10μm (89% of group mean) and 5.57 non-pedunculated spines/10μm (98% of group mean). Panel D shows a dendrite at 1wk post-LFPI, with 9.51 pedunculated spines/10μm (96% of group mean) and 6.34 non-pedunculated spines/10μm (92% of group mean); note that spine density was not quantified in the beaded region of this dendrite. Also, not all spines counted are in focus in the micrographs. Scale bar, 10μm.

TABLE 1 – Spine densities and *n* values.

Dendritic Spine Density (spines/micron ± SEM)

		Control		FK506+2hr		FK506+23hr		LFPI+1hr				LFPI+24hr				LFPI+1wk				LFPI+24hr, +FK506			
								Contra		Ipsi		Contra		Ipsi		Contra		Ipsi		Contra		Ipsi	
		mean	SEM	mean	SEM	mean	SEM	mean	SEM	mean	SEM	mean	SEM	mean	SEM	mean	SEM	mean	SEM	mean	SEM	mean	SEM
Layer II/III Neocortex																							
Apical	Total Spine Density	1.20	± 0.08	1.20	± 0.07	1.24	± 0.08	1.22	± 0.07	1.16	± 0.06	1.12	± 0.07	0.94	± 0.04	1.20	± 0.06	1.10	± 0.09	1.31	± 0.06	1.15	± 0.09
	Pedunculated	0.74	± 0.05	0.71	± 0.05	0.78	± 0.06	0.75	± 0.05	0.69	± 0.04	0.64	± 0.04	0.52	± 0.02	0.70	± 0.04	0.68	± 0.06	0.84	± 0.04	0.76	± 0.06
	Non-Pedunculated	0.46	± 0.04	0.49	± 0.03	0.46	± 0.03	0.47	± 0.03	0.48	± 0.03	0.48	± 0.03	0.42	± 0.02	0.50	± 0.03	0.43	± 0.04	0.47	± 0.04	0.39	± 0.04
	$n_{neurons}$	14		14		13		14		15		14		19		13		14		15		13	
Basilar	Total Spine Density	1.07	± 0.04	1.28	± 0.07	1.38	± 0.06	1.14	± 0.05	1.28	± 0.05	0.97	± 0.05	0.94	± 0.04	1.26	± 0.04	1.26	± 0.11	1.38	± 0.07	1.23	± 0.10
	Pedunculated	0.65	± 0.03	0.79	± 0.04	0.84	± 0.03	0.72	± 0.04	0.78	± 0.04	0.53	± 0.03	0.51	± 0.03	0.70	± 0.04	0.75	± 0.06	0.84	± 0.06	0.76	± 0.05
	Non-Pedunculated	0.42	± 0.02	0.49	± 0.04	0.54	± 0.04	0.42	± 0.03	0.50	± 0.02	0.44	± 0.03	0.42	± 0.02	0.52	± 0.02	0.51	± 0.05	0.54	± 0.02	0.46	± 0.05
	$n_{neurons}$	13		17		16		13		19		17		22		14		13		12		14	
Hippocampus CA1																							
Apical	Total Spine Density	1.36	± 0.08	1.65	± 0.09	1.73	± 0.08	1.65	± 0.07	1.65	± 0.06	1.61	± 0.08	1.51	± 0.05	1.91	± 0.07	2.06	± 0.09	1.67	± 0.09	1.70	± 0.10
	Pedunculated	0.83	± 0.04	0.92	± 0.06	1.06	± 0.04	1.02	± 0.05	0.97	± 0.04	0.89	± 0.05	0.86	± 0.04	1.15	± 0.05	1.26	± 0.07	1.04	± 0.07	1.13	± 0.06
	Non-Pedunculated	0.52	± 0.05	0.64	± 0.04	0.67	± 0.05	0.64	± 0.03	0.68	± 0.04	0.71	± 0.05	0.65	± 0.04	0.76	± 0.04	0.80	± 0.04	0.64	± 0.03	0.57	± 0.05
	$n_{neurons}$	14		16		14		13		14		15		13		14		13		13		14	
Basilar	Total Spine Density	1.48	± 0.11	1.55	± 0.06	1.67	± 0.08	1.51	± 0.08	1.42	± 0.06	1.49	± 0.07	1.36	± 0.06	1.88	± 0.08	1.82	± 0.08	1.56	± 0.06	1.64	± 0.09
	Pedunculated	0.92	± 0.08	0.98	± 0.04	1.05	± 0.07	0.86	± 0.05	0.85	± 0.04	0.82	± 0.05	0.76	± 0.04	1.15	± 0.04	1.13	± 0.06	0.99	± 0.04	1.09	± 0.07
	Non-Pedunculated	0.56	± 0.04	0.57	± 0.03	0.62	± 0.03	0.65	± 0.05	0.58	± 0.03	0.67	± 0.04	0.61	± 0.04	0.72	± 0.05	0.69	± 0.04	0.57	± 0.04	0.56	± 0.03
	$n_{neurons}$	12		20		14		14		17		18		12		14		13		16		13	
Hippocampus CA3																							
Apical	Total Spine Density	1.24	± 0.11	1.30	± 0.08	1.41	± 0.07	1.22	± 0.11	1.17	± 0.07	1.25	± 0.06	1.40	± 0.06	1.54	± 0.12	1.62	± 0.07	1.33	± 0.10	1.47	± 0.13
	Pedunculated	0.72	± 0.08	0.76	± 0.05	0.82	± 0.05	0.71	± 0.07	0.69	± 0.04	0.65	± 0.04	0.73	± 0.05	0.93	± 0.08	0.96	± 0.05	0.81	± 0.05	0.91	± 0.07
	Non-Pedunculated	0.52	± 0.04	0.53	± 0.04	0.59	± 0.04	0.51	± 0.05	0.49	± 0.04	0.57	± 0.04	0.60	± 0.03	0.61	± 0.06	0.66	± 0.04	0.51	± 0.05	0.56	± 0.06
	$n_{neurons}$	10		14		14		10		14		13		16		13		14		13		13	
Basilar	Total Spine Density	1.28	± 0.09	1.25	± 0.07	1.35	± 0.09	1.19	± 0.07	1.02	± 0.08	1.07	± 0.06	1.19	± 0.05	1.60	± 0.07	1.71	± 0.12	1.29	± 0.07	1.30	± 0.07
	Pedunculated	0.73	± 0.05	0.74	± 0.05	0.83	± 0.06	0.65	± 0.04	0.60	± 0.05	0.57	± 0.03	0.64	± 0.04	0.99	± 0.06	1.02	± 0.09	0.81	± 0.05	0.81	± 0.04
	Non-Pedunculated	0.55	± 0.04	0.51	± 0.04	0.52	± 0.04	0.54	± 0.04	0.42	± 0.04	0.50	± 0.03	0.54	± 0.02	0.61	± 0.03	0.69	± 0.05	0.48	± 0.04	0.49	± 0.04
	$n_{neurons}$	12		17		14		17		13		16		19		14		13		14		14	
Dentate Gyrus																							
	Total Spine Density	1.43	± 0.06	1.48	± 0.07	1.51	± 0.05	1.31	± 0.07	1.35	± 0.06	1.30	± 0.06	1.24	± 0.04	1.71	± 0.09	1.67	± 0.07	1.52	± 0.05	1.62	± 0.06
	Pedunculated	0.83	± 0.04	0.90	± 0.04	0.93	± 0.03	0.77	± 0.04	0.77	± 0.04	0.68	± 0.04	0.67	± 0.03	0.97	± 0.06	0.99	± 0.04	0.94	± 0.03	0.97	± 0.03
	Non-Pedunculated	0.60	± 0.03	0.58	± 0.03	0.59	± 0.03	0.54	± 0.04	0.57	± 0.03	0.62	± 0.03	0.57	± 0.03	0.63	± 0.04	0.69	± 0.03	0.58	± 0.02	0.65	± 0.03
	$n_{neurons}$	27		27		27		27		27		27		27		27		27		27		27	

CHAPTER II

MECHANISMS OF DENDRITIC SPINE REMODELING IN A RAT MODEL OF TRAUMATIC BRAIN INJURY

INTRODUCTION

A traumatic brain injury (TBI) occurs every 19 seconds in the United States [219] and is a leading cause of death and disability. TBI typically involves both an immediate, mechanical destruction of tissue as well as prolonged reactive processes such as excitotoxicity which develop over a period of hours to days. This secondary injury can affect cellular function well beyond the site of impact and so may be responsible for many of the long-lasting neurological deficits associated with TBI [220,221]. However, this secondary injury may be treatable or even preventable, given the apparent window for therapeutic intervention.

Calcium-regulated systems have been implicated in the spread of neuronal damage following ischemia and TBI [32,35,222]. One such system involves the calcium-regulated phosphatase, calcineurin (CaN) [223,224,225]. CaN mediates many cellular responses to brain injury, including the expression of cytokines [226] and neuronal nitric oxide synthase [227], glial apoptosis [228] and activation [229]. CaN also regulates synaptic plasticity under normal conditions (*e.g.*, [114,230]) and in various pathological states, including prolonged seizure [118], amyloid beta exposure

[231], and TBI [186]. Given its regulation by calcium and role in cellular responses to injury, CaN and its signaling pathways may contribute to the pathology of TBI. Previous research by our laboratory found both an increase in CaN activity and its re-distribution to synapses in the rat forebrain after fluid percussion TBI [224,232]. More recently, we found that these changes coincide with a CaN-dependent loss of dendritic spines in the rat neocortex and hippocampus after fluid percussion TBI [233]. However, it is unclear how CaN is involved in this spine loss. Several signaling pathways which connect CaN activity to spine loss have been characterized *in vitro* (for review, see [183]). One such pathway involves remodeling the spine's actin-rich cytoskeleton by the actin-binding protein, cofilin [23,118,211]. Another pathway involves the targeted proteolysis of the spine-stabilizing protein, SPAR (spine-associated Rap guanosine triphosphatase activating protein) [12,142]. While these pathways have been demonstrated in other injury models, it is unclear whether they can explain the spine loss we observed in the TBI model [233]. Therefore, the present study examined the activity and temporal profile of these CaN-dependent pathways in the fluid percussion model of TBI. We report significant changes in CaN activity and in its downstream substrates. Together with our companion paper [233], these experiments characterize cellular mechanisms through which TBI can cause dendritic spine loss.

MATERIALS AND METHODS

All animal use procedures were performed in strict accordance with the Guide for the Care and Use of Laboratory Animals described by the National Institutes of Health and was approved by the Virginia Commonwealth University Institutional Animal Care

and Use Committee. Animal subjects received *ad libitum* access to food and water and were maintained on 12-hour light/dark cycles throughout the experiment. A total of 105 adult, male Sprague-Dawley rats (90 day old; 350-400g) were used in this study. These rats were randomly distributed among the following treatment groups: controls (naïve, age-matched; n=20), FK506-only (n=4), TBI-only (n=76), and TBI+FK506 (n=5).

Fluid percussion injury

The TBI and TBI+FK506 groups were surgically prepared for TBI as follows. First, rats were anesthetized with sodium pentobarbital l (54 mg/kg intraperitoneally; i.p.) or isoflurane (3% isoflurane in a carrier gas mixture of 30% N_2O and 70% O_2) and placed into a stereotactic frame. The scalp was then incised and a 4.8-mm hole was made over the left hemisphere using a manual trephine centered 4mm caudal to bregma and -3mm lateral to the sagittal suture. An anchor screw was inserted into the skull overlying the opposite hemisphere. A modified female Luer-Loc syringe hub (2.6mm inside diameter) was placed over the exposed dura, affixed with a cyanoacrylate adhesive, and then secured with dental acrylic. The hub was filled with sterile saline and the scalp was sutured closed. On the following day, subjects were anesthetized with isoflurane (4min in 4% isoflurane in a carrier mixture of 30% N_2O and 70% O_2) and subjected to fluid percussion of the intact dura over their left parietal cortex. The fluid percussion device used in these experiments is identical to that described by Dixon and colleagues [187]. Immediately after fluid percussion injury, the Luer-Loc fitting, screw, and dental cement were removed from the skull and the scalp was sutured closed. Subjects were then placed in a supine position and the time at

which they righted themselves was recorded. Upon recovery of righting reflexes, subjects were returned to home cages and monitored daily. At 1hr post-TBI, some rats (n=5; "TBI+FK506") received a single injection of FK506 (5mg/kg; i.p.; Astellas Pharma Inc., Tokyo, Japan). As a drug control group, additional age-matched Sprague-Dawley rats ("FK506 only"; n=4) were administered FK506 (5mg/kg; i.p.) and then sacrificed 23hr after drug administration.

Isolation and homogenization of brain regions

Rats were briefly anesthetized with isoflurane and quickly decapitated at the following times after TBI: 1hr (n=7); 6hr (n=4); 12hr (n=5); 18hr (n=13); 24hr (n=18); 24hr+FK506 (n=5); 48hr (n=4); 1wk (n=5); 2wk (n=6); and 4wk (n=5). Age-matched control rats and FK506-only rats were sacrificed along with TBI rats and in the same manner. Brains were rapidly dissected on an iced Petri dish to reduce postmortem enzyme activity. Ipsilateral and contralateral hemispheres of neocortex and hippocampus were dissected whole and separately homogenized with 10 strokes (up and down) at 12,000 rpm using a motorized homogenizer (TRI-R Instruments, Inc., Rockville Center, NY). Brain regions were homogenized in ice-cold homogenization buffer containing 7mM EGTA, 5mM EDTA, 1mM dithiothreitol, 0.3 mM phenylmethylsulfonylfluoride, and 300mM sucrose. Neocortical hemispheres and hippocampal hemispheres were homogenized in 4mL and 2mL of buffer, respectively. Homogenates were aliquoted and stored at -80°C until use. Homogenates from the same animals were used for multiple experiments whenever possible. To control for

storage artifact in the Western analyses of phosphorylated cofilin, samples from post-TBI animals were normalized to equivalently-stored control samples.

pNPP assay of CaN activity

CaN activity was measured using the procedure of Pallen and Wang [234], as optimized by Kurz *et al.* [224,235]. Briefly, all reaction tubes were prepared on ice and contained the following: 25mM MOPS (pH 7.0), 1mM DTT, 2mM p-nitrophenyl phosphate (pNPP) (Sigma-Aldrich; St Louis, MO, U.S.A.). Tubes used to measure basal CaN activity also contained 2mM EGTA and 2mM EDTA. Tubes used to measure maximal CaN activity contained the same reagents as basal reactions, with the addition of 2mM $MnCl_2$. Manganese activates CaN much more strongly than calcium in the pNPP assay and is therefore used to reveal changes in maximal CaN activity [224]. Final reaction volumes were 1mL. Prior to use, the protein concentrations of all homogenate samples were determined using the method of Bradford [236]. Reactions were initiated by the addition of 50µg/mL brain homogenate. Reactions were incubated at 37°C for 30min in a shaking water bath. Tubes were then removed from the water bath and placed in ice to stop the reaction. Absorbance of the reaction mixture was immediately measured at 405nm in a spectrophotometer (UV-2101, Shimadzu Scientific Instruments, Inc., Columbia, MD). Absorbance units were converted to nmol of pNP produced by comparison to a pNP concentration standard absorption curve.

Western analysis

Brain samples were normalized using the Bradford method, resolved by sodium dodecyl sulfate polyacrylamide gel electrophoresis (SDS-PAGE) (Mini-Protean II system, Bio-Rad, Hercules, CA, U.S.A.), and transferred to nitrocellulose membrane using the Trans-blot system (Bio-Rad). Transfer quality was confirmed by staining the blots with a reversible protein stain, Ponceau S (Sigma-Aldrich), according to the manufacturer's instructions. After de-staining, blots were twice immersed for 15 minutes in blocking solution containing phosphate buffered saline (PBS, pH 7.4), 0.05% (v/v) polyoxyethylene sorbitan monolaurate (Tween 20), and 2.5% blotting grade dry milk (Bio-Rad). Blots were then incubated overnight with the appropriate antibody in blocking solution at 4°C. Antibodies were used at the following dilutions: rabbit anti-cofilin, 1:500 (catalog #3842, Chemicon International, Temecula, CA, U.S.A.); rabbit anti-Ser3 phosphorylated cofilin, 1:500 (catalog #3831, Chemicon International); rabbit anti-PSD-95, 1:1000 (catalog #51-9600, Invitrogen, San Diego, CA, U.S.A.); goat anti-E6TP1 ("SPAR"), 1:1000 (catalog #sc-20846, Santa Cruz Biotechnology). Membranes were then washed in 0.05% Tween 20-PBS three times for 10 minutes each. Next, the nitrocellulose was incubated for 45min in the appropriate horseradish peroxidase-conjugated secondary antibody (Thermo Scientific, Waltham, MA, U.S.A.), diluted 1:4000 in blocking solution. The blots were then washed 3 times in PBS for 10min each wash. Immunoreactive bands were revealed by chemiluminescence (Pierce Femto or Pico Luminol Substrate, Pierce, Rockford, IL, U.S.A.) and exposed to x-ray films (Kodak X-OMAT) which were then developed on a Kodak X-OMAT developer. The mean optical densities of immunoreactive bands were measured by computer-assisted densitometry (GS-800 Calibrated Densitometer, Bio-Rad) and compared to a linear

concentration curve as described previously [237]. In the SPAR and PSD-95 experiments, data were normalized to whole-lane optical densities obtained from the same Ponceau S stained blots [238].

Statistical analysis

Group means were statistically analyzed with GraphPad Prism 4.0 (Graph-Pad Software, San Diego, CA, U.S.A.). All comparisons were made by one-way analysis of variance (ANOVA). *Post hoc* analyses were conducted with either Tukey's test (only data related to Figure 19) or Dunnett's test (all other data). Groups were considered significantly different if $p < 0.05$. All data are presented as group mean ± standard deviation. Sample sizes (*n* values) are shown on the figures.

RESULTS

Lateral fluid percussion TBI

Adult male rats received a traumatic brain injury by fluid percussion of the dura overlying their left parietal cortex. The mean fluid percussion pressure was 2.22 ± 0.11atm and did not differ significantly across groups (F [9,64]=1.111, p=0.3678). A common correlate of injury severity is the latency between injury and the recovery of the righting reflex ("righting time") [191]. In the present study, the mean righting time was 7.00 ± 3.19min. This mean righting time corresponds to an injury of moderate severity (*e.g.,* [239]). Righting time did not differ significantly across groups (F [9,63]=0.9287, p=0.5068). Some subjects (n=3) exhibited apnea immediately following injury and were mechanically ventilated until spontaneous respirations resumed (mean duration, 25 ±

5sec). The acute mortality rate associated with LFPI in this study was approximately 3% (2 of 76 rats died within 7 days of LFPI and so were excluded from all other data).

Lateral TBI enhanced the enzymatic activity of calcineurin

To determine the effect of lateral TBI on CaN activity, ipsilateral and contralateral hemispheres of neocortex and hippocampus were dissected, separately homogenized, and subjected to a well-characterized pNPP assay [118,224,235,240] (see Materials and Methods). Using this approach, CaN activity was measured either in the absence of stimulating cations ("basal CaN activity"), or in the presence of stimulating cations ("maximal CaN activity").

Lateral TBI had a significant effect on basal CaN activity in the ipsilateral hippocampus, when compared to analogous tissue from control animals (F [8,56]=5.617, $p<0.0001$; Figure 13A). *Post hoc* analysis indicates that this effect was delayed, as basal CaN activity at 1hr post-TBI did not differ significantly from controls ($p>0.05$). By 6hr post-TBI, however, basal CaN activity in this region had increased significantly over control levels ($p<0.01$). The increase was transient, as basal CaN activity did not differ significantly from controls at 12hr, 18hr, or 24hr post-TBI ($p>0.05$, each time point). Basal CaN activity increased again at 1wk post-TBI relative to controls ($p<0.01$). This increase also appeared to be transient, as basal CaN activity at 2wk and 4wk post-TBI did not differ significantly from controls ($p>0.05$, each time point).

The contralateral hippocampus also showed a significant change in basal CaN activity after lateral TBI, when compared to controls (F [8,56]=5.524, $p<0.0001$; Figure 13B). Like the ipsilateral hippocampus, basal CaN activity in the contralateral

hippocampus was unchanged at 1hr post-TBI ($p>0.05$) but increased significantly by 6hr post-TBI, relative to controls ($p<0.01$). Basal CaN activity at 12hr post-TBI was also significantly elevated over control levels ($p<0.01$). This increase was transient, as basal CaN activity returned to control levels by 18hr post-TBI and remained near control levels at the subsequent time points ($p>0.05$, each time point). Overall, lateral TBI caused delayed, transient increases in basal CaN activity in the ipsilateral hippocampus and in the contralateral hippocampus.

The maximal enzymatic activity of CaN was also altered by lateral TBI. In the ipsilateral hippocampus, for example, TBI had a significant effect on maximal CaN activity, relative to controls (F [8,56]=3.283, p=0.0039; Figure 13C). The effect was delayed though, as maximal CaN activity at 1hr and 6hr post-TBI did not differ significantly from controls ($p>0.05$, each time point). By 12hr post-TBI, however, ipsilateral hippocampus showed a significant increase in maximal CaN activity over control levels ($p<0.05$). This increase did not persist, as maximal CaN activity was not significantly altered at 18hr post-TBI, nor at the later time points, relative to controls ($p>0.05$, each time point).

The contralateral hippocampus also showed significant changes in maximal CaN activity after lateral TBI, compared to controls (F [8,56]=4.791, p=0.0002; Figure 13D). As with basal CaN activity, maximal CaN activity was unchanged at 1hr post-TBI ($p>0.05$) but increased significantly at 6hr and 12hr post-TBI, relative to controls ($p<0.01$ and $p<0.05$, respectively). The increase did not persist though, as maximal CaN activity had returned to control levels by 18hr post-TBI and remained near control levels at the subsequent time points ($p>0.05$, each time point). Thus, lateral TBI caused delayed but

transient increases in maximal CaN activity in the ipsilateral hippocampus and in the contralateral hippocampus.

Lateral TBI altered CaN phosphatase activity in the neocortex as well. In the ipsilateral neocortex, for example, lateral TBI had a significant effect on basal CaN activity and maximal CaN activity relative to controls (basal CaN activity, F [7,43]=5.519, p=0.0001, Figure 14A; maximal CaN activity, F [7,43]=3.264, p=0.0072, Figure 14C). The effect was delayed though, as neither basal nor maximal CaN activity differed significantly from controls at the acute time points, 1hr, 6hr, 12hr, and 24hr post-TBI ($p>0.05$, each time point). By 1wk post-TBI, however, ipsilateral neocortex showed significant increases in both basal CaN activity and maximal CaN activity, compared to control levels (basal CaN activity, $p<0.01$, Figure 14A; maximal CaN activity, $p<0.05$, Figure 14C). Basal and maximal CaN activity were also increased above control levels at 2wk post-TBI (basal CaN activity, $p<0.05$, Figure 14A; maximal CaN activity, $p<0.01$, Figure 14C) but returned to control levels by 4wk post-TBI ($p>0.05$; Figure 14A,C).

The contralateral neocortex also underwent significant changes in basal and maximal CaN activity after lateral TBI, when compared to control tissue (basal CaN activity, F [7,43]=3.483, p=0.0048, Figure 14B; maximal CaN activity, F [7,43]=3.088, p=0.0100, Figure 14D). These too were delayed changes, as neither basal nor maximal CaN activity differed significantly from controls at 1hr, 6hr, 12hr, 24hr, 1wk, or 2wk post-TBI ($p>0.05$, each time point; Figure 14B,D). By 4wk post-TBI, both basal and maximal CaN activity had increased significantly above control levels ($p<0.01$; Figure 14B,D). The data thus demonstrate delayed but transient increases in CaN activity in the

ipsilateral neocortex, followed weeks later by an increase in CaN activity in the contralateral neocortex.

Lateral TBI caused time- and region-dependent changes in pSer3-cofilin immunoreactivity

To further characterize the TBI-induced changes in CaN activity, we examined the effect of TBI on cofilin, an endogenous protein which is activated downstream of CaN [131,241]. Cofilin is an actin-binding and -depolymerizing protein critically involved in both functional and structural remodeling of excitatory synapses [23,242]. CaN activation leads to de-phosphorylation of a key serine 3 (Ser3) residue on cofilin, resulting in an increase in cofilin activity [131,241]. To test whether lateral TBI affects cofilin Ser3 phosphorylation, ipsilateral and contralateral hemispheres of neocortex and hippocampus were dissected after lateral fluid percussion injury, separately homogenized, and subjected to Western analysis with a phospho-specific antibody recognizing the inactivated, serine 3-phosphorylated cofilin (pSer3-cofilin). This analysis revealed apparent, time-dependent changes in pSer3-cofilin immunoreactivity in hippocampal and neocortical structures (Figure 15). In both the ipsilateral and contralateral hippocampi, for example, pSer3-cofilin immunoreactivity appeared to decrease acutely, within 1hr of TBI, and remain decreased at 24hr post-TBI (Figure 15A,B). However, in animals allowed to recover for 1wk after injury, pSer3-cofilin immunoreactivity appeared to return to control levels. A different trend was observed in the neocortex, where pSer3-cofilin immunoreactivity appeared to increase or remain

unchanged at 1hr post-TBI, but then decrease at the subsequent time points (Figure 15C,D).

To further investigate the apparent changes in pSer3-cofilin immunoreactivity, additional Westerns were performed for quantitative analysis (Figure 16). These experiments confirmed that lateral TBI caused time- and region-dependent changes in pSer3-cofilin immunoreactivity. For example, lateral TBI significantly altered pSer3-cofilin immunoreactivity in the ipsilateral hippocampus, when compared to analogous tissue from controls (F [6,48]=7.953, $p<0.0001$; Figure 16A). At 1hr post-TBI in the ipsilateral hippocampus, pSer3-cofilin immunoreactivity appeared to decrease relative to control levels, though *post hoc* analysis indicates that this decrease was not statistically significant (1hr post-TBI *vs*. controls, $p>0.05$). Nor did pSer3-cofilin immunoreactivity at 12hr post-TBI differ significantly from controls ($p>0.05$). However, a significant decrease in pSer3-cofilin immunoreactivity was observed at 24hr post-TBI, relative to controls ($p<0.05$). This decrease did not persist, as pSer3-cofilin immunoreactivity had returned to control levels by 1wk post-TBI ($p>0.05$), and was elevated above control levels at 2wk post-TBI ($p<0.01$). Surprisingly, at 4wk post-TBI, pSer3-cofilin immunoreactivity again fell below control levels ($p<0.05$).

The contralateral hippocampus also underwent significant changes in pSer3-cofilin immunoreactivity after lateral TBI, relative to controls (F [6,48]=13.60, $p<0.0001$; Figure 16B). Like the ipsilateral hippocampus, the contralateral hippocampus showed an acute, TBI-induced decrease in pSer3-cofilin immunoreactivity. Specifically, at 1hr, 12hr, and 24hr post-TBI in the contralateral hippocampus, pSer3-cofilin immunoreactivity was significantly below control levels ($p<0.01$, each time point). As

observed in the ipsilateral hemisphere, pSer3-cofilin immunoreactivity returned to control levels by 1wk post-TBI and did not change significantly thereafter (1wk, 2wk, or 4wk post-TBI, $p>0.05$). Overall, the data demonstrate an acute, decrease in apparent pSer3-cofilin immunoreactivity in both hemispheres of the hippocampus.

Lateral TBI also caused significant changes in pSer3-cofilin immunoreactivity in the neocortex, though these changes differed from those observed in the hippocampus. In the ipsilateral neocortex, TBI had a significant effect on pSer3-cofilin immunoreactivity, when compared to controls (F [6,47]=17.27, $p<0.0001$; Figure 16C). However, in contrast to what was observed of the hippocampal fractions, lateral TBI caused an initial increase in pSer3-cofilin immunoreactivity in the ipsilateral neocortex. *Post hoc* analysis shows that, at 1hr post-TBI, pSer3-cofilin immunoreactivity in the ipsilateral neocortex was significantly increased above control levels ($p<0.01$). This initial increase was followed by a decrease, as pSer3-cofilin fell substantially below control levels by 12hr post-TBI ($p<0.01$). pSer3-cofilin immunoreactivity was significantly decreased at all subsequent time points as well, relative to controls (24hr post-TBI, $p<0.01$; 1wk post-TBI, $p<0.05$; 2wk post-TBI, $p<0.01$; 4wk post-TBI, $p<0.01$).

The contralateral neocortex also showed changes in pSer3-cofilin immunoreactivity after lateral TBI (F [6,47]=12.61, $p<0.0001$; Figure 16D), changes which were similar to those observed of the ipsilateral neocortex. As in the ipsilateral neocortex, pSer3-cofilin immunoreactivity in the contralateral neocortex increased over control levels by 1hr post-TBI ($p<0.01$). However, pSer3-cofilin immunoreactivity returned to control levels by 12hr post-TBI ($p>0.05$). The downward trend continued at 24hr post-TBI, when pSer3-cofilin immunoreactivity decreased substantially below

control levels ($p<0.01$). The pSer3-cofilin immunoreactivity at 1wk and 2wk post-TBI appeared reduced when compared to controls, but not to a statistically significant extent ($p>0.05$, each time point). At 4wk post-TBI though, pSer3-cofilin immunoreactivity was significantly below control levels ($p<0.01$), similar to what was observed of the ipsilateral side. In general, lateral TBI caused acute, but transient increases in pSer3-cofilin immunoreactivity, followed by delayed but persistent decreases, bilaterally in the neocortex

Lateral TBI generally caused a transient increase in total cofilin protein

To determine whether TBI-induced changes in pSer3-cofilin immunoreactivity were due to quantitative changes in cofilin protein, Western analyses were repeated with an antibody recognizing total cofilin protein, regardless of Ser3 phosphorylation. This antibody was generated using the same peptide sequence as the pSer3-specific antibody, but without the phosphate at the Ser3 residue. These analyses revealed significant changes in total cofilin immunoreactivity, though nearly all of these changes were increases.

Lateral TBI significantly altered total cofilin immunoreactivity in the ipsilateral hippocampus relative to analogous tissue from control animals (F [6,48]=40.10, $p<0.0001$; Figure 17A). *Post hoc* analysis indicates that total cofilin immunoreactivity at 1hr and 12hr post-TBI in the ipsilateral hippocampus was significantly above control levels ($p<0.05$ and $p<0.01$, respectively). The increase was transient, as total cofilin immunoreactivity at 24hr and 1wk post-TBI did not differ significantly from controls

(p>0.05, each time point). Total cofilin immunoreactivity increased above control levels again, at 2wk post-TBI (p<0.01), but returned to control levels by 4wk post-TBI (p>0.05).

The contralateral hippocampus also underwent significant changes in total cofilin immunoreactivity after lateral TBI, relative to controls (F [6,49]=6.342, p<0.0001; Figure 17B). In contrast to the ipsilateral hippocampus, acute changes in total cofilin immunoreactivity were not observed in the contralateral hippocampus, as total cofilin immunoreactivity did not differ significantly from controls at 1hr or 12hr post-TBI (p>0.05, each time point). Nor did total cofilin immunoreactivity change significantly at 24hr or 1wk post-TBI, relative to controls (p>0.05, each time point). As observed of the ipsilateral hippocampus, however, total cofilin immunoreactivity increased above control levels at 2wk post-TBI (p<0.01) but then returned to control levels by 4wk post-TBI (p>0.05). Overall, lateral TBI caused acute and delayed increases in total cofilin immunoreactivity in each hemisphere of hippocampus, but no significant decrease at any time point tested.

Lateral TBI altered total cofilin immunoreactivity in the neocortex as well. In the ipsilateral neocortex, TBI had a significant effect on total cofilin immunoreactivity, compared to controls (F [6,49]=11.20, p<0.0001; Figure 17C). In contrast to the hippocampal data, *post hoc* analysis revealed a decrease in total cofilin immunoreactivity in the ipsilateral neocortex at 1hr post-TBI (p<0.01). This decrease was transient, as total cofilin immunoreactivity had returned to control levels by 12hr post-TBI (p>0.05). Total cofilin immunoreactivity remained near control levels at 24hr and 1wk post-TBI (p>0.05, each time point) but then increased at 2wk post-TBI, relative to controls (p<0.01). Similar to what was observed of the hippocampus, the increase at

2wk post-TBI did not persist, as total cofilin immunoreactivity at 4wk post-TBI in the ipsilateral neocortex did not differ significantly from controls ($p>0.05$).

The contralateral neocortex, like the hippocampus, did not show a significant loss of total cofilin immunoreactivity after lateral TBI, at any time point tested. However, TBI did have a significant effect on total cofilin immunoreactivity in the contralateral neocortex relative to controls (F [6,49]=5.228, p=0.0003; Figure 17D). In contrast the ipsilateral neocortex, total cofilin immunoreactivity at 1hr post-TBI in the contralateral neocortex did not differ significantly from controls ($p>0.05$). Nor was there a significant change in total cofilin immunoreactivity at 12hr post-TBI, relative to controls ($p>0.05$). At 24hr post-TBI, however, total cofilin immunoreactivity increased significantly above control levels ($p<0.01$). This increase did not last, as total cofilin immunoreactivity had returned to control levels by 1wk post-TBI ($p>0.05$) and did not differ significantly from controls at 2wk or 4wk post-TBI ($p>0.05$). In general, lateral TBI caused delayed but transient increases in total cofilin immunoreactivity in each hemisphere of neocortex, but a decrease only at 1hr post-TBI in the ipsilateral hemisphere.

Lateral TBI resulted in time- and region-specific changes in the percentage of Ser3 phosphorylated cofilin

To correct for TBI-induced changes in cofilin protein expression, pSer3-cofilin immunoreactivity data were normalized to total cofilin immunoreactivity data for each tissue sample. This yielded a ratio of pSer3-cofilin to total cofilin ("p/t cofilin") for each animal, allowing us to determine whether TBI affected the proportion of Ser3-

phosphorylated cofilin. Statistical analysis of these data revealed significant changes in p/t cofilin after lateral TBI, as detailed below.

Lateral TBI significantly altered p/t cofilin in the ipsilateral hippocampus, when compared to controls (F [6,47]=10.71, p<0.0001; Figure 18A). *Post hoc* analysis indicates that p/t cofilin was significantly decreased at 1hr, 12hr, and 24hr post-TBI, relative to controls (p<0.01, each time point). This decrease did not persist, as p/t cofilin at 1wk and 2wk post-TBI did not differ significantly from controls (p>0.05, each time point). At 4wk post-TBI, however, p/t cofilin again decreased below control levels (p<0.01).

The contralateral hippocampus also underwent significant changes in p/t cofilin after lateral TBI, relative to controls (F [6,48]=16.76, p<0.0001; Figure 18B). Like the ipsilateral hippocampus, contralateral hippocampus showed acute and delayed decreases in p/t cofilin. At 1hr, 12hr, and 24hr post-TBI in the contralateral hippocampus, for example, p/t cofilin was substantially below control levels (p<0.01, each time point). The decrease appeared to be transient, as p/t cofilin did not differ significantly from controls at 1wk post-TBI (p>0.05). However, p/t cofilin decreased again by 2wk post-TBI (p<0.01), relative to controls, before returning to control levels by 4wk post-TBI (p>0.05). Overall, lateral TBI resulted in significant alterations in p/t cofilin in both the ipsilateral and the contralateral hippocampus.

Lateral TBI altered p/t cofilin immunoreactivity in the neocortex as well. In the ipsilateral neocortex, for instance, TBI had a significant effect on p/t cofilin, compared to controls (F [6,47]=28.98, p<0.0001; Figure 18C). *Post hoc* analysis shows that p/t cofilin was increased above control levels at 1hr post-TBI (p<0.01). This increase in p/t

cofilin was followed by decreases at 12hr and 24hr post-TBI, relative to controls ($p<0.05$ and $p<0.01$, respectively). By 1wk post-TBI, p/t cofilin had recovered to control levels ($p>0.05$). However, additional decreases in p/t cofilin were observed at 2wk and 4wk post-TBI, relative to controls ($p<0.01$, each time point).

The contralateral neocortex also showed significant changes in p/t cofilin after lateral TBI, relative to controls (F [6,47]=17.37, $p<0.0001$; Figure 18D). As in the ipsilateral neocortex, p/t cofilin at 1hr post-TBI in the contralateral neocortex was significantly above control levels ($p<0.01$). This increase was transient though, as p/t cofilin had returned to control levels by 12hr post-TBI ($p>0.05$). The downward trend continued at 24hr post-TBI, when p/t cofilin decreased substantially below control levels ($p<0.01$). Similar decreases in p/t cofilin were observed at all subsequent time points, 24hr, 1wk, 2wk, and 4wk post-TBI, relative to controls ($p<0.01$, each time point). In general, both the ipsilateral and contralateral hemispheres of neocortex showed acute but transient increases in p/t cofilin, followed by delayed but apparently persistent decreases in p/t cofilin, after lateral TBI.

Post-TBI treatment with FK506 prevented cofilin de-phosphorylation in neocortex but not hippocampus

In vitro studies have shown that CaN negatively regulates the phosphorylation of the cofilin Ser3 residue [241], which could explain how pSer3-cofilin immunoreactivity decreased after TBI in the absence of any overt loss of cofilin protein (see Figures 3 and 4). To test whether CaN caused the apparent de-phosphorylation of cofilin after TBI, we administered a selective CaN inhibitor, FK506 (5mg/kg, i.p.) to rats at 1hr post-

TBI and sacrificed them at 24hr post-TBI ("TBI+FK506"). To control for drug effects, an age-matched group of uninjured rats (n=5) were also injected with FK506 (5mg/kg, i.p.) and then sacrificed 23hr post-injection ("FK506-only"). Whole hemispheres of neocortex and hippocampus were dissected, separately homogenized, and subjected to Western analysis with a phospho-specific antibody recognizing Ser3-phosphorylated cofilin. Data were then compared across the following groups, using one-way ANOVA and Tukey's *post hoc* test: controls, FK506-only, TBI-only, and TBI+FK506. These analyses indicate that FK506 treatment had region-specific effects on pSer3-cofilin immunoreactivity after lateral TBI.

In the ipsilateral hippocampus, for example, pSer3-cofilin immunoreactivity differed significantly between the treated groups and controls (F [3,34]=20.97, $p<0.001$; Figure 19A). *Post hoc* comparisons revealed a significant reduction in pSer3-cofilin immunoreactivity in the TBI+FK506 group relative to either the FK506-only group ($p<0.001$) or controls ($p<0.001$). In addition, pSer3-cofilin immunoreactivity did not differ significantly between the TBI-only and FK506 groups ($p>0.05$).

Like the ipsilateral hippocampus, pSer3-cofilin immunoreactivity in the contralateral hippocampus differed significantly between the treated groups and controls (F [3,32]=36.24, $p<0.0001$; Figure 19B). Also like the ipsilateral hippocampus, the contralateral hippocampus showed a significant loss of pSer3-cofilin immunoreactivity in the FK506+TBI relative to the FK506-only and control groups ($p<0.001$, each), but no significant difference between the FK506+TBI and TBI-only groups ($p>0.05$). The data thus suggest that the FK506 treatment failed to prevent the 24hr post-TBI loss of pSer3-cofilin immunoreactivity in either hemisphere of hippocampus.

The ipsilateral neocortex also showed significant differences in pSer3-cofilin immunoreactivity between the control and treated groups (F [3,33]=10.35, p<0.0001; Figure 19C). In contrast to the hippocampus, however, pSer3-cofilin immunoreactivity in the ipsilateral neocortex did not differ significantly between the TBI+FK506 group and the FK506-only group (p>0.05), nor between the TBI+FK506 group and controls (p>0.05). In addition, pSer3-cofilin immunoreactivity in the FK506+TBI group was increased substantially over that of the TBI-only group (p<0.001). This increase in pSer3-cofilin immunoreactivity was not likely due to an increase in cofilin protein expression, as one-way ANOVA found no significant difference in total cofilin immunoreactivity between the control and treated groups (control, n=20, 100 ± 15% of control; FK506-only, n=4, 97 ± 37% of control; TBI-only, n=10, 113 ± 26% of control; TBI+FK506, n=5, 92 ± 27% of control; F [3,35]=1.320, p=0.2835).

Like the ipsilateral neocortex, pSer3-cofilin immunoreactivity in the contralateral neocortex differed significantly between the control and treated groups (F [3,33]=4.109, p=0.0139; Figure 19D). Also like the ipsilateral side, there was no significant difference in pSer3-cofilin immunoreactivity between the TBI+FK506 group and the control group (p>0.05), or between the TBI+FK506 group and the FK506-only groups (p>0.05). Again, however, there was a significant increase in pSer3-cofilin immunoreactivity in the TBI+FK506 group relative to the TBI-only group (p<0.05) which did not appear to be due to an increase in cofilin protein (total cofilin immunoreactivity: control, n=20, 100 ± 14% of control; FK506-only, n=4, 102 ± 32% of control; TBI-only, n=10, 200 ± 108% of control; TBI+FK506, n=5, 118 ± 42% of control; F [3,35]=6.893, p=0.0009; TBI-only vs. FK506+TBI, p>0.05). The data thus strongly suggest that the FK506 treatment

prevented the 24hr post-TBI loss of pSer3-cofilin immunoreactivity in both the ipsilateral neocortex and contralateral neocortex.

Lateral TBI caused a decrease in PSD-95 immunoreactivity

Pathological activation of CaN and cofilin are associated with the degeneration of excitatory synapses *in vitro* [12,23,211]. To test whether synapse degeneration occurred in our TBI model, Western blots were used to measure the immunoreactivity of a post-synaptic marker protein, PSD-95, in neocortical and hippocampal homogenates obtained 18hr, 24hr, and 48hr after lateral fluid percussion injury. As described below, TBI caused a significant loss of PSD-95 immunoreactivity in ipsilateral neocortex and bilateral hippocampus.

Lateral TBI had a significant effect on PSD-95 immunoreactivity in the ipsilateral hippocampus, when compared to analogous tissue from control animals (F [3,13]=13.75, p=0.0003; Figure 20A). *Post hoc* analysis indicates that PSD-95 immunoreactivity at 18hr, 24hr, and 48hr post-TBI in the ipsilateral hippocampus was significantly below control levels ($p<0.01$, $p<0.05$, and $p<0.01$, respectively). The contralateral hippocampus also showed significant changes in PSD-95 immunoreactivity after lateral TBI, relative to controls (F [3,13]=6.890, p=0.0051; Figure 20B). As in the ipsilateral hippocampus, PSD-95 immunoreactivity in the contralateral hippocampus decreased below control levels at 18hr and 24hr post-TBI ($p<0.05$ and $p<0.01$, respectively). Unlike the ipsilateral hippocampus, however, PSD-95 immunoreactivity in the contralateral hippocampus returned to control levels by 48hr post-TBI ($p>0.05$).

Overall, lateral TBI caused an acute loss of PSD-95 immunoreactivity bilaterally in the hippocampus, though the loss appeared to persist longer in the ipsilateral hemisphere.

Lateral TBI also affected PSD-95 immunoreactivity in the ipsilateral neocortex, when compared to controls (F [3,14]=8.328, p=0.002; Figure 20C). *Post hoc* analysis revealed a significant loss of PSD-95 immunoreactivity in the ipsilateral neocortex at 18hr and 24hr post-TBI, relative to controls ($p<0.01$ and $p<0.05$, respectively). This loss did not persist though, as PSD-95 immunoreactivity at 48hr post-TBI did not differ significantly from controls ($p>0.05$). Unlike the ipsilateral neocortex, the contralateral neocortex showed no significant change in PSD-95 immunoreactivity after TBI, when compared to controls (F [3,13]=2.921, p=0.0739; Figure 20D). The data thus demonstrate an acute but transient loss of PSD-95 immunoreactivity in the ipsilateral neocortex after lateral TBI.

Effect of lateral TBI on SPAR immunoreactivity

Injury to hippocampal neurons *in vitro* can cause a CaN-dependent induction of serum-induced kinase (Snk), resulting in increased proteolysis of SPAR, a protein which is critical to post-synaptic stability [12,145,210]. To determine whether SPAR proteolysis occurred after lateral TBI, SPAR immunoreactivity was measured using Western blots of neocortical and hippocampal homogenates obtained 18hr, 24hr, and 48hr after lateral fluid percussion injury. No significant change in SPAR immunoreactivity was detected in either hemisphere of neocortex or hippocampus, at any post-TBI time point tested, relative to controls (ipsilateral hippocampus, F [3,14]=3.134, p=0.0593; contralateral hippocampus, F [3,13]=0.8802, p=0.4767;

ipsilateral neocortex, F [3,14]=0.3530, p=0.7877; contralateral neocortex, F [3,13]=2.850, p=0.0784; Figure 21). The data therefore suggest that SPAR proteolysis is unlikely to be a mechanism behind the dendritic spine loss observed in neocortex and dentate gyrus at 24hr post-TBI [233].

DISCUSSION

The present study examined the effects of lateral fluid percussion on CaN activity and CaN-dependent signaling in the rat forebrain. An *in vitro* assay revealed significant, time-dependent changes in CaN phosphatase activity in the hippocampus and neocortex after lateral TBI. Changes in CaN activity were further characterized by Western analyses. These analyses measured the effect of lateral TBI on two signaling pathways through which CaN regulates the stability of dendritic spines. The results implicate cellular pathways through which lateral TBI could alter dendritic spine stability. Together with its companion study [233], the present study demonstrates a specific cellular mechanism through which lateral TBI can cause a loss of dendritic spines. This spine loss may be clinically relevant, if it alters inter-neuronal communication and so contributes to cognitive impairment.

Analogous to what our group observed in midline TBI model [224,232], lateral TBI resulted in a delayed, transient change in CaN phosphatase activity in the hippocampus and neocortex. The increase in CaN activity could be explained by an acute increase in CaN protein, as has been reported in a different model of lateral TBI [243]. An alternative hypothesis is that CaN activity is enhanced through some post-translational modification of the enzyme – *e.g.*, a partial proteolytic cleavage which

disinhibits its phosphatase activity [244], as has been proposed in models of central fluid percussion injury [224] and *status epilepticus* [118,235]. Recently, D'Amelio and colleagues reported evidence of a caspase-3 cleaved, constitutively active fragment of CaN in a mouse model of Alzheimer's disease [245]. Enhancement of CaN activity in this manner would agree with our findings from the midline TBI model, wherein no change in CaN holoenzyme expression was observed [224]. However, it is noteworthy that the changes in CaN activity induced by lateral TBI were not as long-lasting as those induced by midline TBI. Specifically, the increase in CaN activity lasted for hours after lateral TBI but for weeks after midline TBI [224].

CaN activity can also influenced by endogenous factors, such as Ca^{2+} binding, that cannot be measured by our *in vitro* assay. These endogenous changes in CaN activity can, however, be measured by the downstream effects on CaN substrates. The present study therefore examined a downstream substrate of CaN, cofilin. CaN activity leads to de-phosphorylation of a key Ser3 residue on cofilin [131], and the removal of this Ser3 phosphate enables cofilin to bind and de-polymerize actin [246]. The breakdown of actin filaments by cofilin is critical to synaptic plasticity and a number of other cellular processes (reviewed in [247]). Therefore, this choice of substrate allowed us not only to indirectly measure CaN activity, but to directly assess the cellular consequences of CaN activity.

The present study found that lateral TBI caused time- and region-dependent changes in pSer3-cofilin immunoreactivity in both the ipsilateral and contralateral hemispheres of hippocampus and neocortex. These changes could be due to changes in cofilin protein expression or Ser3 phosphorylation, or both. While total cofilin

immunoreactivity did change at some post-TBI time points, relative to controls, only once did it correspond to a change in pSer3-cofilin immunoreactivity (*i.e*., at 2wk post-TBI in the ipsilateral hippocampus, pSer3-cofilin increased and total cofilin increased). It is therefore reasonable to conclude that all of the decreases in pSer3-cofilin immunoreactivity we observed were due to decreased Ser3 phosphorylation and not due to decreased cofilin protein expression. Likewise, all but one of the increases in pSer3-cofilin immunoreactivity appeared to be due to increased Ser3 phosphorylation, not to increased cofilin protein expression. A noteworthy example is the loss of pSer3-cofilin which occurred bilaterally in the neocortex at 24hr post-TBI. This loss cannot be attributed alone to a decrease in cofilin protein, because total cofilin immunoreactivity was unchanged in the ipsilateral neocortex at 24hr post-TBI, and actually increased in the contralateral neocortex at this time point, relative to controls. Therefore, the loss of pSer3-cofilin most likely represents Ser3 de-phosphorylation. Previous studies have shown that this de-phosphorylation can occur downstream of CaN activity [131]. Though our *in vitro* assay found no significant change in CaN phosphatase activity at 24hr post-TBI, it is possible that some endogenous (*e.g*., Ca^{2+}-mediated) increase in CaN activity led to the cofilin de-phosphorylation we observed. Consistent with this possibility, the present study found that the CaN inhibitor, FK506, administered 1hr post-TBI, prevented the loss of pSer3-cofilin immunoreactivity bilaterally in the neocortex at 24hr post-TBI. The data thus suggest that a TBI-induced increase in CaN activity leads to cofilin de-phosphorylation in the neocortex at 24hr post-TBI.

The results of the present study strongly suggest that TBI causes cofilin de-phosphorylation bilaterally in the rat forebrain. The resulting increase in cofilin activity

could degrade the actin-rich cytoskeleton of dendritic spines, causing the spines to shrink or collapse [23,118,211]. Since dendritic spines form most of the excitatory synapses in the brain, their collapse may physically de-stabilize and disrupt synapses. Indeed, lateral TBI is associated with synapse degeneration, evident in the loss of synaptic proteins reported in previous studies [207,248] and the loss of PSD-95 immunoreactivity observed in the present study. Thus, a pathological increase in cofilin activity may result in not only a loss of dendritic spines, but a loss of spine synapses [211].

Interestingly, the apparent de-phosphorylation of cofilin observed in the present study coincides with a loss of dendritic spines reported in our companion study [233]. Specifically, the ipsilateral neocortex at 24hr post-TBI shows both cofilin de-phosphorylation (Figure 15) and spine loss [233], and both of which are prevented by a 1hr post-TBI administration of FK506. These studies, along with the evidence from other models (*e.g.*, [23,118,211]), thus implicate cofilin de-phosphorylation as a mechanism of dendritic spine loss in the neocortex (Figure 22, “Cofilin Pathway”).

Surprisingly, the same FK506 treatment failed to block cofilin de-phosphorylation in the hippocampus. We suspect that different timing or mechanisms are involved in cofilin de-phosphorylation in the hippocampus. For example, CaN may have been activated in the hippocampus earlier than in the neocortex after lateral TBI. Indeed, cofilin was significantly de-phosphorylated at 1hr post-TBI in the hippocampus, though it is unclear from the present study whether this de-phosphorylation is CaN-dependent. However, if CaN is responsible for this acute de-phosphorylation of cofilin, then FK506 may need to be administered earlier than 1hr post-TBI to fully prevent CaN activation in

the hippocampus. By 1hr post-TBI, CaN may have already conveyed the signal to de-phosphorylate cofilin, or may have been cleaved into a catalytically active fragment which resists inhibition by FK506 [249].

Though FK506 administration failed to block cofilin de-phosphorylation in the hippocampus, it fully prevented a concurrent loss of dendritic spines in the dentate gyrus [233]. One possible explanation is that FK506 inhibits CaN to varying degrees across the subfields of the hippocampus, perhaps due to differential expression of FK506's partner in inhibiting CaN, FKBP12 [250]. A more plausible explanation is that a different mechanism underlies spine loss in the hippocampus, a mechanism which is CaN-dependent but cofilin-independent. The present study considered one such mechanism: the proteolysis of SPAR. SPAR is a post-synaptic protein which stabilizes dendritic spines in hippocampal neurons [141] (Figure 22, "SPAR Pathway"). In cultured hippocampal neurons, excitotoxic injury triggers a CaN-dependent increase in Snk protein, resulting in an increased proteolysis of SPAR and a corresponding loss of dendritic spines [12]. In contrast to these *in vitro* findings, however, the present study detected no significant change in SPAR immunoreactivity at 18hr, 24hr, or 48hr post-TBI in the hippocampus, nor in the neocortex. One could conclude then that SPAR proteolysis did not occur after lateral TBI and so is not a major mechanism of spine loss in this model. However, our data cannot exclude the possibility that SPAR proteolysis occurred focally - *e.g.*, within the dentate gyrus, the only hippocampal subfield which showed spine loss [233]. Such a spatially-limited change in SPAR protein would not likely be detected in a Western analysis of a whole hippocampal hemisphere. Future

studies using immunohistochemistry or micro-dissection could detect changes in SPAR protein with better spatial resolution.

Considering the findings of the present study and its companion [233], we hypothesize that different, CaN-dependent mechanisms underlie spine loss in the neocortex and dentate gyrus following lateral TBI. In the neocortex, CaN may cause spine loss through activation (de-phosphorylation) of cofilin, whereas in the dentate gyrus, CaN may cause spine loss through a cofilin-independent pathway. These studies do not, however, exclude the possibility of other CaN-dependent mechanisms of spine loss in this model. Further investigation is needed to definitively characterize the mechanisms of spine loss following lateral TBI.

Another interesting parallel between the present study and its companion is found at the 1wk post-TBI time point. By 1wk post-TBI in the present study, cofilin phosphorylation had returned to control levels bilaterally in the hippocampus. This recovery represented a substantial increase in cofilin phosphorylation relative to the preceding time point. At the same 1wk post-TBI time point, our companion study found an increase in dendritic spine density bilaterally in the hippocampus [233]. The increase in cofilin phosphorylation and spine density may be related, as the phosphorylation/inactivation of cofilin would favor the cytoskeletal expansion necessary for spine growth. Therefore, the increase in cofilin phosphorylation during recovery from TBI may play a role in the increase in spine density.

The present study and its companion [233] identify potential mechanisms of dendritic remodeling in the traumatically-injured forebrain. This remodeling could disrupt neuronal circuits, or facilitate aberrant re-wiring, and so contribute to cognitive

impairment and other TBI sequelae. CaN inhibition may help to prevent these sequelae by preserving synaptic circuits following TBI, and so could be a new option for treating a widespread medical problem that currently has few treatment options.

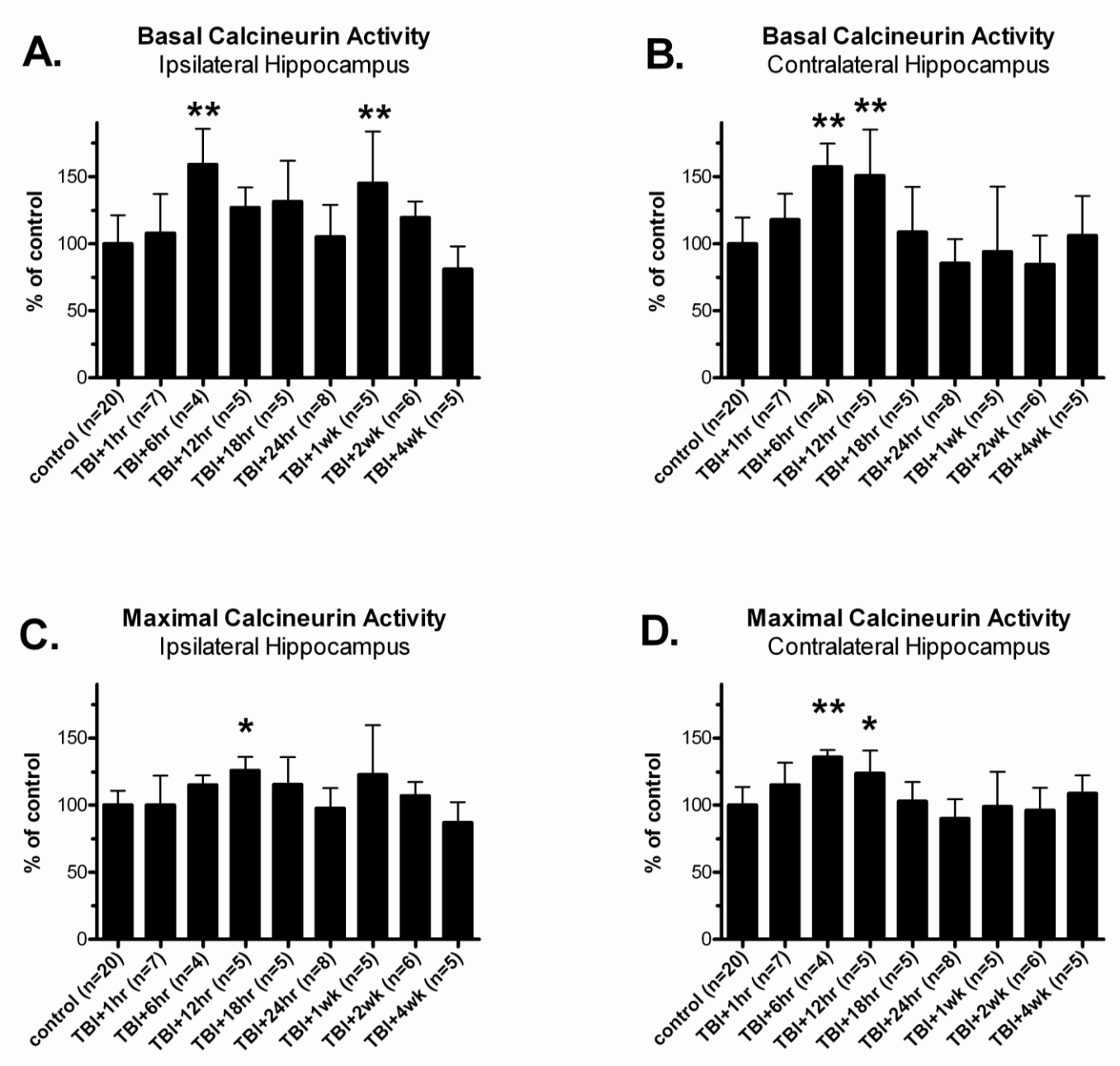
A.
Basal Calcineurin Activity
Ipsilateral Hippocampus
% of control
0
50
100
150
**
**
control (n=20)
TBI+1hr (n=7)
TBI+6hr (n=4)
TBI+12hr (n=5)
TBI+18hr (n=5)
TBI+24hr (n=8)
TBI+1wk (n=5)
TBI+2wk (n=6)
TBI+4wk (n=5)
B.
Basal Calcineurin Activity
Contralateral Hippocampus
% of control
0
50
100
150
**
**
control (n=20)
TBI+1hr (n=7)
TBI+6hr (n=4)
TBI+12hr (n=5)
TBI+18hr (n=5)
TBI+24hr (n=8)
TBI+1wk (n=5)
TBI+2wk (n=6)
TBI+4wk (n=5)
C.
Maximal Calcineurin Activity
Ipsilateral Hippocampus
% of control
0
50
100
150
*
control (n=20)
TBI+1hr (n=7)
TBI+6hr (n=4)
TBI+12hr (n=5)
TBI+18hr (n=5)
TBI+24hr (n=8)
TBI+1wk (n=5)
TBI+2wk (n=6)
TBI+4wk (n=5)
D.
Maximal Calcineurin Activity
Contralateral Hippocampus
% of control
0
50
100
150
**
*
control (n=20)
TBI+1hr (n=7)
TBI+6hr (n=4)
TBI+12hr (n=5)
TBI+18hr (n=5)
TBI+24hr (n=8)
TBI+1wk (n=5)
TBI+2wk (n=6)
TBI+4wk (n=5)

FIGURE 13 - Lateral TBI enhanced calcineurin phosphatase activity in the hippocampus. Hippocampal tissue was isolated from adult rats at specific times after lateral fluid percussion injury, homogenized, and subjected to an *in vitro* assay of CaN enzymatic activity (see Materials and Methods). CaN activity was measured either in the absence of stimulating cations ("basal CaN activity"), or in the presence of stimulating cations ("maximal CaN activity"). In the ipsilateral hippocampus, these experiments revealed increases in basal CaN activity at 6hr and 1wk post-TBI, relative to controls (A). Similarly, in the contralateral hippocampus, increases in basal CaN activity were detected at 6hr and 12hr post-TBI, relative to controls (B). Lateral TBI also affected the maximal activity of CaN, causing increases at 12hr post-TBI in the ipsilateral hippocampus (C) and at 6hr and 12hr post-TBI in the contralateral hippocampus (D), compared to controls. All comparisons were made by one-way ANOVA with Dunnett's *post hoc* test. *p<0.05, **p<0.01

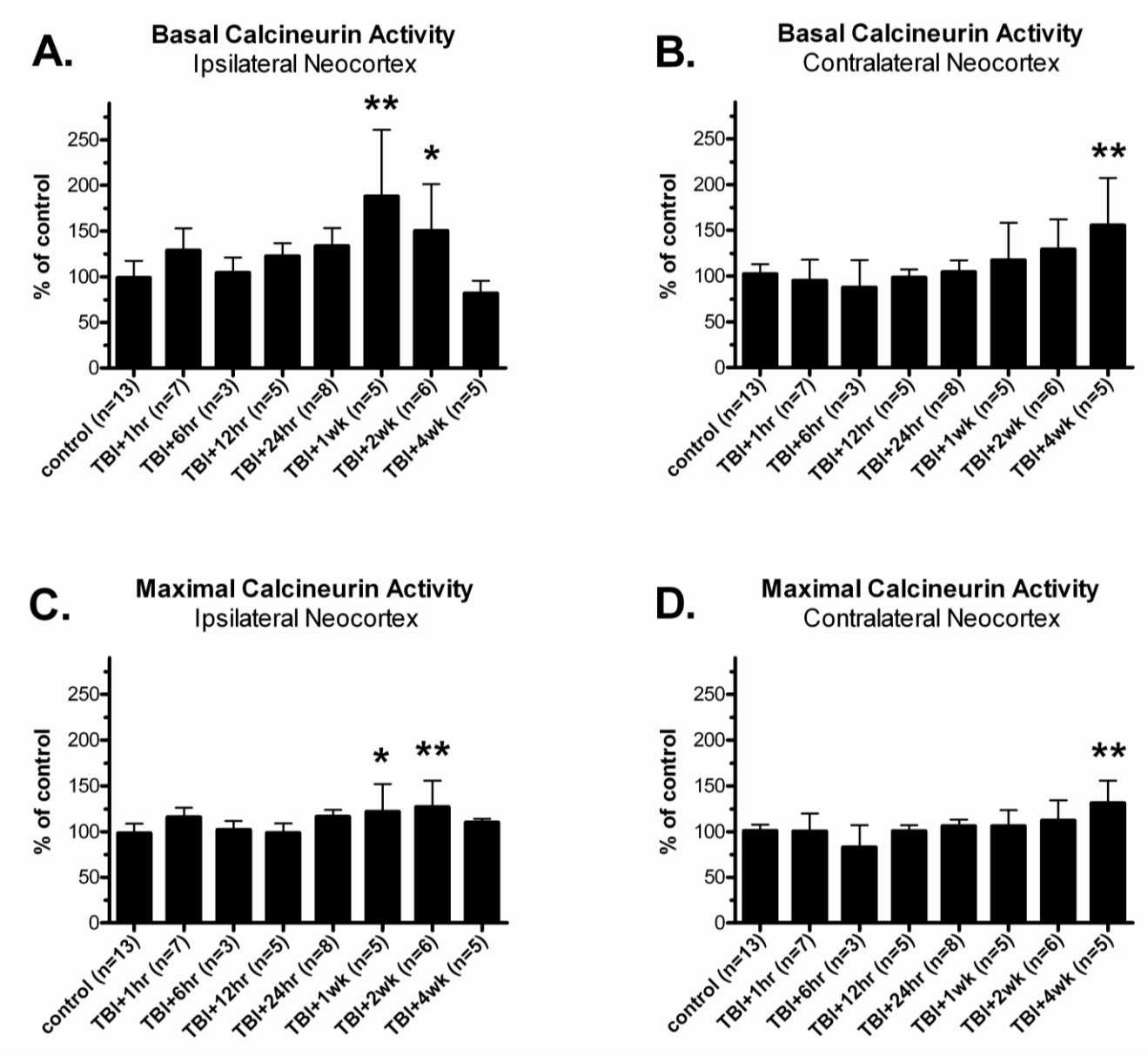
A.
Basal Calcineurin Activity
Ipsilateral Neocortex
% of control
0
50
100
150
200
250
**
*
control (n=13)
TBI+1hr (n=7)
TBI+6hr (n=3)
TBI+12hr (n=5)
TBI+24hr (n=8)
TBI+1wk (n=5)
TBI+2wk (n=6)
TBI+4wk (n=5)
B.
Basal Calcineurin Activity
Contralateral Neocortex
% of control
0
50
100
150
200
250
**
control (n=13)
TBI+1hr (n=7)
TBI+6hr (n=3)
TBI+12hr (n=5)
TBI+24hr (n=8)
TBI+1wk (n=5)
TBI+2wk (n=6)
TBI+4wk (n=5)
C.
Maximal Calcineurin Activity
Ipsilateral Neocortex
% of control
0
50
100
150
200
250
*
**
control (n=13)
TBI+1hr (n=7)
TBI+6hr (n=3)
TBI+12hr (n=5)
TBI+24hr (n=8)
TBI+1wk (n=5)
TBI+2wk (n=6)
TBI+4wk (n=5)
D.
Maximal Calcineurin Activity
Contralateral Neocortex
% of control
0
50
100
150
200
250
**
control (n=13)
TBI+1hr (n=7)
TBI+6hr (n=3)
TBI+12hr (n=5)
TBI+24hr (n=8)
TBI+1wk (n=5)
TBI+2wk (n=6)
TBI+4wk (n=5)

FIGURE 14 - Lateral TBI enhanced calcineurin phosphatase activity in the neocortex. Neocortical tissue was isolated from adult rats at specific times after lateral fluid percussion injury, homogenized, and subjected to an *in vitro* assay of CaN enzymatic activity (see Materials and Methods). CaN activity was measured either in the absence ("basal CaN activity") or presence ("maximal CaN activity") of stimulating cations. In the ipsilateral neocortex, basal CaN activity increased significantly above control levels by 1wk and 2wk post-TBI (A). The contralateral neocortex also showed an increase in basal CaN activity, but weeks later, at 4wk post-TBI, compared to controls (B). The maximal activity of CaN also changed after lateral TBI, increasing significantly over control levels at 1wk and 2wk post-TBI in the ipsilateral neocortex (C), and at 4wk post-TBI in the contralateral neocortex (D). All comparisons were made by one-way ANOVA with Dunnett's *post hoc* test. *$p<0.05$, **$p<0.01$

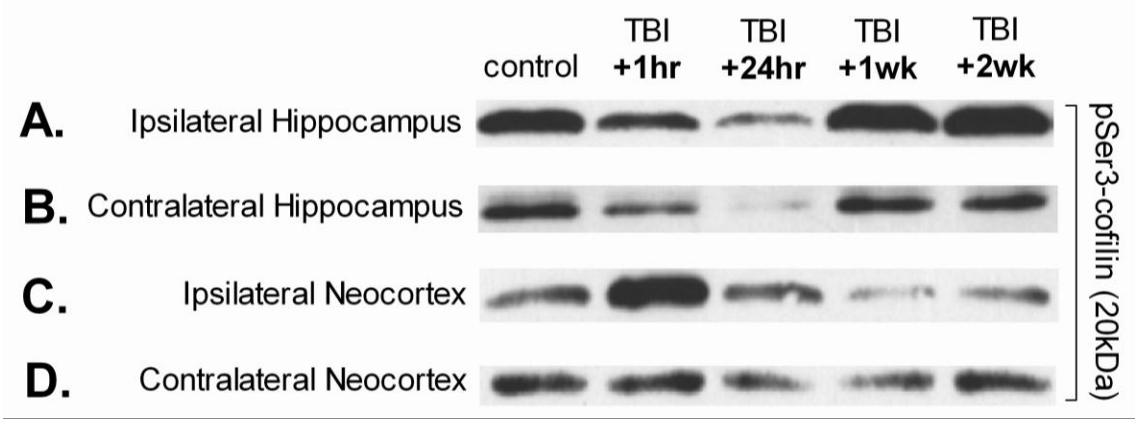

FIGURE 15 - Lateral TBI caused apparent changes in pSer3-cofilin immunoreactivity. Western analysis was performed on crude homogenates of whole ipsilateral and contralateral hemispheres of hippocampus and neocortex dissected from adult rats 1hr, 24hr, 1wk, or 2wk after lateral TBI, and from age-matched control rats. The immunoreactivity of Ser3 phosphorylated cofilin (pSer3-cofilin) was detected with a phospho-specific antibody. Results suggest that the hippocampus and neocortex underwent time- and region-dependent changes in pSer3-immunoreactivity after lateral TBI. In both the ipsilateral and contralateral hippocampi, for example, pSer3-cofilin immunoreactivity appeared to decrease below control levels by 1hr post-TBI and remain decreased at 24hr post-TBI (A,B). However, by 1wk post-TBI, pSer3-cofilin immunoreactivity appeared to have increased to control levels or beyond. A different trend was observed in the neocortex, where pSer3-cofilin immunoreactivity seemed to initially increase (C) or remain unchanged (D) at 1hr post-TBI, but then decrease at later time points (C,D).

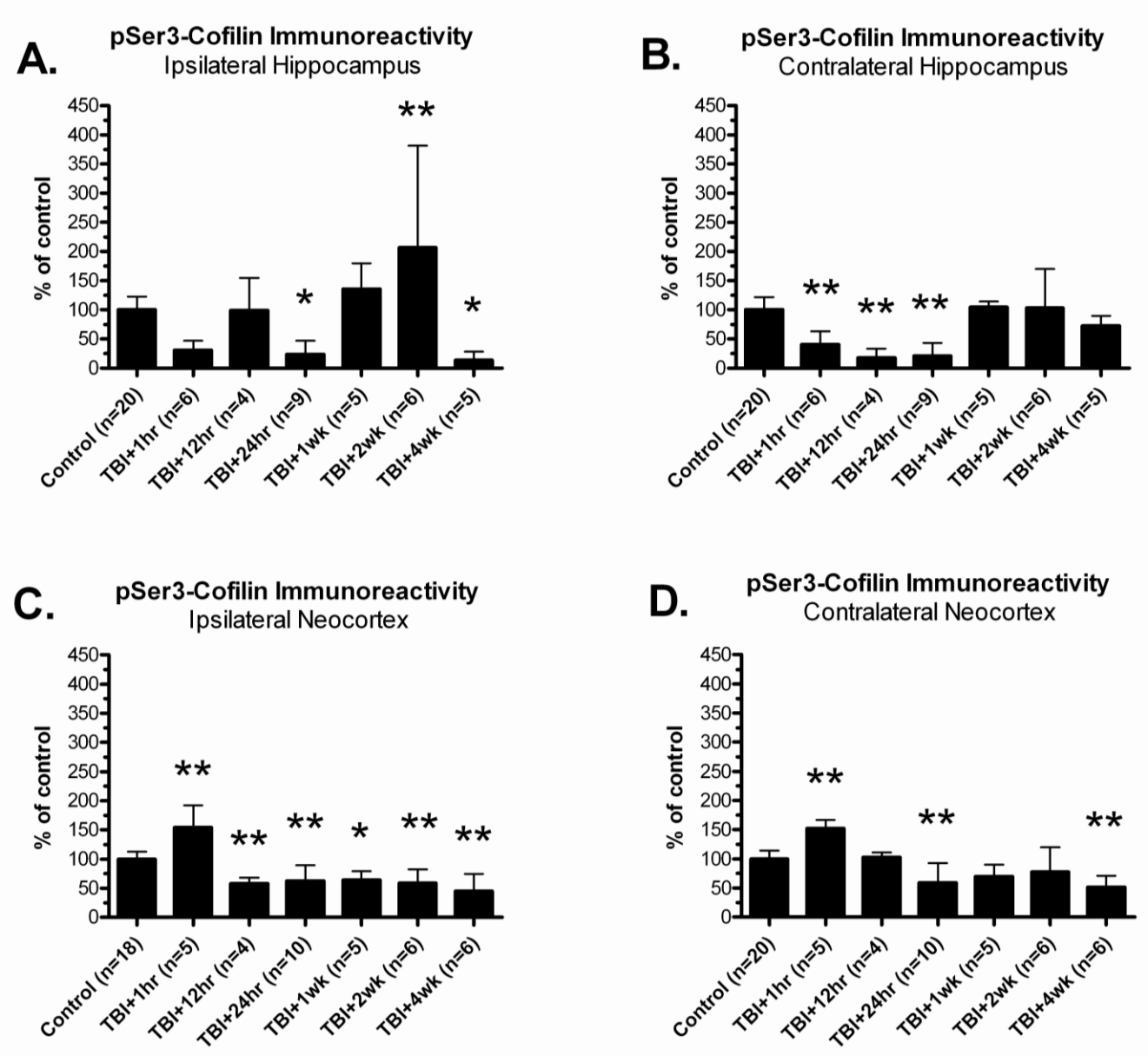
A.
pSer3-Cofilin Immunoreactivity
Ipsilateral Hippocampus
% of control
450
400
350
300
250
200
150
100
50
0
**
*
*
Control (n=20)
TBI+1hr (n=6)
TBI+12hr (n=4)
TBI+24hr (n=9)
TBI+1wk (n=5)
TBI+2wk (n=6)
TBI+4wk (n=5)
B.
pSer3-Cofilin Immunoreactivity
Contralateral Hippocampus
% of control
450
400
350
300
250
200
150
100
50
0
**
**
**
Control (n=20)
TBI+1hr (n=6)
TBI+12hr (n=4)
TBI+24hr (n=9)
TBI+1wk (n=5)
TBI+2wk (n=6)
TBI+4wk (n=5)
C.
pSer3-Cofilin Immunoreactivity
Ipsilateral Neocortex
% of control
450
400
350
300
250
200
150
100
50
0
**
**
**
*
**
**
Control (n=18)
TBI+1hr (n=5)
TBI+12hr (n=4)
TBI+24hr (n=10)
TBI+1wk (n=5)
TBI+2wk (n=6)
TBI+4wk (n=6)
D.
pSer3-Cofilin Immunoreactivity
Contralateral Neocortex
% of control
450
400
350
300
250
200
150
100
50
0
**
**
**
Control (n=20)
TBI+1hr (n=5)
TBI+12hr (n=4)
TBI+24hr (n=10)
TBI+1wk (n=5)
TBI+2wk (n=6)
TBI+4wk (n=6)

FIGURE 16 - Lateral TBI caused time- and region-dependent changes in pSer3-cofilin immunoreactivity. Ipsilateral and contralateral hemispheres of hippocampus and neocortex were dissected from post-TBI rats and their age-matched controls, separately homogenized, and subjected to immunoblotting with antibodies recognizing the serine 3 phosphorylated form of cofilin (pSer3-cofilin). Results indicate significant changes in pSer3-cofilin immunoreactivity following lateral TBI, relative to controls. In the ipsilateral hippocampus, for example, pSer3-cofilin decreased significantly at 24hr post-TBI, increased at 2wk post-TBI, but then decreased again at 4wk post-TBI, relative to controls (A). The contralateral hippocampus also underwent an acute decrease in pSer3-cofilin immunoreactivity, at 1hr, 12hr, and 24hr post-TBI, compared to controls (B). The neocortex showed a different pattern of changes in pSer3-cofilin immunoreactivity, with an increase at 1hr post-TBI followed by decreases at subsequent time points, in both the ipsilateral neocortex (C) and contralateral neocortex (D), relative to controls. Specifically, pSer3-cofilin immunoreactivity decreased below control levels at 12hr post-TBI and all later time points in the ipsilateral neocortex (C), and at 24hr and 4wk post-TBI in the contralateral neocortex (D). All comparisons were made by one-way ANOVA with Dunnett's *post hoc* test. *p<0.05, **p<0.01

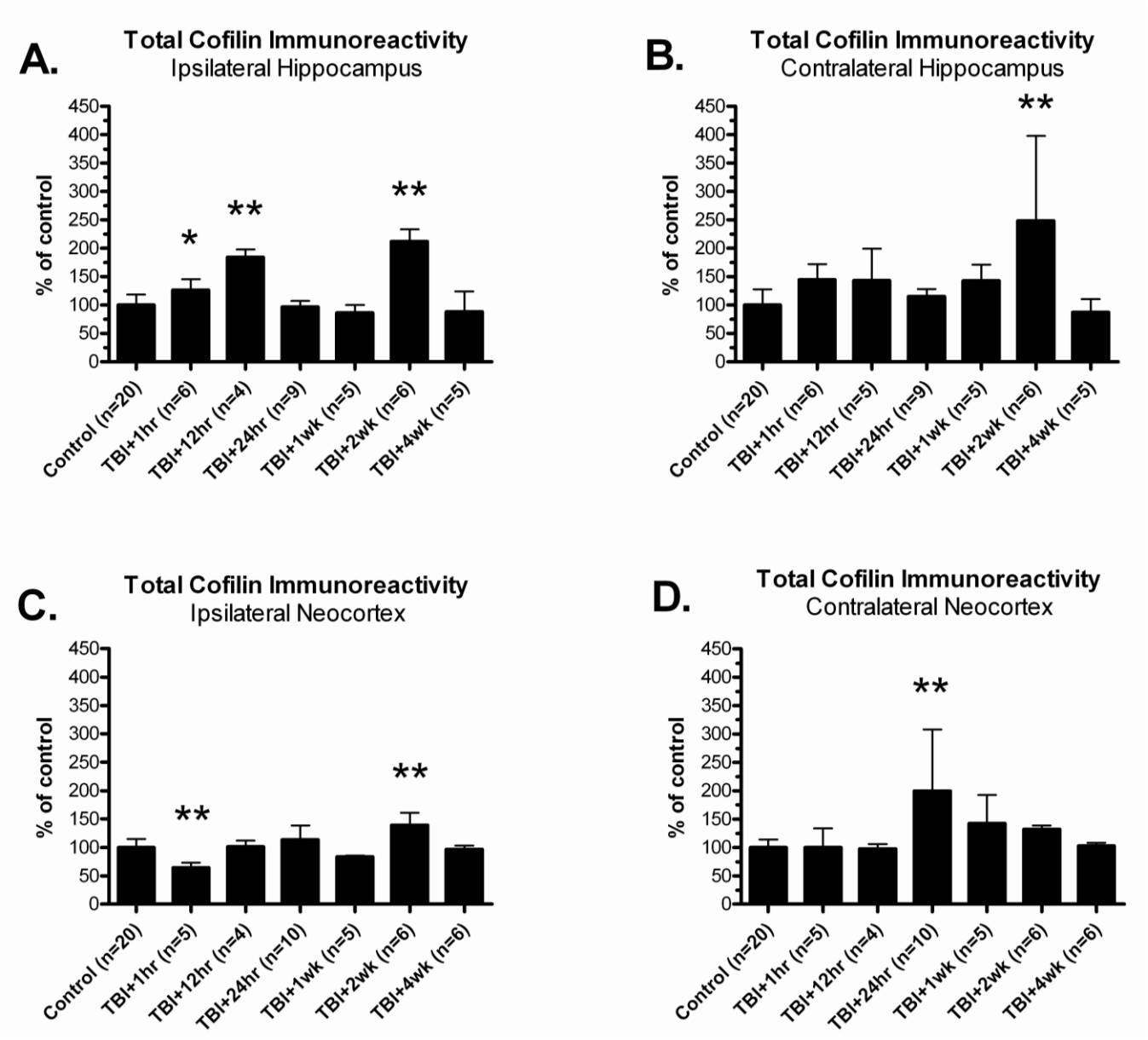
A.
Total Cofilin Immunoreactivity
Ipsilateral Hippocampus
% of control
450
400
350
300
250
200
150
100
50
0
*
**
**
Control (n=20)
TBI+1hr (n=6)
TBI+12hr (n=4)
TBI+24hr (n=9)
TBI+1wk (n=5)
TBI+2wk (n=6)
TBI+4wk (n=5)
B.
Total Cofilin Immunoreactivity
Contralateral Hippocampus
% of control
**
Control (n=20)
TBI+1hr (n=6)
TBI+12hr (n=5)
TBI+24hr (n=9)
TBI+1wk (n=5)
TBI+2wk (n=6)
TBI+4wk (n=5)
C.
Total Cofilin Immunoreactivity
Ipsilateral Neocortex
% of control
**
**
Control (n=20)
TBI+1hr (n=5)
TBI+12hr (n=4)
TBI+24hr (n=10)
TBI+1wk (n=5)
TBI+2wk (n=6)
TBI+4wk (n=6)
D.
Total Cofilin Immunoreactivity
Contralateral Neocortex
% of control
**
Control (n=20)
TBI+1hr (n=5)
TBI+12hr (n=4)
TBI+24hr (n=10)
TBI+1wk (n=5)
TBI+2wk (n=6)
TBI+4wk (n=6)

FIGURE 17 - Lateral TBI generally caused a transient increase in total cofilin immunoreactivity. Western analyses were repeated using an antibody recognizing cofilin regardless of Ser3 phosphorylation status ("total cofilin"). Analyses revealed time- and region-dependent changes in total cofilin immunoreactivity, relative to controls. In the ipsilateral hippocampus, for example, total cofilin immunoreactivity increased at 1hr, 12hr, and 2wk post-TBI, relative to controls (A). In the contralateral hippocampus, total cofilin immunoreactivity also increased above control levels, but only weeks later, at 2wk post-TBI (B). Unlike all other brain regions tested, the ipsilateral neocortex decreased in total cofilin immunoreactivity, at 1hr post-TBI, relative to controls. However, total cofilin immunoreactivity returned to control levels by 12hr post-TBI, and then increased above control levels weeks later, at 2wk post-TBI (C). The contralateral neocortex underwent a delayed increase in total cofilin immunoreactivity, at 24hr post-TBI, relative to controls (D). All comparisons were made by one-way ANOVA with Dunnett's *post hoc* test. $*p<0.05$, $**p<0.01$

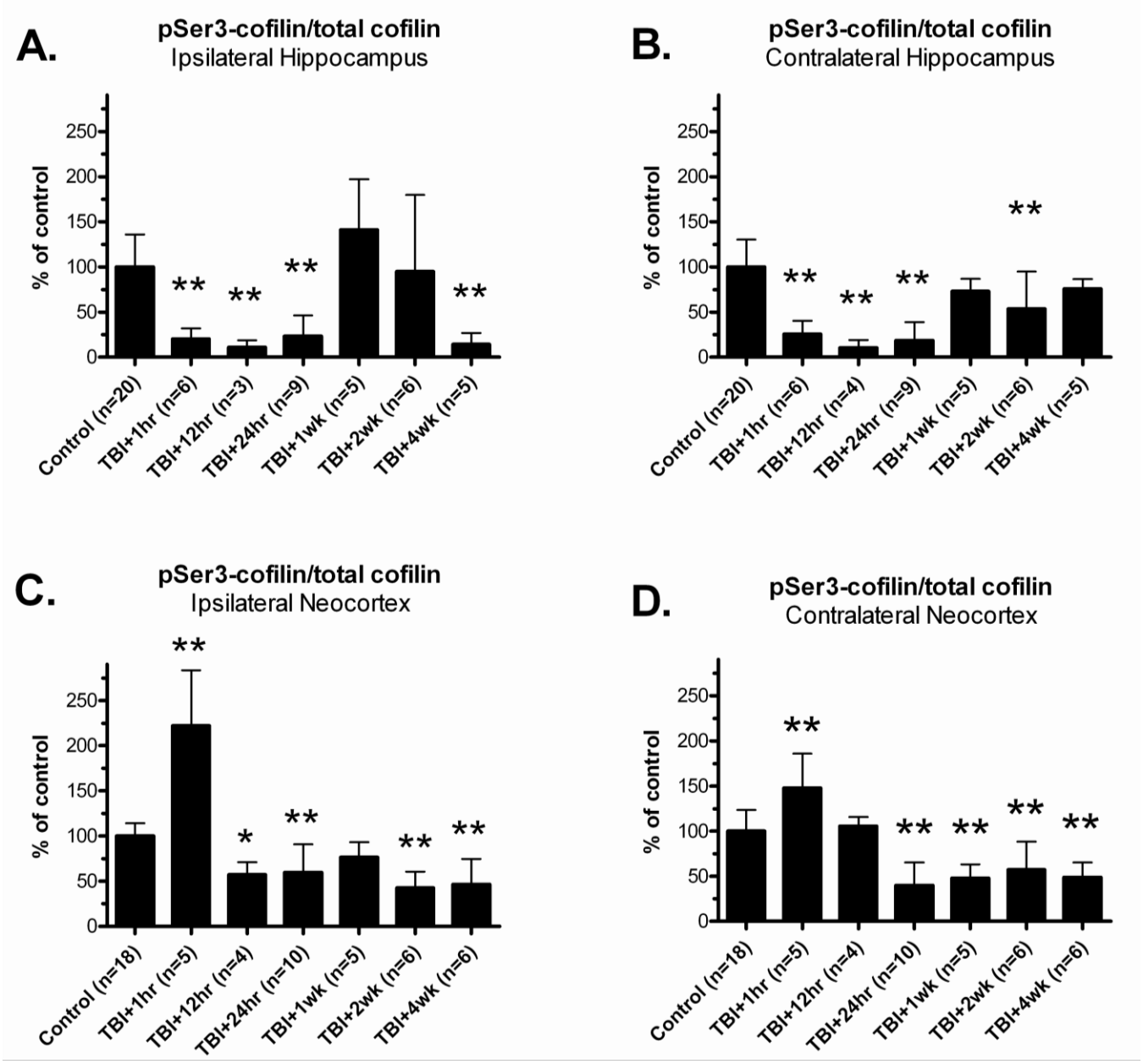
A.
pSer3-cofilin/total cofilin
Ipsilateral Hippocampus
% of control
0
50
100
150
200
250
**
**
**
**
Control (n=20)
TBI+1hr (n=6)
TBI+12hr (n=3)
TBI+24hr (n=9)
TBI+1wk (n=5)
TBI+2wk (n=6)
TBI+4wk (n=5)
B.
pSer3-cofilin/total cofilin
Contralateral Hippocampus
% of control
0
50
100
150
200
250
**
**
**
**
Control (n=20)
TBI+1hr (n=6)
TBI+12hr (n=4)
TBI+24hr (n=9)
TBI+1wk (n=5)
TBI+2wk (n=6)
TBI+4wk (n=5)
C.
pSer3-cofilin/total cofilin
Ipsilateral Neocortex
% of control
0
50
100
150
200
250
**
*
**
**
**
Control (n=18)
TBI+1hr (n=5)
TBI+12hr (n=4)
TBI+24hr (n=10)
TBI+1wk (n=5)
TBI+2wk (n=6)
TBI+4wk (n=6)
D.
pSer3-cofilin/total cofilin
Contralateral Neocortex
% of control
0
50
100
150
200
250
**
**
**
**
**
Control (n=18)
TBI+1hr (n=5)
TBI+12hr (n=4)
TBI+24hr (n=10)
TBI+1wk (n=5)
TBI+2wk (n=6)
TBI+4wk (n=6)

FIGURE 18 - Lateral TBI caused time- and region-dependent changes in the proportion of Ser3-phosphorylated cofilin. To determine whether TBI affected the proportion of Ser3 phosphorylated cofilin, pSer3-cofilin immunoreactivity data were normalized to total cofilin immunoreactivity data for each sample, yielding a ratio of pSer3-cofilin to total cofilin ("p/t cofilin"). Analysis of these data identified time- and region-dependent changes in p/t cofilin. In the ipsilateral hippocampus, for example, p/t cofilin was significantly below control levels at 1hr, 12hr, and 24hr post-TBI, and again at 4wk post-TBI (A). In the contralateral hippocampus, a similar reduction in p/t cofilin was observed at 1hr, 12hr, and 24hr post-TBI, and then at 2wk post-TBI, relative to controls (B). The ipsilateral neocortex showed an increase in p/t cofilin at 1hr post-TBI, followed by decreases in p/t cofilin at 12hr, 24hr, 2wk and 4wk post-TBI, relative to controls (C). A similar pattern was observed in the contralateral neocortex, where p/t cofilin was significantly above control levels at 1hr post-TBI but then dropped below control levels at 24hr, 1wk, 2wk, and 4wk post-TBI (D). All comparisons were made by one-way ANOVA with Dunnett's *post hoc* test. *$p<0.05$, **$p<0.01$

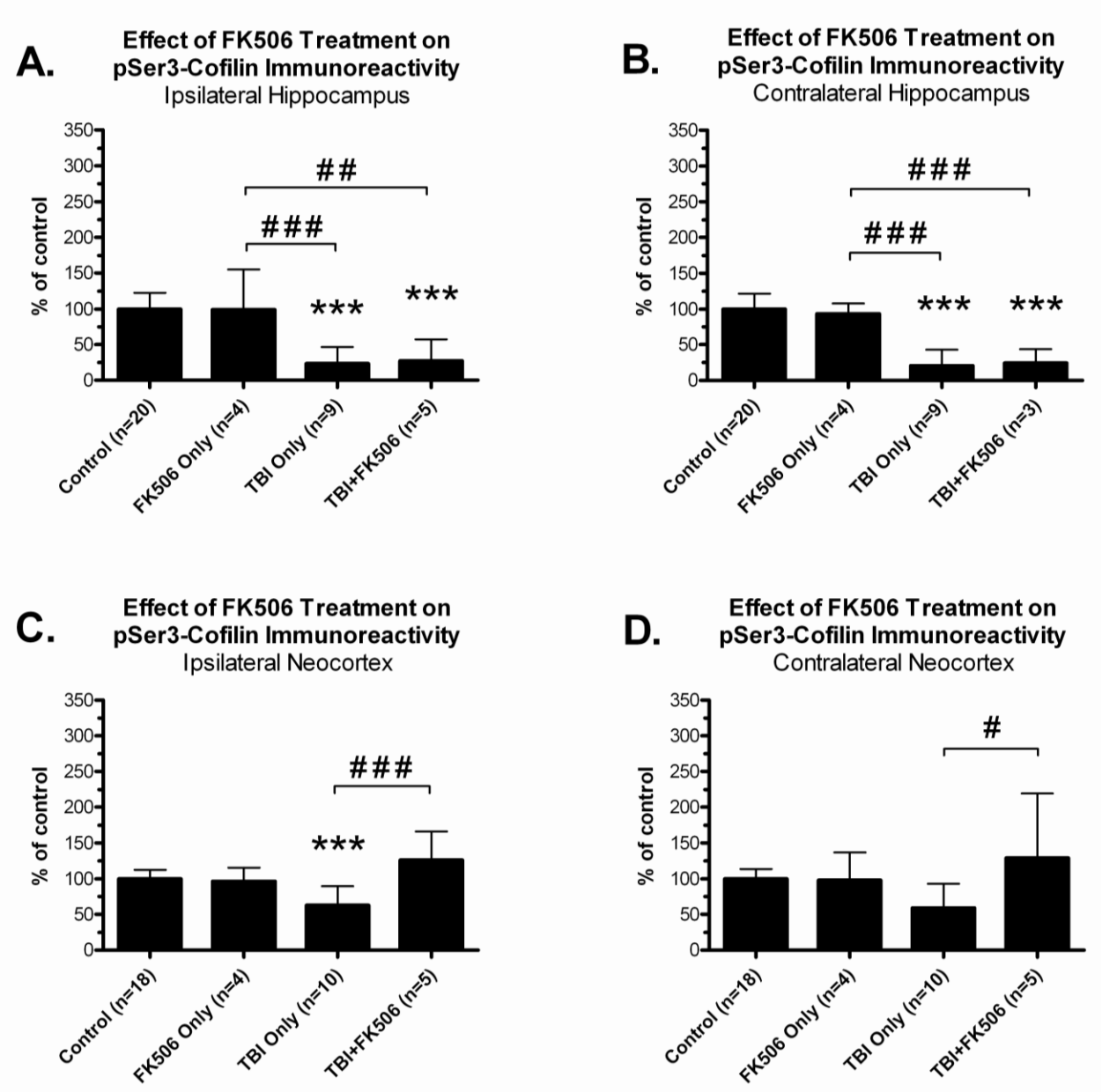
A.
Effect of FK506 Treatment on
pSer3-Cofilin Immunoreactivity
Ipsilateral Hippocampus
% of control
350
300
250
200
150
100
50
0
##
###
***
***
Control (n=20)
FK506 Only (n=4)
TBI Only (n=9)
TBI+FK506 (n=5)
B.
Effect of FK506 Treatment on
pSer3-Cofilin Immunoreactivity
Contralateral Hippocampus
% of control
350
300
250
200
150
100
50
0
###
###
***
***
Control (n=20)
FK506 Only (n=4)
TBI Only (n=9)
TBI+FK506 (n=3)
C.
Effect of FK506 Treatment on
pSer3-Cofilin Immunoreactivity
Ipsilateral Neocortex
% of control
350
300
250
200
150
100
50
0
###
***
Control (n=18)
FK506 Only (n=4)
TBI Only (n=10)
TBI+FK506 (n=5)
D.
Effect of FK506 Treatment on
pSer3-Cofilin Immunoreactivity
Contralateral Neocortex
% of control
350
300
250
200
150
100
50
0
#
Control (n=18)
FK506 Only (n=4)
TBI Only (n=10)
TBI+FK506 (n=5)

FIGURE 19 – A 1hr post-TBI administration of FK506 prevented the 24hr post-TBI loss of pSer3-cofilin immunoreactivity in the neocortex. Adult rats received either lateral fluid percussion TBI alone ("TBI only,"), TBI followed by a 1hr post-TBI injection of FK506 (5mg/kg; i.p.; "TBI+FK506"), FK506 injection but no TBI ("FK506 only"), or no treatment ("control"). Treated groups were sacrificed at 24hr post-TBI (or 23hr post-injection), along with equivalently-aged control rats. Ipsilateral and contralateral hemispheres of hippocampus and neocortex were dissected, separately homogenized, and subjected to immunoblotting with antibodies recognizing either the serine 3-phosphorylated cofilin (pSer3-cofilin). Statistical analysis identified region-specific effects of FK506 treatment on pSer3-cofilin phosphorylation. For example, FK506 treatment did not prevent the loss of pSer3-cofilin at 24hr post-TBI, in either the ipsilateral hippocampus (A) or contralateral hippocampus (B). In the neocortex, however, FK506 treatment completely blocked the loss of pSer3-cofilin at 24hr post-TBI in both the ipsilateral (C) and contralateral (D) hemispheres. All comparisons were made by one-way ANOVA with Tukey's *post hoc* test. **p*<0.05 *vs*. controls; ***p*<0.01 *vs*. controls; ****p*<0.001 *vs*. controls; # *p*<0.05 *vs*. other bracketed group; ## *p*<0.01 *vs*. other bracketed group; ### *p*<0.001 *vs*. other bracketed group

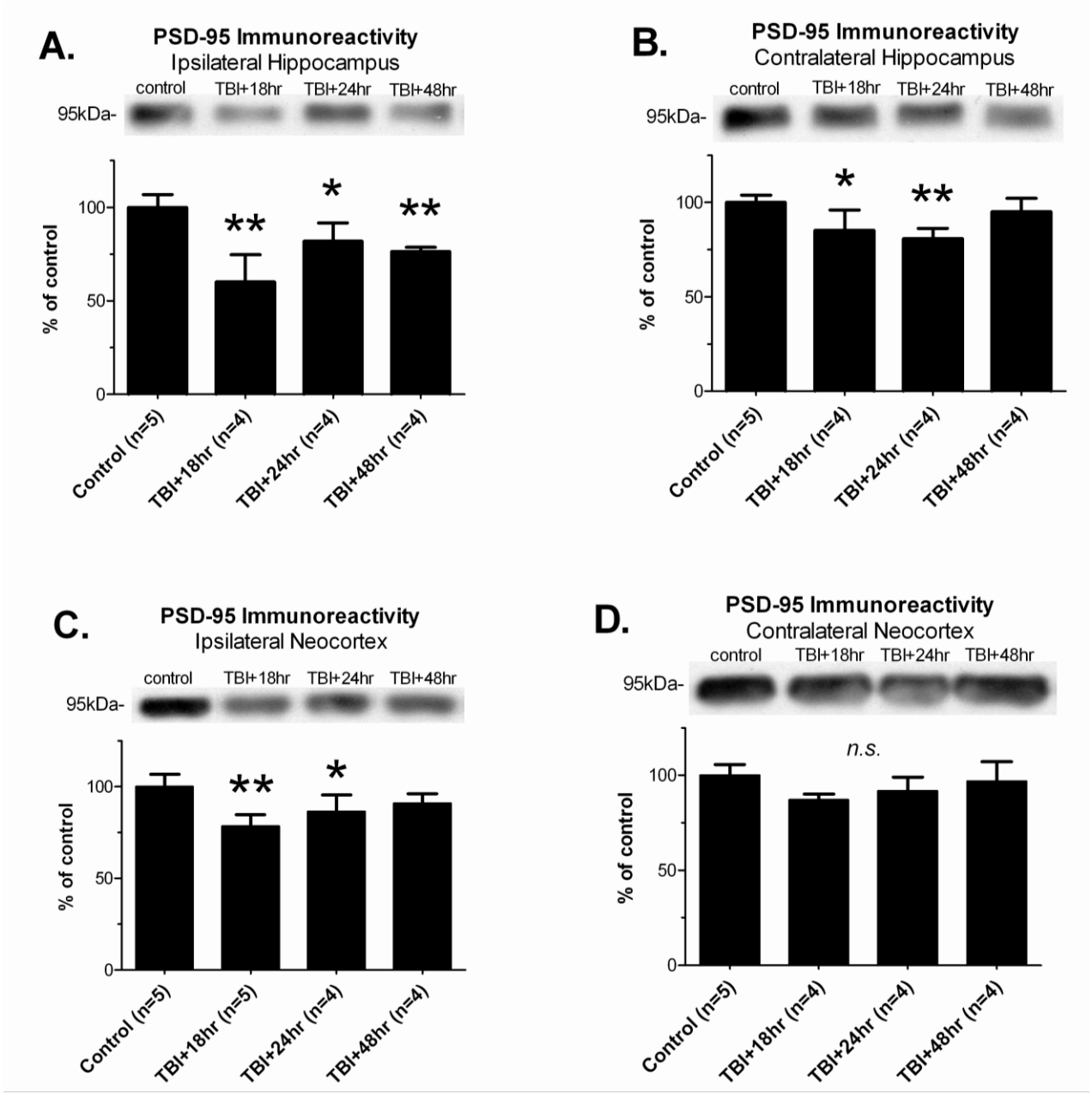
A.
PSD-95 Immunoreactivity
Ipsilateral Hippocampus
control
TBI+18hr
TBI+24hr
TBI+48hr
95kDa-
% of control
100
50
0
**
*
**
Control (n=5)
TBI+18hr (n=4)
TBI+24hr (n=4)
TBI+48hr (n=4)
B.
PSD-95 Immunoreactivity
Contralateral Hippocampus
control
TBI+18hr
TBI+24hr
TBI+48hr
95kDa-
% of control
100
50
0
*
**
Control (n=5)
TBI+18hr (n=4)
TBI+24hr (n=4)
TBI+48hr (n=4)
C.
PSD-95 Immunoreactivity
Ipsilateral Neocortex
control
TBI+18hr
TBI+24hr
TBI+48hr
95kDa-
% of control
100
50
0
**
*
Control (n=5)
TBI+18hr (n=5)
TBI+24hr (n=4)
TBI+48hr (n=4)
D.
PSD-95 Immunoreactivity
Contralateral Neocortex
control
TBI+18hr
TBI+24hr
TBI+48hr
95kDa-
n.s.
% of control
100
50
0
Control (n=5)
TBI+18hr (n=4)
TBI+24hr (n=4)
TBI+48hr (n=4)

FIGURE 20 - Lateral TBI caused a loss of PSD-95 immunoreactivity. Ipsilateral and contralateral hemispheres of hippocampus and neocortex were dissected from adult rats at 18hr, 24hr, and 48hr after lateral fluid percussion TBI, separately homogenized, and subjected to immunoblotting with antibody recognizing the post-synaptic protein, PSD-95. Lateral TBI caused a significant loss of PSD-95 immunoreactivity at 18hr, 24hr, and 48hr post-TBI in the ipsilateral hippocampus (A) and at 18hr and 24hr post-TBI in the contralateral hippocampus (B), relative to controls. In the ipsilateral neocortex, PSD-95 immunoreactivity also decreased significantly below control levels, at 18hr and 24hr post-TBI (C). In the contralateral neocortex, however, PSD-95 immunoreactivity did not differ significantly from controls, at any time point tested (D). . All comparisons were made by one-way ANOVA with Dunnett's post-hoc test. *$p < 0.05$; **$p < 0.01$; *n.s.*, no significant differences

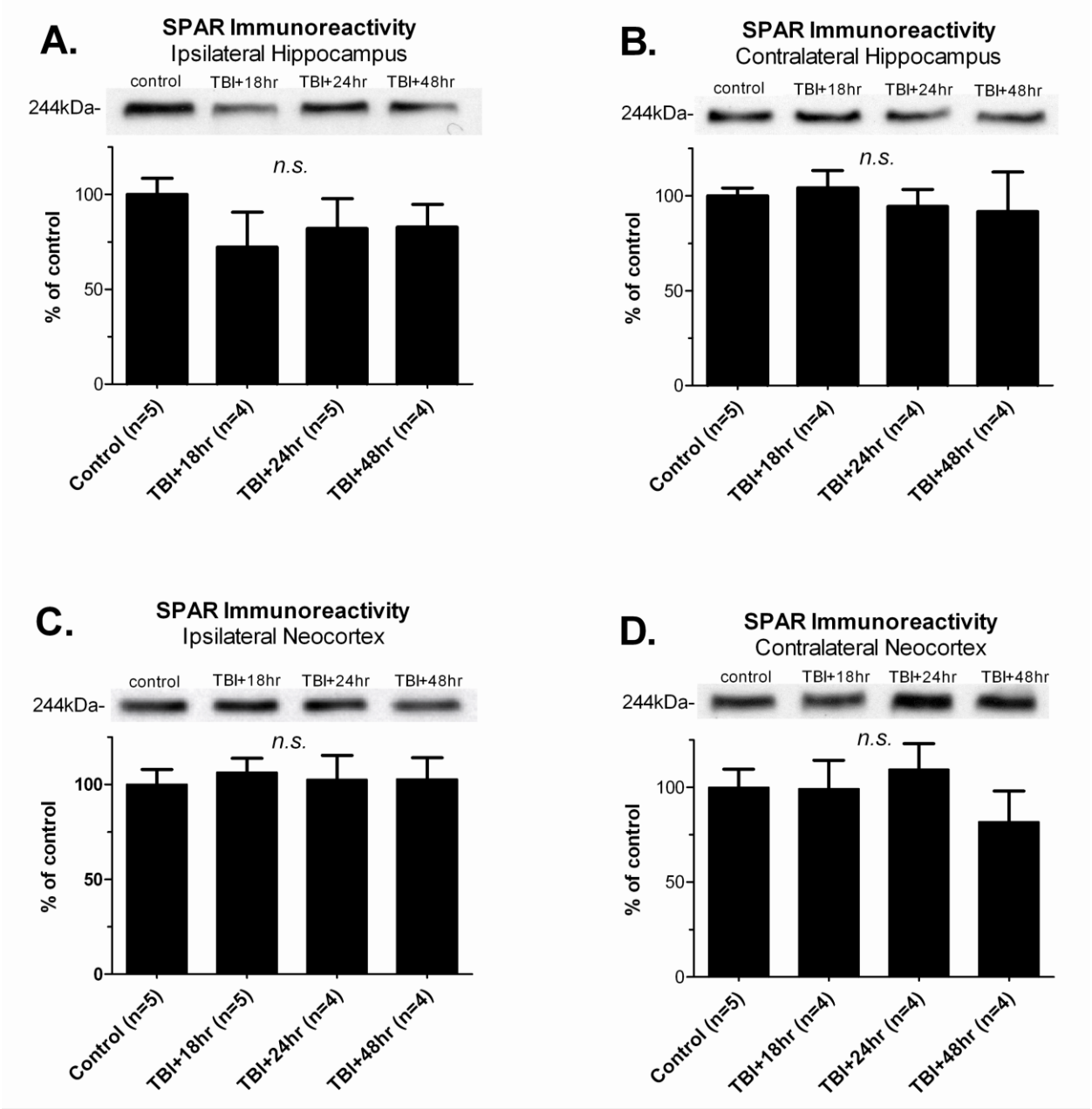
A.
SPAR Immunoreactivity
Ipsilateral Hippocampus
control
TBI+18hr
TBI+24hr
TBI+48hr
244kDa-
n.s.
% of control
100
50
0
Control (n=5)
TBI+18hr (n=4)
TBI+24hr (n=5)
TBI+48hr (n=4)
B.
SPAR Immunoreactivity
Contralateral Hippocampus
control
TBI+18hr
TBI+24hr
TBI+48hr
244kDa-
n.s.
% of control
100
50
0
Control (n=5)
TBI+18hr (n=4)
TBI+24hr (n=4)
TBI+48hr (n=4)
C.
SPAR Immunoreactivity
Ipsilateral Neocortex
control
TBI+18hr
TBI+24hr
TBI+48hr
244kDa-
n.s.
% of control
100
50
0
Control (n=5)
TBI+18hr (n=5)
TBI+24hr (n=4)
TBI+48hr (n=4)
D.
SPAR Immunoreactivity
Contralateral Neocortex
control
TBI+18hr
TBI+24hr
TBI+48hr
244kDa-
n.s.
% of control
100
50
0
Control (n=5)
TBI+18hr (n=4)
TBI+24hr (n=4)
TBI+48hr (n=4)

FIGURE 21 – Effect of lateral TBI on SPAR immunoreactivity. Ipsilateral and contralateral hemispheres of hippocampus and neocortex were dissected from adult rats at 18hr, 24hr, and 48hr after lateral fluid percussion TBI, separately homogenized, and subjected to immunoblotting with an antibody recognizing SPAR. No change in SPAR immunoreactivity was detected at any time point tested, in the ipsilateral hippocampus (A), contralateral hippocampus (B), ipsilateral neocortex (C), or contralateral neocortex (D), relative to controls. All comparisons were made by one-way ANOVA with Dunnett's *post hoc* test. *n.s.*, no significant differences

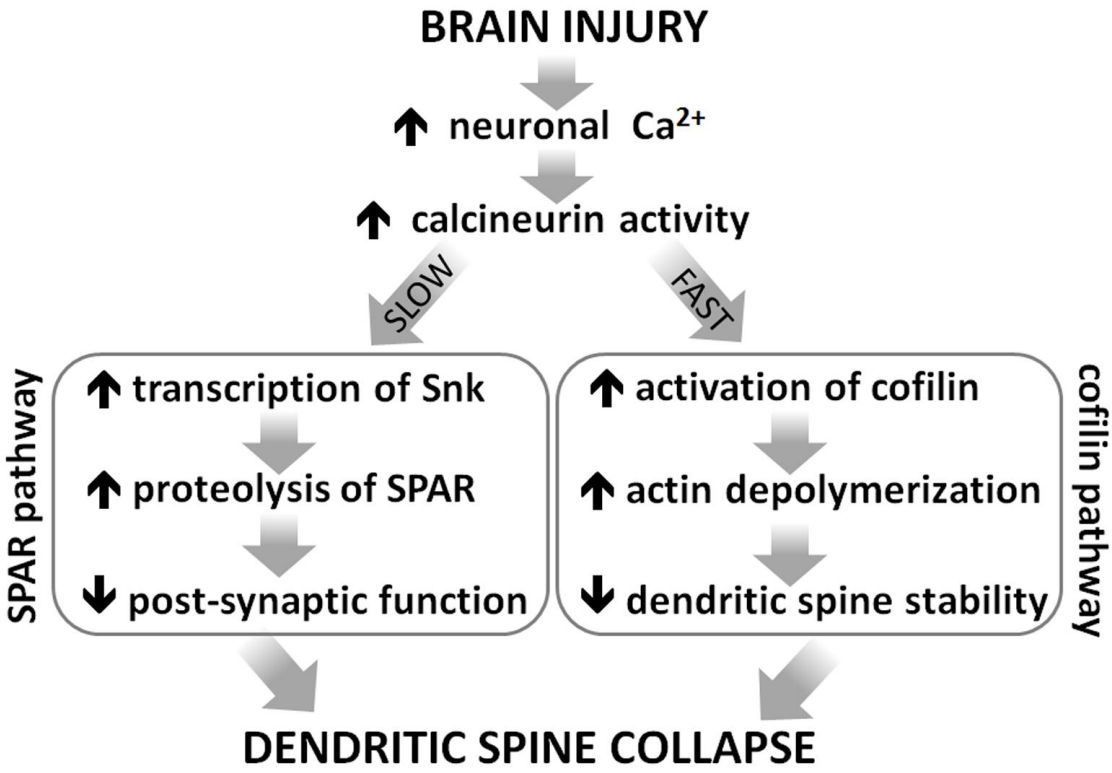
BRAIN INJURY
↑ neuronal Ca^{2+}
↑ calcineurin activity
SLOW
FAST
SPAR pathway
↑ transcription of Snk
↑ proteolysis of SPAR
↓ post-synaptic function
↑ activation of cofilin
↑ actin depolymerization
↓ dendritic spine stability
cofilin pathway
DENDRITIC SPINE COLLAPSE

FIGURE 22 – Calcineurin-dependent mechanisms by which brain injury could cause dendritic spine collapse. Brain injury can cause an increase in the activity of the calcium-sensitive phosphatase, calcineurin (CaN). CaN-dependent signaling can then lead to dendritic spine collapse through regionally-distinct signaling pathways. In the neocortex, for example, CaN activity may lead to a rapid de-phosphorylation/activation of the actin-depolymerizing protein, cofilin. Excessive cofilin activity could disrupt the spine's actin-rich cytoskeleton, resulting in spine shrinkage or de-stabilization [23]. In the hippocampus, however, a different mechanism may be involved - a mechanism involving CaN but not cofilin. For example, an injury-induced increase in CaN activity can lead to a transcriptional up-regulation of Snk (serum-inducible kinase), ultimately resulting in the targeted proteolysis of a spine-stabilizing protein, SPAR (spine-associated Rap guanosine triphosphatase activating protein) [12]. SPAR loss is associated with degeneration of post-synaptic function and structure, including spine loss [12,141,145]. Therefore, cofilin activation and SPAR proteolysis represent different mechanisms by which CaN may cause spine loss. Evidence from the present study favors cofilin activation as a regional mechanism of spine loss after TBI but does not rule out focal involvement of SPAR proteolysis.

CHAPTER III

TRAUMATIC BRAIN INJURY CAUSES A TACROLIMUS-SENSITIVE INCREASE IN NON-CONVULSIVE SEIZURES IN A RAT MODEL OF POST-TRAUMATIC EPILEPSY

INTRODUCTION

Every 16 minutes in the U.S., a traumatic brain injury (TBI) occurs which results in chronic, recurrent seizures [160,163]. This form of acquired epilepsy, known as post-traumatic epilepsy, is often refractory to medications or surgery [168,169] and so can be a lifelong disability for the victim and a financial burden which extends to their community. An ideal therapy would prevent or limit the development of post-traumatic epilepsy, but no such therapy has yet been found [171]. A better understanding of how the injured brain becomes epileptic, a process called epileptogenesis, should reveal novel opportunities for preventing post-traumatic epilepsy.

Epileptogenesis is thought to begin within minutes to hours after brain injury [176,177], though the underlying mechanisms are still unknown. One hypothesis is that a pathological increase in intracellular calcium triggers molecular changes which culminate in neuronal hyperexcitability [33,251]. Calcium-sensitive enzymes which regulate neuronal excitability may thus play a critical role in epileptogenesis. Indeed, animal models of acquired epilepsy have implicated a calcium-sensitive phosphatase, calcineurin [251,252,253,254]. Recent research by our lab suggests that calcineurin

may also be involved in the epileptogenesis after TBI. In a study of lateral fluid percussion TBI in rats, a well-characterized model of post-traumatic epilepsy [173,255], we identified an acute post-injury increase in calcineurin activity [186]. This increase could facilitate epileptogenesis through the dysregulation of hyperpolarizing cyclic nucleotide-gated (HCN) channels [254] or voltage-gated potassium channels ($K_V2.1$) [256]. An increase in calcineurin activity may also alter excitatory synaptic circuits by destabilizing dendritic spines [11,12,118,204,211,233], potentially creating opportunities for maladaptive plasticity [78]. The increase in calcineurin activity we observed after TBI could therefore be an early but critical step in epileptogenesis.

The present study characterized the importance of calcineurin activity in a rat model of post-traumatic epilepsy. We administered the calcineurin inhibitor, Tacrolimus (FK506), to adult rats 1 hour after lateral fluid percussion TBI and then monitored spontaneous seizure activity 5 weeks or 33 weeks later. The results indicate a significant disease-modifying effect of Tacrolimus in this model of post-traumatic epilepsy.

MATERIALS AND METHODS

Animal Use and Housing Conditions

All animal care and use complied with the Guide for the Care and Use of Laboratory Animals described by the National Institutes of Health and was approved in advance by the Virginia Commonwealth University Institutional Animal Care and Use Committee. Animals received *ad libitum* access to food and water and were kept in temperature- and humidity-controlled housing on 12 hour light/dark cycles throughout

the experiment. The present study involved a total of 49 male, Sprague-Dawley rats acquired as adults (90 day old) and randomly assigned to treatment groups in two experiments. Experiment 1 assessed spontaneous seizure activity at 33 weeks post-TBI and involved the following treatment groups: controls (naïve, age-matched rats; n=7), sham TBI (n=3), TBI Only (n=10), and TBI+TAC (n=14). Experiment 2 examined spontaneous seizure activity at 5 weeks post-TBI in different rats assigned to the same treatment groups: control (naïve, age-matched rats; n=4), TBI Only (n=5), and TBI+TAC (n=6).

Lateral Fluid Percussion Injury

The procedure for lateral fluid percussion injury has been described previously [186,233] and was identical for Experiments 1 and 2. All rats except controls were each anesthetized with 3% isoflurane in a carrier gas mixture of 30% N_2O and 70% O_2 and placed into a stereotactic frame. A 5mm circular craniotomy was made over the left hemisphere using a manual trephine centered between Lambda and Bregma (approximately -4.4mm Bregma), and midway between the sagittal suture and the lateral ridge. A modified syringe hub was placed over the craniotomy, affixed to the skull with a cyanoacrylate adhesive, and then secured with dental acrylic. The hub was filled with sterile saline and the scalp was sutured closed over the hub. On the following day, the same rats were anesthetized with isoflurane (4min of 4% isoflurane in a carrier mixture of 30% N_2O and 70% O_2) and subjected to fluid percussion of the intact dura over their left parietal cortex. Sham TBI rats received the same dose of isoflurane but no fluid percussion. The fluid percussion device used in Experiment 1 is identical to that

described by Dixon and colleagues (Dixon *et al.*, 1987). A newer model of this device was used in Experiment 2. Fluid percussion pressure was measured at the time of fluid impact, by an external pressure transducer adjacent to the hub. The Luer-Loc fitting, screw, and dental cement were removed from the skull and the scalp was sutured closed immediately after fluid percussion injury (or, in sham TBI rats, immediately after discontinuation of isoflurane anesthesia). If apnea occurred immediately following TBI, rats were mechanically ventilated with room air until spontaneous respiration resumed. Immediately following injury, rats were placed in a supine position and the time at which they righted themselves was recorded. Body temperature was maintained for at least 1 hour after injury by placement on a heating pad set to "low." Rats were then returned to their home cages and monitored daily. Some rats (TBI+TAC) received a single injection of Tacrolimus (5mg/kg; intraperitoneal, i.p.; Astellas Pharma Inc., Tokyo, Japan) 1 hour after TBI.

Video-Electrocorticography

Each rat was anesthetized with 3% isoflurane in a carrier gas mixture of 30% N_2O and 70% O_2. The scalp was then incised and reflected, and surgical steel screws with Teflon-coated leads (1.6mm long shafts, 10mm long leads; Plastics One, Norfolk, VA, U.S.A.) were implanted over the frontal cortex (3.5mm anterior to Bregma, +/- 2.5mm lateral to midline), the right parietal cortex (2.0mm posterior to Bregma, +2.5mm lateral to midline) and the left parietal/occipital cortex (8.0mm posterior to Bregma, -2.5mm lateral to midline). To protect underlying brain tissue, electrode screws were inserted into the skull to a depth of no more than 0.8mm (*i.e.,* half of the electrode screw

length). Next, the tips of each electrode lead were inserted into a plastic electrode platform (Plastics One), the entire headset was then secured in place with dental acrylic, and the scalp was sutured closed around the base of the headset. Rats were then allowed to recover for at least 3 days prior to EEG recording, after which they were lightly sedated with isoflurane (*i.e.,* to the point of slowing reflexes) and connected to a video-ECoG system (BMSI 5000, Nicolet, Middleton, WI, U.S.A.). A bipolar montage was used, with individual traces representing the voltage difference between (from top trace to bottom) the two frontal leads, the two ipsilateral leads, the two contralateral leads, and the two posterior leads. In Experiment 1, video-ECoG was recorded for at least 12 hours per rat. In Experiment 2, video-ECoG was recorded daily, or every other day, until at least 40 hours were recorded in total per rat. To ensure the quality of video data for behavioral analysis, recordings were scheduled so that at least two-thirds of video would be recorded during light hours.

Analysis of Spontaneous Seizures (Experiments 1 and 2)

Video-ECoG data in Experiment 1 were analyzed offline by three identically-trained reviewers, one of whom was blinded to treatment groups. In Experiment 2, all video-ECoG data were analyzed offline by a single reviewer who was blinded to treatment groups. All ECoG traces were visually reviewed for electrographic seizures, defined as paroxysmal, rhythmic trains of spikes, waves, or spike-waves with amplitude at least double that of baseline (*i.e.*, the 3-second epoch preceding the event) and a duration of 5 seconds or longer. The duration of ECoG discharge was interpreted as seizure duration. To characterize ECoG power distribution, spectral analysis with

Insight II software was performed on a representative sample of seizures (200Hz sampling of ≥3 second epochs; Persyst Corporation, Prescott, AZ). To estimate the average frequency of seizures (seizures per hour) for each rat, the number of seizures observed on video-ECoG was divided by the number of video-ECoG hours reviewed. Seizure behavior was scored by comparison to a modified Racine scale [257]: sudden freezing was scored as a "0," facial twitching as a "1," head bobbing as a "2," forelimb clonus as a "3," rearing as a "4," and falling or jumping as a "5." Seizures with a Racine score of 0 to 2 were considered "non-convulsive," whereas those with a Racine score of 3 to 5 were identified as "convulsive." Seizures were characterized as "non-convulsive" (Racine stage 0 to 2) or "convulsive" (Racine stage 3 to 5) according to the corresponding behavior.

Ethosuximide and fos-Phenytoin Challenges (Experiment 1)

A subset of rats in Experiment 1 was used for additional experiments involving conventional anti-seizure medications. Any epileptic, post-TBI rats with a functioning ECoG headset were included in these experiments, regardless of treatment group. These rats were administered a single dose of either ethosuximide ("ETX"; 25mg/kg; i.p.; Sigma Aldrich, St. Louis, MO, U.S.A.) or *fos*-phenytoin ("fPHT;" 40mg/kg; i.p. APP Pharmaceuticals, LLC, Schaumburg, IL, U.S.A.) while being monitored with video-ECoG. At least 2 hours of video-ECoG were recorded prior to drug administration, and at least another 2.5 hours were recorded thereafter. A reviewer blind to the time of drug administration then visually reviewed ECoG traces for electrographic seizures (see criteria above). Seizure frequency (seizures/hour) and duration were calculated for the

2 hour period preceding drug administration and for a 2 hour period beginning 30 minutes after drug administration, to allow time for drug absorption. All pre- and post-drug data were normalized to pre-drug data for each rat. To characterize time-dependent changes in seizure frequency, seizure frequency was also calculated for 30 minute segments of each video-ECoG recording. To control for hourly fluctuations in seizure frequency which were not related to drug administration, analyses were repeated on previously recorded video-ECoG of the same rats, in which the recording conditions were the same except that no drugs were administered.

Histology and Analysis of Neocortical Volume (Experiments 1 and 2)

Rats were deeply anesthetized with a euthanasia cocktail (390mg/kg of pentobarbital, 50mg/kg of phenytoin; i.p.) and then transcardially perfused with room-temperature 0.9% saline followed by phosphate-buffered 4% paraformaldehyde (Pease's fixative). Brains were extracted whole and then immersed in Pease's fixative overnight at 4ºC. Brains were examined grossly for evidence of electrode injury, typically appearing as a small (<1mm) brown lesion on the surface of the neocortex underlying an electrode. Any rats showing such injury were excluded from all analyses. Brains were blocked to remove tissue rostral to Bregma and caudal to Lambda. Tissue blocks were then sectioned in the coronal plane by vibratome (Leica, Wetzler, Germany). Sections were cut slowly and at a thickness of 75µm to minimize fraying and folding of peri-lesional tissue. Beginning at the hippocampal commissure (-0.8mm Bregma), every eighth section was retained until 9 sections were collected per brain (1-in-8 series, 600µm intervals; last section at -5.6mm Bregma). This range permitted

analysis of tissue located 3.6mm rostral and 1.2mm caudal to the site of fluid percussion impact. Slide-mounted sections were stained with thionine, dehydrated in ethanol, cleared in xylene, and coverslipped with Permount (Thermo Scientific). Sections were then imaged through a macro lens (0.5x) on a light microscope (Nikon Eclipse E800M). Images were opened in ImageJ [258], which was then used to trace the borders of the ipsilateral and contralateral neocortex and measure the enclosed area. The area of the ipsilateral neocortex was then divided by that of the contralateral neocortex, yielding a ratio ("RatioCx") for each brain section [259]. An analogous procedure was used to calculate a ratio of the hippocampal hemispheres (RatioHp). Regional boundaries and distances from Bregma were defined according to a stereotaxic atlas [188].

Statistical Analysis

The normality of data distribution was assessed by Shapiro Wilk test (α=0.05). Normal data were compared by paired Student's t test, unpaired Student's t test, or one-way analysis of variance (ANOVA) with Tukey's *post hoc* test (for paired, single, or multiple comparisons, respectively), including the following: FPI pressure, subject age, post-TBI time, and pre *vs*. post-fPHT seizure frequency and duration. Non-normal data were compared by Wilcoxon matched-pairs signed rank test, Mann Whitney test, or Kruskall-Wallis test with a *post hoc* Mann Whitney test (for paired, single, or multiple comparisons, respectively), including the following: righting reflex latency; seizure frequency; seizure duration; total seizure time; pre- *vs*. post-ETX seizure frequency; RatioCx; RatioHp. Acute mortality rate, prevalence of seizures, and prevalence of thalamic calcifications were compared across groups using a Chi-square test.

Spearman's test was used to assess the correlation between seizure frequency and each histological measure (RatioCx, RatioHp, and thalamic calcifications). When testing for a correlation between seizure frequency and thalamic calcifications, each rat was scored as a "1" or "0" depending on the presence or absence of calcifications, respectively. All statistical analyses were performed with an alpha level of 0.05, using GraphPad Prism (version 5.0; GraphPad Software, La Jolla, CA, U.S.A.). Data are reported as mean ± standard deviation (SD) in the text but are illustrated as mean ± standard error of the mean (SEM) in the figures. *N* values represent the number of rats, unless stated otherwise.

RESULTS

The present study used a total of 49 male, Sprague-Dawley rats acquired as adults (90 day old) and randomly assigned to treatment groups in two experiments. Rats were subjected to traumatic brain injury (TBI) by lateral fluid percussion and then monitored for spontaneous seizure activity at either 33 weeks post-TBI (Experiment 1) or 5 weeks post-TBI (Experiment 2).

Mortality and Severity of Lateral Fluid Percussion Injury

To ensure that TBI severity was comparable between Experiments 1 and 2, we examined two correlates of TBI severity, the latency to recovery of righting reflex after TBI ("righting time") and the acute mortality rate (*i.e.*, within 7 days of TBI). Overall, the average righting time was 9.1 ± 3.8 minutes and the average mortality rate was 14%. Neither righting time nor acute mortality rate differed significantly between experiments

(righting time, p=0.4599; acute mortality rate, χ^2 [5]=3.461, p=0.6293), thus indicating that TBI severity was equivalent between the two experiments.

EXPERIMENT 1 – Adult, male Sprague-Dawley rats (n=34; 14 ± 1 weeks old) were administered lateral fluid percussion TBI or a sham injury (n=3), or were kept as age-matched controls (n=7). At 1 hour post-TBI, rats received either a single dose of the calcineurin inhibitor, Tacrolimus (5mg/kg; i.p.; "TBI+TAC"; n=14) or no injection ("TBI Only"; n=10). Age at the time of TBI (or sham) did not differ significantly among treatment groups (F [2,16]=0.4307, p=0.6574; Table 1). Three rats died within 7 days of TBI (acute mortality rate, 13%), including one rat humanely sacrificed due to severe motor impairment. Acute mortality rate varied across treatment groups but not to a statistically significant extent (mortality rates by treatment: TBI Only, 20%; TBI+TAC, 7%; χ^2 [2]=0.8816, p=0.6435). The rats which died acutely after TBI were excluded from all analyses, as were the additional two rats that died after 7 days post-TBI but before data collection. Three of the surviving rats (TBI+TAC group) exhibited apnea immediately following TBI and were mechanically ventilated with room air until spontaneous respirations resumed (mean duration of ventilation, 1.8 ± 1.1 minutes). Fluid percussion pressure (surviving rats) and righting time (all rats) were measured as correlates of injury severity. Among the rats surviving TBI and used for video-ECoG analysis, fluid percussion pressure averaged 2.7 ± 0.1 atmospheres and righting time averaged 9.5 ± 4.2 minutes (Table 1). Neither fluid percussion pressure nor righting time differed significantly between TBI Only and TBI+TAC rats (fluid percussion pressure, t [15]=1.495, p=0.1558; righting time, p=0.5622), which demonstrates that TBI severity was equivalent between these groups.

EXPERIMENT 2 – Adult, male Sprague-Dawley rats (n=15; 14 ± 1 weeks old) were administered lateral fluid percussion TBI, followed 1 hour later by either Tacrolimus (n=6; TBI+TAC) or no injection (n=5; TBI Only). Uninjured littermates were kept as age-matched controls (n=4; Control). Two rats in the TBI+TAC group died within 7 days of TBI (acute mortality rate, 33%) and so were excluded from analysis. All other rats survived until completion of the experiment. Overall, the acute mortality rate associated with TBI in Experiment 2 was 18%. Fluid percussion pressure and acute mortality were again used to approximate injury severity. The mean fluid percussion pressure among surviving rats was 2.36 ± 0.04 atmospheres, and the mean righting time was 8.3 ± 2.8 minutes (Table 1). Neither injury measure differed significantly between TBI Only and TBI+TAC rats (fluid percussion pressure, t [7]=1.562, p=0.1622; righting time, p=0.9048), indicating that the severity of TBI was equivalent between these groups.

Video-Electrocorticography Revealed Two Distinct Types of Late Post-Traumatic Seizures (Experiment 1)

We used simultaneous video-ECoG to monitor spontaneous seizure activity at 33 ± 5 weeks after TBI or sham, or at the equivalent age in control rats (Figure 1A,B). One rat (sham TBI) was excluded from analysis due to a surgical injury of the neocortex which occurred during implantation of the ECoG electrodes. Age at time of video-ECoG did not differ significantly among treatment groups (F [3,22]=2.539; p=0.0827; Table 1). On average, video-ECoG was recorded over the course of 8 ± 7 days for a total of 51 ± 15 hours per rat (Table 1). In one case the ECoG headset detached from a rat after

only two days of recording, limiting that rat's ECoG record to 12.4 hours. We confirmed electrode depth by examining the neocortex *post-mortem*. Two rats (TBI Only and TBI+TAC) were each found to have a small (<1mm) neocortical lesion at an electrode site and so were excluded from all analyses. The remaining 1,315 hours of ECoG data were visually reviewed for electrographic seizures, defined as paroxysmal, rhythmic trains of spikes, waves, or spike-waves, lasting 5 seconds or longer and with an amplitude at least double that of baseline ECoG activity.

All rats exhibited arrhythmic, low-amplitude ECoG activity during awake behavior (Figure 1C). In sharp contrast to this baseline activity were observed two distinct types of electrical seizures. One seizure type appeared on the ECoG as a burst of high-voltage spikes, followed by low-voltage fast activity which evolved into high-voltage spikes and waves (Figure 1D,E). Spectral analysis of these seizures showed dominant power in the delta (<4Hz) and theta (4 to 8Hz) ranges (Figure 1E). Analysis of the corresponding video revealed a tonic contraction followed by forelimb clonus, rearing, and falling (*i.e.*, progression from Racine stage 3 to 5) – we therefore classified these events as "convulsive seizures." Previous studies of lateral fluid percussion TBI have reported similar seizures [173,259].

The present study identified convulsive seizures in two rats (TBI+TAC) during video-ECoG recording months after TBI. These seizures occurred at a rate of 0.05 ± 0.04 per hour and lasted an average of 95 ± 14 seconds (n=5 seizures; range 78 – 110 seconds). A third rat (TBI Only) exhibited a convulsive seizure prior to video-ECoG, at 13 weeks post-TBI, but no additional seizures during video-ECoG. Overall, only 5

convulsive seizures were recorded, rarity which precluded further analysis of these seizures.

The second type of seizure we observed was distinct in terms of electrographic appearance, spectral profile, and behavioral correlate. This type of seizure appeared on the ECoG as a rhythmic train of spike-waves, beginning abruptly or building-up rapidly across all four ECoG leads, and lasting for tens of seconds (Figure 1F). These discharges had a spike frequency of 6 to 8Hz, peak spectral power in the theta (4 to 8Hz) and beta (12 to 18Hz) ranges (Figure 1G), and could be interrupted by alerting stimuli such as sudden changes in lighting or noise (data not shown). The corresponding video showed subtle but stereotyped changes in behavior, ranging from behavioral arrest (or immobility) to head bobbing (Racine stage 0 to 2) - we termed these events “non-convulsive seizures.” Similar seizures have been described in studies of adult rats following lateral [255] or parasagittal fluid percussion TBI [172,255,260] or neonatal hypoxic injury [261].

We identified spontaneous, non-convulsive seizures at 33 weeks post-TBI in 94% rats (16 of 17), prevalence similar to that observed months after parasagittal fluid percussion TBI [172,260]. One rat (TBI Only) did not exhibit any non-convulsive seizures on video-ECoG, only a single convulsive seizure which occurred prior to video-ECoG recording (see above). The two other rats with convulsive seizures also exhibited non-convulsive seizures, though convulsive and non-convulsive seizures were never observed on the same day in the same rat. A total of 3,279 non-convulsive seizures were identified in the video-ECoG record of TBI rats.

Previous ECoG studies have reported idiopathic seizure activity in uninjured Sprague-Dawley rats, typically beginning around 7-8 months of age (*e.g.*, [172,260]). Accordingly, the present study identified non-convulsive seizures in 3 of 7 control rats and 2 of 2 sham TBI rats (average age, 10 ± 2 months). The seizures in control and sham TBI rats were similar electrographically, characterized by a generalized onset, a spike-wave morphology, and peak spectral power in the theta and beta ranges (Figure 2A). The corresponding video showed behavioral freezing (or immobility) lasting at least as long as the electrographic discharge.

TBI and Age Each Increased the Frequency and Duration of Non-Convulsive Seizures

The non-convulsive seizures of age-matched control and sham TBI rats resembled those of TBI rats (Figure 2A-C). We therefore compared treatment groups in terms of seizure prevalence, frequency, or duration. Prevalence was calculated as the percentage of rats observed to have at least 1 seizure during video-ECoG monitoring. Non-convulsive seizures appeared to be more prevalent in TBI Only rats (83%) than in control and sham TBI rats (56%, combined), though the difference was not statistically significant (χ^2 [1]=0.8365, p=0.3604).

We also compared the frequency of non-convulsive seizures across groups (Figure 2D). Data from control and sham TBI rats were pooled for this analysis, since these groups did not differ significantly in seizure frequency (control, 2.1 ± 2.5 seizures per hour; Sham TBI, 0.4 ± 0.1 seizures per hour; t [3]=0.9146, p=0.4279). Controls and sham TBI rats together exhibited 1.4 ± 1.9 non-convulsive seizures per hour (n=243 seizures). The frequency of non-convulsive seizures was 5-fold higher in TBI Only rats

than in controls/shams (TBI Only rats, 7.0 ± 3.6 non-convulsive seizures per hour; n=1,713 seizures; TBI Only *vs*. controls/shams, t [8]=3.075, p=0.0152).

We then analyzed the duration of non-convulsive seizures (Figure 2E). Data from control and sham TBI rats were again pooled, since seizure duration did not differ significantly between these groups (control, 7 ± 1 seconds; sham TBI, 6 ± 0 seconds; t [3]=1.656, p=0.1963). The mean duration of non-convulsive seizures in controls/shams was 6.8 ± 1.2 seconds. The durations of non-convulsive seizures in TBI Only rats was twice as long as in controls/shams (13.6 ± 11.6 seconds; t [8]=2.887, p=0.0203; Figure 2E). In addition, the longest non-convulsive seizure recorded in controls/shams was 15 seconds, but in TBI Only rats was 181 seconds.

An increase in seizure frequency and duration could mean that more time per hour is spent in a seizure state. To test this possibility, we multiplied the averages of seizure frequency and seizure duration for each rat. This analysis indicated that TBI Only rats averaged ten-fold more time per hour in a seizure state than did controls/shams (p=0.0159; Figure 2F). Thus, non-convulsive seizures in TBI Only rats were significantly more frequent and longer-lasting than in controls/shams.

Previous ECoG studies have shown that idiopathic seizures become more frequent with age in Sprague-Dawley rats (*e.g.*, [260]). To confirm this in the present study, we performed video-ECoG monitoring on uninjured rats that were 5 months older than the controls/shams (older rats, n=2, 12 video-ECoG hours per rat). The older rats exhibited spontaneous seizures which were electrographically and behaviorally similar to those of the age-matched controls/shams (data not shown). However, seizure frequency differed significantly between the older and younger rats (p=0.0206).

Specifically, the older rats exhibited 9.7 ± 0.4 seizures per hour (n=232 seizures), a 7-fold increase in frequency over that of controls/shams (p<0.05; Dunn's *post hoc* test). Interestingly, seizure frequency in older rats was comparable to that of TBI Only rats (p>0.05).

Older rats also differed from the younger rats in terms of seizure duration (p=0.0168). Specifically, the idiopathic seizures of older rats lasted 24.5 ± 4.0 seconds on average (range, 5 – 129 seconds), significantly longer than those of the younger controls/shams (p<0.05; Dunn's). However, seizure duration did not differ significantly between the older rats and the TBI Only rats (p>0.05; Dunn's). The preliminary data thus indicate that idiopathic seizures increase in frequency and duration with age, and suggest that TBI may accelerate this process.

Tacrolimus Administered at One Hour Post-TBI Reduced the Frequency of Non-Convulsive Seizures Months Later

Our lab recently demonstrated that calcineurin activity in the rat cortex increases within hours of lateral fluid percussion TBI [186], suggesting that calcineurin may be involved in post-traumatic epileptogenesis. We therefore administered a calcineurin inhibitor, Tacrolimus (5mg/kg; i.p.; TBI+TAC; n=12) to rats 1 hour after lateral fluid percussion TBI and then monitored the rats by video-ECoG alongside their untreated counterparts (TBI Only) at 33 ± 5 weeks post-TBI. As mentioned above, 1 TBI+TAC rat was excluded from analysis due to a small (<1mm) neocortical lesion at an electrode site. Data from the remaining TBI+TAC rats (n=11) are summarized below.

Like the TBI Only rats, TBI+TAC rats exhibited spontaneous non-convulsive seizures months after lateral TBI (Figure 3A). The prevalence of these seizures did not differ significantly between TBI+TAC rats and TBI Only rats (100% and 83%, respectively; $\chi^2[1]=1.948$, $p=0.1628$). We then compared TBI groups in terms of seizure frequency and duration. This analysis indicated that non-convulsive seizures were significantly less frequent in the TBI+TAC group than in the TBI Only group ($p=0.0414$; Figure 3B). However, seizure duration did not differ significantly between the TBI groups ($p=0.2127$; Figure 3C). Multiplying seizure frequency by seizure duration for each rat revealed that TBI+TAC rats averaged significantly less seizure time per hour than did TBI Only rats ($p=0.0414$; Figure 3D). The data overall indicate that administering Tacrolimus at 1 hour post-TBI reduced the frequency of spontaneous non-convulsive seizures months later.

Differences in seizure frequency between groups could be explained by differences in the light/dark dependency of seizures. For example, since most video-ECoG was recorded during light hours, seizure frequency could be underestimated if more seizures occurred during the dark hours. Plotting seizure onset times on a Raster did not suggest any light/dark dependence (Figure 4A), and seizure frequency did not differ significantly between light hours and dark hours of ECoG recording (for each treatment group, $p>0.05$ for light *vs*. dark seizure frequency; paired Student's t test; Figure 4B).

Review of the raster plots also revealed a clustering pattern to the non-convulsive seizures, especially in the brain injured rats (Figure 4A). To confirm the apparent clustering, we averaged the time between seizures for each rat and then

compared group means (Figure 4C). A binned analysis indicated that about 50% of non-convulsive seizures occurred within seconds of one another in the TBI Only and TBI+TAC rats. In the controls/shams however, only about 25% of non-convulsive seizures occurred within seconds of one another. The apparent increase in seizure clustering in TBI rats could be due to an increase in seizure frequency. However, seizure frequency did not differ significantly between the TBI+TAC and controls/shams (p>0.05), though seizures tended to cluster more in the TBI+TAC rats (Figure 4C). The data thus suggest that TBI enhances clustering of non-convulsive seizures, independent of the change in seizure frequency.

Nearly one-third of the ECoG data in Experiment 1 were reviewed blind to treatment group (28% overall; by treatment group, 0% control/sham, 34% TBI Only, and 43% TBI+TAC). The remaining data were reviewed without blinding and so may have been subject to experimenter bias. To control for this potential confound, we tested whether blinding affected seizure identification in the ECoG reviewers. Three ECoG recordings (~18 ECoG hours total) were analyzed independently by two reviewers, one of whom was blinded to treatment group. The blinded reviewer counted 8.0 ± 5.3 seizures per recording, whereas the unblinded reviewer counted 8.3 ± 4.6 seizures per recording. Paired analysis confirmed that seizure counts did not differ significantly between the blinded and unblinded reviews (p=0.7728; Wilcoxon). The data suggest that blinding ECoG reviewers to treatment group in the present study did not confound seizure identification.

Ethosuximide and fos-Phenytoin Differentially Affected the Frequency of Spontaneous Non-Convulsive Seizures

The conventional anti-seizure medication, ethosuximide (ETX), is effective against multiple types of spontaneous non-convulsive seizures in rat models. For example, a single dose of ETX (50mg/kg; i.p.) can reduce both the frequency of absence seizures in a genetic model [262] and the frequency of partial seizures in an iron-induced neocortical injury model [263]. To determine whether ETX had a similar effect on non-convulsive seizures in the present study, we administered ETX (50mg/kg; i.p.) to a subset of epileptic rats (n=6) during video-ECoG. This testing took place 1 week after the rats were monitored for spontaneous seizure activity. To ensure that a decrease in seizure frequency could be detected, we only included rats which had exhibited a high frequency of non-convulsive seizures (≥ 5 seizures/hr; n=6 rats).

We assessed seizure frequency and duration during the 2-hour period immediately preceding ETX administration ("pre-ETX period") and for the 2-hour period beginning 30 minutes after ETX administration ("post-ETX period"). During the pre-ETX period, rats averaged 7.0 ± 9.3 non-convulsive seizures per hour, lasting 14.3 ± 10.8 seconds. Compared to the pre-ETX period, seizure frequency decreased by 92% in the post-ETX period (p=0.0313, Wilcoxon; Figure 5A,D). The decrease in seizure frequency was equivalent between TBI rats and uninjured rats (TBI rats, 96 ± 8% decrease; older, uninjured rats, 83 ± 24% decrease; t [4]=1.082; p=0.3402). We did not compare seizure duration between the pre-ETX and post-ETX periods, because only 1 rat exhibited seizures during the post-ETX period (post-ETX seizure duration, 10.1 ± 3.5

seconds). The data overall suggest that ETX reduces the frequency of spontaneous non-convulsive seizures.

We then treated a different group of epileptic rats (n=4) with another anti-seizure medication, *fos*-phenytoin (fPHT; 40mg phenytoin equivalents/kg; i.p.), the pro-drug form of phenytoin. In contrast to ETX, phenytoin has shown contrary effects in rat models of non-convulsive seizures. Phenytoin can aggravate absence seizures in genetic models [264,265] at doses which inhibit partial seizures during electrical [266] or chemical kindling [267]. The present study used fPHT instead of phenytoin, because fPHT is more reliably absorbed when administered intraperitoneally but has shown similar pharmacokinetics and dose-equivalent efficacy in a rat model of partial seizures [268]. Rats in the present study were administered fPHT 9 ± 6 weeks after monitoring for spontaneous seizure activity. To ensure that bi-directional changes in seizure frequency could be detected, we only included rats which exhibited a moderate frequency of non-convulsive seizures (≈ 2/hr; n=4 rats) at 33 weeks post-TBI.

We measured seizure frequency and duration in the 2-hour period immediately preceding fPHT administration ("pre-fPHT period") and in the 2-hour period beginning 30 minutes after fPHT administration ("post-fPHT period"). One rat exhibited no seizures during the pre- or post-fPHT periods. All other rats showed non-convulsive seizures during both periods, averaging 1.6 ± 1.3 seizures per hour in the pre-fPHT period, and 6.1 ± 3.3 seizures per hour in the post-fPHT period (Figure 5B,D). Despite the nearly 4-fold increase in seizure frequency, a paired analysis found no significant difference in seizure frequency between the pre- and post-fPHT periods (t [4]=2.423,

p=0.0725). Nor did seizure duration change significantly after fPHT treatment (pre-fPHT, 9.7 ± 6.4 seconds; post-fPHT, 8.9 ± 5.5 seconds; *t* [4]=0.5512, *p*=0.6108).

The changes in seizure frequency following ETX and fPHT treatment could represent either normal fluctuations or drug effects. To compare these possibilities, we reviewed previous ECoG of the rats later used in the ETX and fPHT experiments. The recording conditions for these ECoG were the same as in the ETX and fPHT experiments, except that no drug was administered. We assessed non-convulsive seizure frequency in 2-hour periods which were analogous to the pre- and post-drug periods in the ETX and fPHT experiments. A paired analysis found no significant difference in seizure frequency between the first and second 2-hour periods, either among the rats later treated with ETX or among those later treated with fPHT (*p*=0.4615 and 0.2785, respectively; Wilcoxon; Figure 5C,D). Therefore, the changes in seizure frequency following administration of ETX and fPHT most likely represent drug effects.

Tacrolimus Did Not Protect against Cortical Atrophy or Thalamic Calcifications following TBI (Experiment 1)

Lateral fluid percussion TBI causes progressive degeneration of ipsilateral cortex over the course of a year [269], and the degeneration of certain cortical regions correlates with the incidence of late spontaneous seizures [259]. Therefore, to determine the location and extent of cortical degeneration in the present study, we sacrificed the rats of Experiment 1 at 43 ± 8 weeks post-TBI (or sham) and processed them for histology, along with age-matched controls. Groups did not differ significantly either in age at sacrifice or in time between TBI and sacrifice (age at sacrifice, *F*

[2,20]=1.438, p=0.2610; time between TBI and sacrifice, F [2,14]=0.1998, p=0.8212; Table 1). Gross examination of fixed brains from TBI rats revealed an opaque lesion, 1mm or more in diameter, at or just ventral to the site of fluid percussion impact. We collected coronal sections at 0.6mm intervals between 0.8mm and 5.6mm caudal to Bregma, stained the sections with thionine and examined them by light microscopy (Figure 6A,B). Most TBI brains showed at least 1 opaquely-stained lesion in the ipsilateral thalamus (Figure 6C and inset in Figure 6B). We interpreted these lesions as thalamic calcifications, based on similar findings in previous studies of fluid percussion TBI [172,259]. Thalamic calcifications were identified in nearly all TBI rats but never in control rats (Figure 6C). However, the prevalence of these calcifications did not differ significantly between TBI Only and TBI+TAC rats (χ^2 [1]=0.7804; p=0.3770; Figure 6C). Nor did the presence of calcifications correlate with seizure frequency, either within or across groups (p>0.05). The data therefore suggest that thalamic calcifications were not related to the frequency of non-convulsive seizures after lateral TBI.

Initial examinations also suggested atrophy of the ipsilateral neocortex in all TBI rats. To quantify the apparent atrophy, we used ImageJ to trace the ipsilateral and contralateral neocortex in micrographs and then measure the area enclosed by the tracing (Figure 6B). The traced area of the ipsilateral (left) neocortex was then divided by that of the contralateral (right) neocortex in each brain section, yielding a ratio of the two hemispheres ("RatioCx") [259]. This analysis revealed significant differences in RatioCx among the treatment groups, as described below.

NEOCORTEX - The RatioCx in control brains was consistent along the rostro-caudal axis, averaging 0.98 ± 0.01 when measured from -0.8mm through -5.6mm

Bregma (Figure 6D). Cross-comparison of the mean RatioCx revealed significant differences among treatment groups (mean RatioCx, p=0.0022; Figure 6D$_2$). *Post hoc* analysis indicated, for example, that the RatioCx was significantly decreased in TBI Only rats relative to controls (p=0.0043). The RatioCx in TBI+TAC rats was also decreased from control levels (p=0.0002). The decrease in RatioCx in TBI+TAC rats appeared to be comparable to that of TBI Only rats, as the TBI groups did not differ significantly from one another (p=0.6787). RatioCx decreased most likely due to atrophy of the ipsilateral neocortex, since the area of the contralateral neocortex did not differ significantly across treatment groups (control, 10.6 ± 1.4 arbitrary units, A.U.; TBI Only, 9.9 ± 0.3 A.U.; TBI+TAC, 10.4 ± 0.9 A.U.; p=0.3228, Kruskal-Wallis) [259]. The data thus demonstrate substantial atrophy of the ipsilateral neocortex by 43 weeks post-TBI, and agree with previous findings that Tacrolimus does not prevent neocortical atrophy following TBI [270,271].

Previous research has shown that the risk of spontaneous seizures increases with the severity of neocortical atrophy following lateral fluid percussion TBI [259]. We therefore used linear correlation to test whether seizure frequency and neocortical atrophy were related. However, mean RatioCx did not correlate with the frequency of non-convulsive seizures, either within TBI groups or when all TBI groups were combined (each, p>0.05). The data thus suggest that neocortical atrophy is not related to non-convulsive seizure frequency after lateral TBI.

We did not perform correlational analysis on convulsive seizure data due to lack of data. It is worth noting, however, that the two rats exhibiting convulsive seizures on video-ECoG also had the most severe neocortical atrophy (*i.e.,* first and second lowest

mean RatioCx among all rats). Quantitative analysis revealed that the RatioCx was significantly decreased in these two rats, when compared to the TBI rats in which no convulsive seizures were observed (t [13]=4.563, p=0.0005). The data therefore support previous research showing a correlation between neocortical atrophy and convulsive seizures after lateral TBI [259].

HIPPOCAMPUS – We also assessed atrophy in the hippocampus, since previous research has linked hippocampal asymmetry related to the incidence of late non-convulsive seizures after fluid percussion TBI [260]. In the present study, we estimated hippocampal atrophy by tracing the ipsilateral and contralateral hippocampi, measuring the enclosed areas (Figure 6B), and then calculating a ratio of ipsilateral to contralateral area ("RatioHp"). Analysis of RatioHp was limited to Bregma levels -3.2mm through -5.6mm for two reasons. First, hippocampal gray matter was not present in the sections representing -0.8mm and -1.4mm Bregma. Second, the rostral end of the hippocampus appeared to have shifted caudally after TBI, confounding the RatioHp in those sections (Figure 6E).

RatioHp in controls was consistent along the rostro-caudal axis, averaging 1.03 ± 0.03 when measured from Bregma levels -3.2mm to -5.6mm (Figure 6E). As with RatioCx, RatioHp differed significantly among treatment groups (mean RatioHp, p=0.0028; Figure 6E$_2$). In particular, RatioHp in TBI Only rats was significantly decreased relative to controls (p=0.0087). TBI+TAC rats also showed a loss of RatioHp when compared to controls (p=0.0005), but not when compared to TBI Only rats (p=0.3710). As with RatioCx, RatioHp most likely decreased due to changes in the ipsilateral hippocampus, since the area of the contralateral hippocampus did not differ

significantly across treatment groups (control, 4.6 ± 0.4 arbitrary units, A.U.; TBI Only, 4.2 ± 0.4 A.U.; TBI+TAC, 4.6 ± 0.7 A.U.; p=0.3646, Kruskal-Wallis). Overall, the data suggest that the ipsilateral hippocampus underwent a significant change in volume and/or shape by 43 weeks post-TBI. While this change is consistent with previous reports of hippocampal asymmetry after fluid percussion injury [260], it did not appear to be related to the expression of non-convulsive seizures, since RatioHp did not correlate with non-convulsive seizure frequency (within or across the TBI groups, p>0.05).

Seizures Were Not Observed at 5 Weeks Post-TBI (Experiment 2)

Spontaneous non-convulsive seizures can begin a few weeks after lateral fluid percussion TBI and increase in both frequency and severity over months [255]. To characterize the timing of seizure development in the present study, we subjected a different set of rats to lateral fluid percussion TBI and then monitored spontaneous seizure activity by video-ECoG 5 weeks later (Experiment 2; Figure 7A). The severity of TBI in Experiment 2 was equivalent to that in Experiment 1 (see Results above), and the treatment groups were also the same - rats received either a single dose of Tacrolimus (5mg/kg; i.p.; “TBI+TAC”; n=4) or no injection (“TBI Only”; n=5) at 1 hour post-TBI. At 5 weeks post-TBI, injured rats and their uninjured littermates (n=4) were monitored by simultaneous video-ECoG. Video-ECoG was recorded 12 ± 1 hours per rat, beginning in the morning and completed the same day. A trained observer who was blinded to treatment group then visually reviewed video-ECoG data offline for evidence of seizure activity.

Low-voltage, arrhythmic electrographic activity was observed during awake behavior in all rats. In contrast to the baseline ECoG activity were observed paroxysmal discharges lasting less than 5 seconds. These epileptiform discharges were observed occasionally (<1/hr) in all TBI rats (Figure 7B) and in one control rat (Figure 7C). However, epileptiform activity lasting longer than 5 seconds was not observed in any rat. The data thus confirms previous reports that seizure prevalence and/or frequency increases over months following fluid percussion TBI [172,255,260].

DISCUSSION

The present study describes several major findings related to the long-term electrographic and anatomical consequences of lateral TBI. For example, video-ECoG revealed two distinct types of spontaneous seizures in adult rats months after TBI. These seizure types included convulsive seizures which were infrequent but lasted for minutes, and non-convulsive seizures which were frequent but lasted tens of seconds on average. A subset of age-matched, uninjured rats exhibited idiopathic seizures, and these idiopathic seizures were electrographically and behaviorally similar to the non-convulsive seizures seen months after TBI. However, the idiopathic seizures were far less frequent and shorter lasting than the non-convulsive seizures of TBI rats. Interestingly, administering a calcineurin inhibitor, Tacrolimus (TBI+TAC) at 1 hour post-TBI significantly decreased the frequency of non-convulsive seizures months later but did not protect against cortical atrophy or thalamic calcifications. A second video-ECoG experiment performed at 5 weeks post-TBI revealed epileptiform discharges but no

seizures, suggesting that both the convulsive and non-convulsive seizures have a delayed onset. The context and implications of the major findings are discussed below.

Studies of post-traumatic epilepsy in human patients and rodent models suggest that epileptogenesis begins within minutes to hours of TBI [176,177]. Our previous research identified an increase calcineurin activity in the minutes to hours following lateral fluid percussion TBI [186]. This increase in calcineurin activity could be an early but critical event in the development of post-traumatic epilepsy, as has been proposed in other models of acquired epilepsy (reviewed in [251]). Consistent with this possibility, the present study demonstrated that administering a calcineurin inhibitor, Tacrolimus, 1 hour after TBI reduced the frequency of spontaneous non-convulsive seizures months later. This finding may shed light on the timing and mechanisms by which non-convulsive seizures develop after TBI, as it reveals a Tacrolimus-sensitive mechanism which is engaged acutely after TBI. Though only a single dose of Tacrolimus was administered in the present study, previous studies suggest that brain levels can remain stable for days [272]. It is therefore possible that Tacrolimus inhibited calcineurin activity for days after TBI, potentially blocking the increase in calcineurin activity our lab previously identified in this model [186]. Importantly, these findings suggest that pharmacological intervention at a clinically-relevant time point can alter the course of epilepsy development after TBI.

Further research is needed to characterize the role of calcineurin in epileptogenesis. One possibility is that a pathological increase in calcineurin activity leads to the dysregulation of hyperpolarization-activated cation (HCN) channels [254]. Calcineurin has been shown to downregulate gating of HCN channels, resulting in

neuronal hyperexcitability [254], and a reduction in HCN channel expression in rat cortex is associated with epileptogenesis after *status epilepticus* [273,274]. HCN channelopathy may also explain the spontaneous non-convulsive seizures observed in the present study. HCN channels are downregulated in subthalamic nuclei in the tottering mouse, a genetic model of spontaneous non-convulsive seizures [275]. In addition, mice lacking a subtype of HCN channels (HCN2) also exhibit spontaneous non-convulsive seizures [276]. It is therefore possible that TBI induces (or exacerbates) the development of spontaneous non-convulsive seizures through a calcineurin-dependent dysregulation of HCN channels, and that this process begins within hours or days of TBI.

Calcineurin may also mediate epileptogenesis through its effects on the immune system or in synaptic circuits. For example, calcineurin mediates pro-inflammatory signaling by interleukin-1β and tumor necrosis factor-α, and these signaling pathways have been strongly implicated in epileptogenesis [226,277,278,279]. An alternative but not exclusive possibility is that calcineurin facilitates epileptogenesis by destabilizing dendritic spines. Various injury models have shown that drugs which inhibit calcineurin activity also block the loss of dendritic spines after injury, including the spine loss we observed in the neocortex and dentate gyrus after lateral TBI [11,12,118,233]. Since dendritic spines bear the majority of excitatory synapses in the adult cortex [5], a widespread and persistent loss of spines could equate to deafferentation. Deafferentation can induce epileptiform activity in the neocortex [280,281,282], potentially through a homeostatic increase in network excitability [283]. In addition, studies of human epileptic tissue have found that spine loss in the dentate gyrus

correlates with an abnormal prolonging of excitatory post-synaptic responses [284,285], which could support seizure activity.

Previous studies of the lateral fluid percussion model have reported either convulsive seizures or non-convulsive seizures in the months following TBI [173,255]. For example, Kharatishvili and colleagues (2006) described infrequent but long-lasting convulsive seizures in up to 50% of rats after TBI, but did not note any non-convulsive seizures [173]. In contrast, a study by Curia *et al.* (2011) found frequent but short-lasting non-convulsive seizures in nearly all rats after TBI, but did not note any convulsive seizures [255]. The present study is thus the first (to our knowledge) in which both types of seizures were identified after TBI, and in the same rats. Methodological differences could explain the discrepant findings in previous studies. For example, adolescent rats (1 month old) like those used in the Curia *et al.* (2011) study may be less likely to develop convulsive seizures after fluid percussion TBI than the adult rats used in the present study and in the Kharatishvili *et al.* (2006). Age-dependency is characteristic of other models of acquired epilepsy – for example, rats younger than 25 days are less likely to develop spontaneous convulsive seizures following experimental *status epilepticus* [286,287].

While the post-traumatic seizures observed in the present study resemble those seen in previous studies, questions remain about the nature of the non-convulsive seizures. Specifically, it is unclear whether these seizures represent an acquired form of partial epilepsy [288], or an exacerbated form of idiopathic, absence-like epilepsy [289,290]. Previous studies have reported that the non-convulsive seizures are focal in origin [172], involve limbic regions, and can be electrographically differentiated from

idiopathic seizures on the basis of waveform and localization [260]. Subsequent research also determined that the non-convulsive seizures were insensitive to the anti-seizure drug, carisbamate [291], at dosages above those which suppress absence seizures in rat models [292] (but see also [293]). Overall, the evidence from previous studies suggests that the non-convulsive seizures are partial seizures, like those frequently seen in human post-traumatic epilepsy [166,288]. The non-convulsive seizures in the present study, however, more closely resembled absence seizures. For example, the seizures we observed typically had a generalized onset, spike-wave morphology, and dominant spectral power in the theta and beta ranges. These electrographic features are typical of absence seizures in rats [294]. Also, the non-convulsive seizures we observed could be interrupted by sensory stimulation, suppressed by ETX, and exacerbated by *fos*-phenytoin - also characteristic of absence seizures [262,264,265,295] (but see also [263,296,297]). However, further investigation is needed to confirm that the non-convulsive seizures we observed months after TBI were absence seizures.

Studies of other rat models suggest that brain injury can cause or exacerbate absence-like seizures in rats. For example, focal thrombolytic damage to rat neocortex has been shown to impair the excitability of thalamic reticular neurons [298], cells which normally inhibit thalamocortical circuits implicated in involved in absence seizures [299]. More diffuse brain injuries may also give rise to absence seizures. For example, rats develop absence-like seizures weeks to months after pilocarpine-induced *status epilepticus* [300,301] . For example, Francois and colleagues (2011) found that administering adult male Sprague-Dawley rats the anti-seizure drug, carisbamate (90 or

120mg/kg), after pilocarpine-induced *status epilepticus* reduced by half the number of rats developing late convulsive seizures [300]. These rats instead developed frequent, non-convulsive seizures which were not observed in rats with convulsive seizures, and which were electrographically, behaviorally, and pharmacologically similar to absence seizures [300]. Though the authors note that a third of age-matched controls also showed absence-like seizures, the seizures in post-SE rats were nearly ten-fold more frequent than in controls [300]. Likewise in the present study, non-convulsive seizures in brain injured rats study were similar in phenotype to idiopathic seizures, but were significantly more frequent and longer lasting. Together these studies suggest that brain injury can increase the frequency of absence-like seizures in adult rats [290].

TABLE 2 – TBI Severity, Age, and Video-ECoG Duration.

Exp. #	Treatment Group	*N*	TBI Severity		Age (weeks) at Time of			Video-ECoG per Rat (hours)
			FPI pressure (atm)	Righting Time (min)	TBI/Sham	video-ECoG	Histology	
1	Control	7	n/a	n/a	n/a	43.2 ± 8.1	43.8 ± 8.3	42.4 ± 7.9
	Sham TBI	2	n/a	n/a	15.0 ± 0.6	45.0 ± 0.0	62.1 ± 0.0	43.7 ± 4.3
	TBI Only	6	2.74 ± 0.11	9.2 ± 5.0	14.0 ± 0.7	50.8 ± 4.2	56.2 ± 2.3	58.6 ± 28.3
	TBI+TAC	11	2.67 ± 0.07	9.7 ± 4.0	14.1 ± 1.6	45.6 ± 3.1	56.6 ± 9.3	52.6 ± 5.6
2	Control	4	n/a	n/a	n/a	19.8 ± 0.1	19.9 ± 0.1	10.8 ± 0.7
	TBI Only	5	*2.34 ± 0.04	8.5 ± 3.7	13.0 ± 0.0	17.9 ± 0.1	17.9 ± 0.1	11.7 ± 0.9
	TBI+TAC	6	*2.38 ± 0.03	8.2 ± 1.4	14.0 ± 0.6	19.2 ± 0.5	19.4 ± 0.4	12.3 ± 0.3

**Experiments 1 and 2 involved different FPI devices that were separately calibrated, which may explain the difference in FPI pressure between experiments*

Values represent mean ± standard deviation.

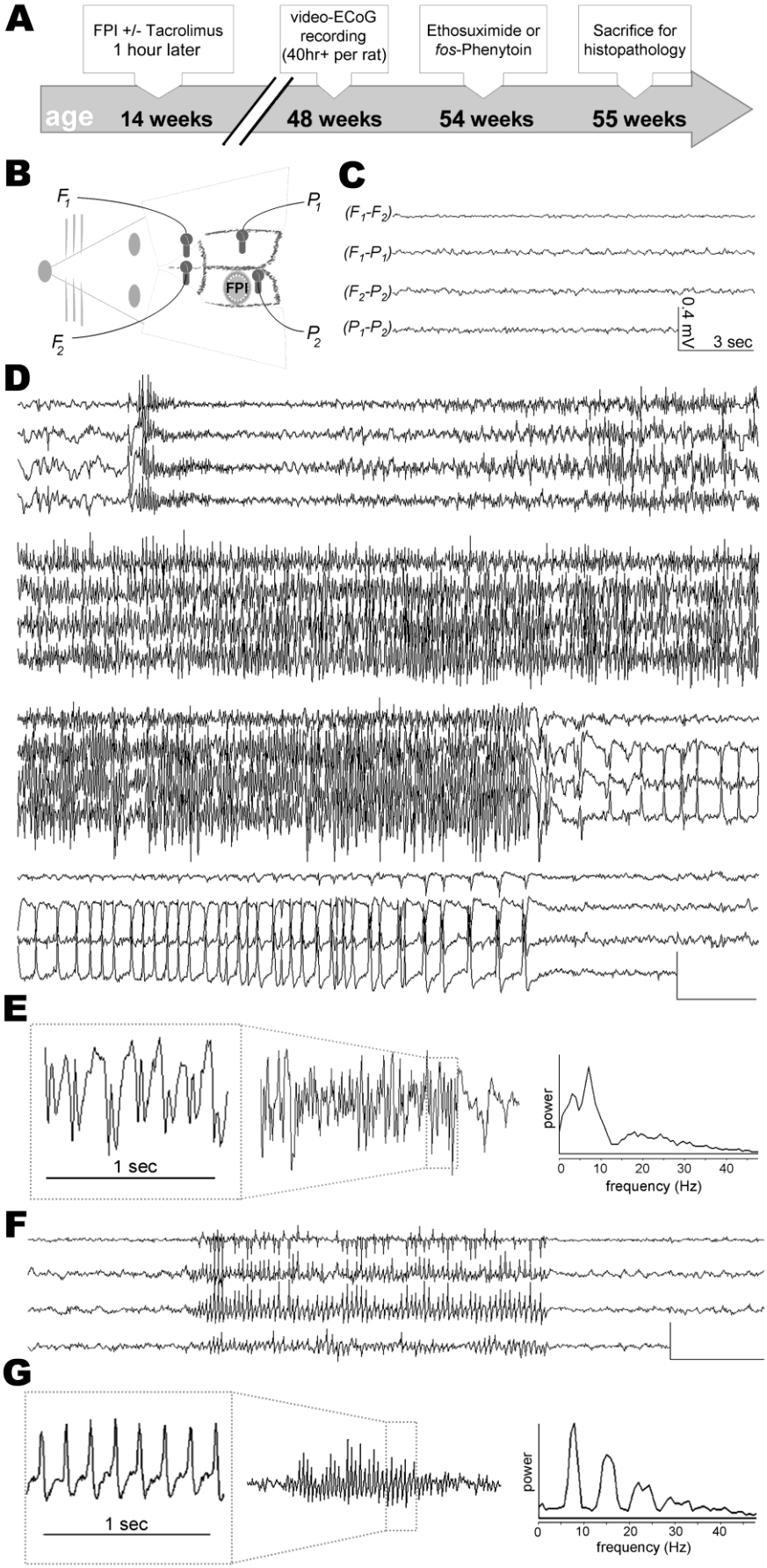
A
FPI +/- Tacrolimus
1 hour later
video-ECoG
recording
(40hr+ per rat)
Ethosuximide or
fos-Phenytoin
Sacrifice for
histopathology
age
14 weeks
48 weeks
54 weeks
55 weeks
B
F1
P1
FPI
F2
P2
C
(F1-F2)
(F1-P1)
(F2-P2)
(P1-P2)
0.4 mV
3 sec
D
E
1 sec
power
0
10
20
30
40
frequency (Hz)
F
G
1 sec
power
0
10
20
30
40
frequency (Hz)

FIGURE 23 – Video-Electrocorticography Revealed Two Distinct Types of Late Post-Traumatic Seizures. Adult, male Sprague-Dawley rats were subjected to lateral fluid percussion TBI or sham TBI and then monitored for spontaneous seizure activity 33 ± 5 weeks later, alongside age-matched uninjured controls. **A**) Timeline of Experiment 1. **B**) Placement of fluid percussion impact (FPI) and epidural electrodes for electrocorticography (ECoG). **C**) Arrhythmic, low-voltage ECoG activity typical of awake behavior in all rats, shown as bipolar montage. **D**) Representative ECoG of convulsive (tonic-clonic) seizures observed months after TBI. **E**) On left, enlarged ECoG trace showing irregular spike-and-wave waveform of convulsive seizures. On right, spectral analysis of a 3 second epoch showing typical distribution of power during a convulsive seizure. **F**) Representative example of ECoG of non-convulsive seizure. **G**) On left, enlarged ECoG trace revealing spike-wave waveform of non-convulsive seizures. On right, spectral analysis of a 3 second epoch showing typical distribution of power during a non-convulsive seizure. All scale bars, 0.4mV by 3sec.

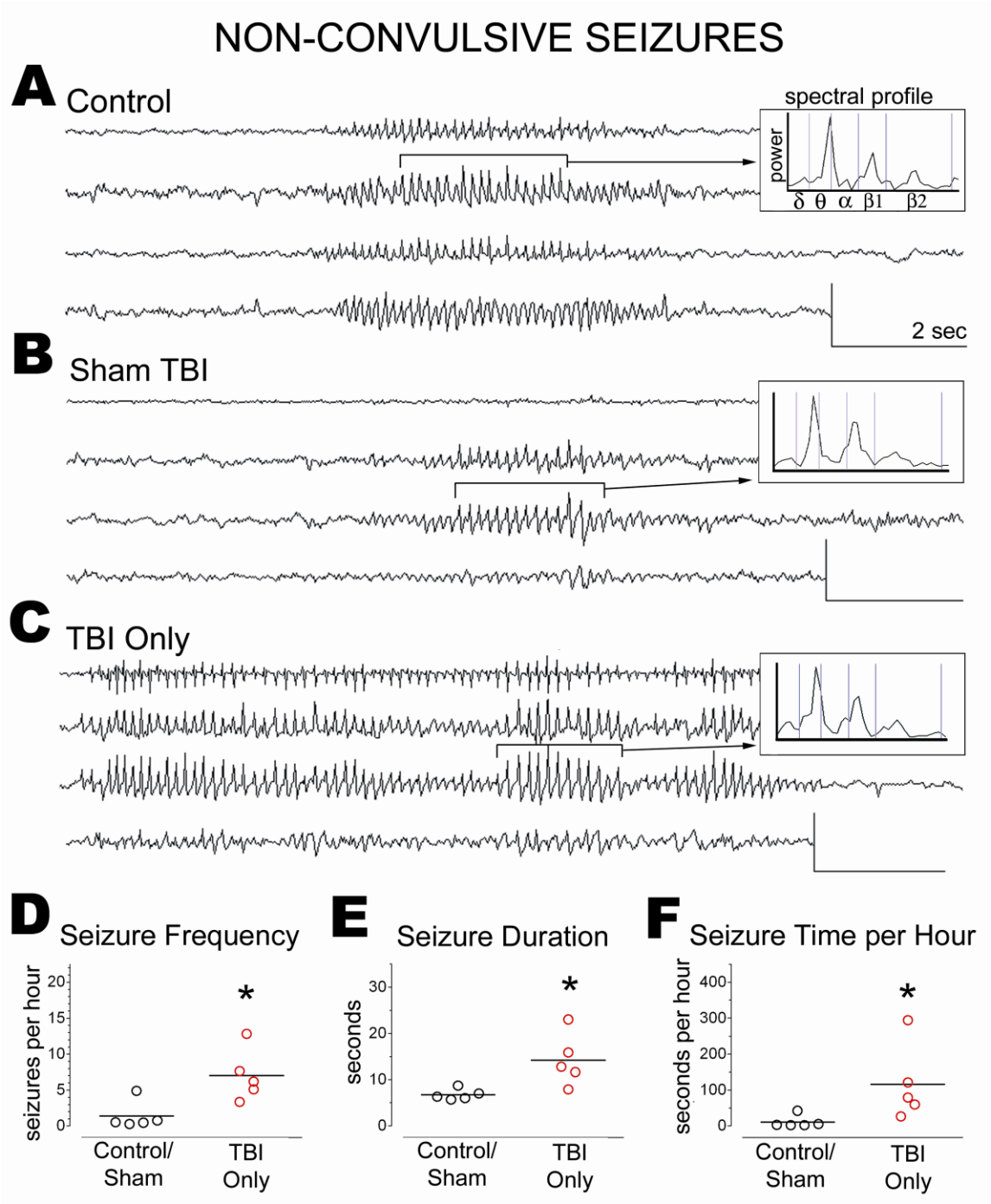
NON-CONVULSIVE SEIZURES
A
Control
spectral profile
power
δ θ α β1 β2
2 sec
B
Sham TBI
C
TBI Only
D
Seizure Frequency
seizures per hour
20
15
10
5
0
*
Control/
Sham
TBI
Only
E
Seizure Duration
seconds
30
20
10
0
*
Control/
Sham
TBI
Only
F
Seizure Time per Hour
seconds per hour
400
300
200
100
0
*
Control/
Sham
TBI
Only

FIGURE 24 – Late Post-Traumatic Seizures Could Be Distinguished from Idiopathic Seizures by Frequency and Duration. Video-ECoG was performed on male Sprague-Dawley rats 33 weeks after lateral fluid percussion TBI ("TBI Only") or sham ("Sham TBI"), or at the equivalent age in uninjured littermates ("Control"). **A** – **C**) Representative ECoG and spectral profiles of non-convulsive seizures in an uninjured control rat, a Sham TBI rat, and a TBI Only rat. **D, E**) Non-convulsive seizures were significantly more frequent and longer lasting in TBI Only rats than in controls/shams. **F**) TBI Only rats spent on average significantly more time in a non-convulsive seizure than did controls/shams. Circles and bars on graphs denote individual means and group means, respectively. Means compared by Kruskal-Wallis test with *post hoc* Mann Whitney tests. Scale bars, 0.4mV by 2 seconds. *, $p<0.05$

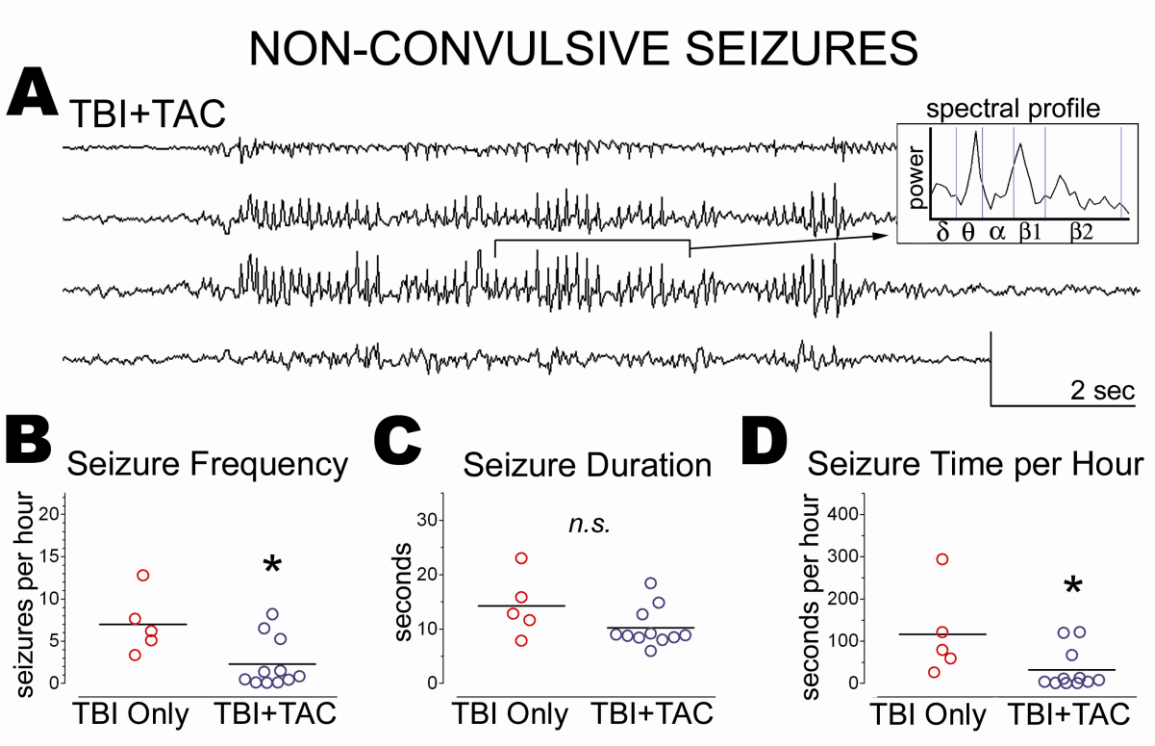

FIGURE 25 – Administering Tacrolimus Acutely after TBI Decreased the Frequency of Late Non-Convulsive Seizures. Rats were administered a calcineurin inhibitor, Tacrolimus (5mg/kg; i.p.; "TBI+TAC") or no injection ("TBI Only") 1 hour after lateral fluid percussion TBI, and then monitored by video-ECoG approximately 33 weeks later. **A**) A typical non-convulsive seizure in a TBI+TAC rat and its spectral profile. **B**) TBI+TAC rats exhibited significantly fewer non-convulsive seizures per hour than did TBI Only rats. **C**) The average duration of non-convulsive seizures did not differ significantly between TBI+TAC and TBI Only rats. **D**) TBI+TAC rats averaged significantly less time per hour in a non-convulsive seizure than did TBI Only rats. Circles and bars on graphs denote individual means and group means, respectively. Means compared by Kruskal-Wallis test with *post hoc* Mann Whitney tests. All scale bars, 0.4mV by 2 seconds. * $p<0.05$

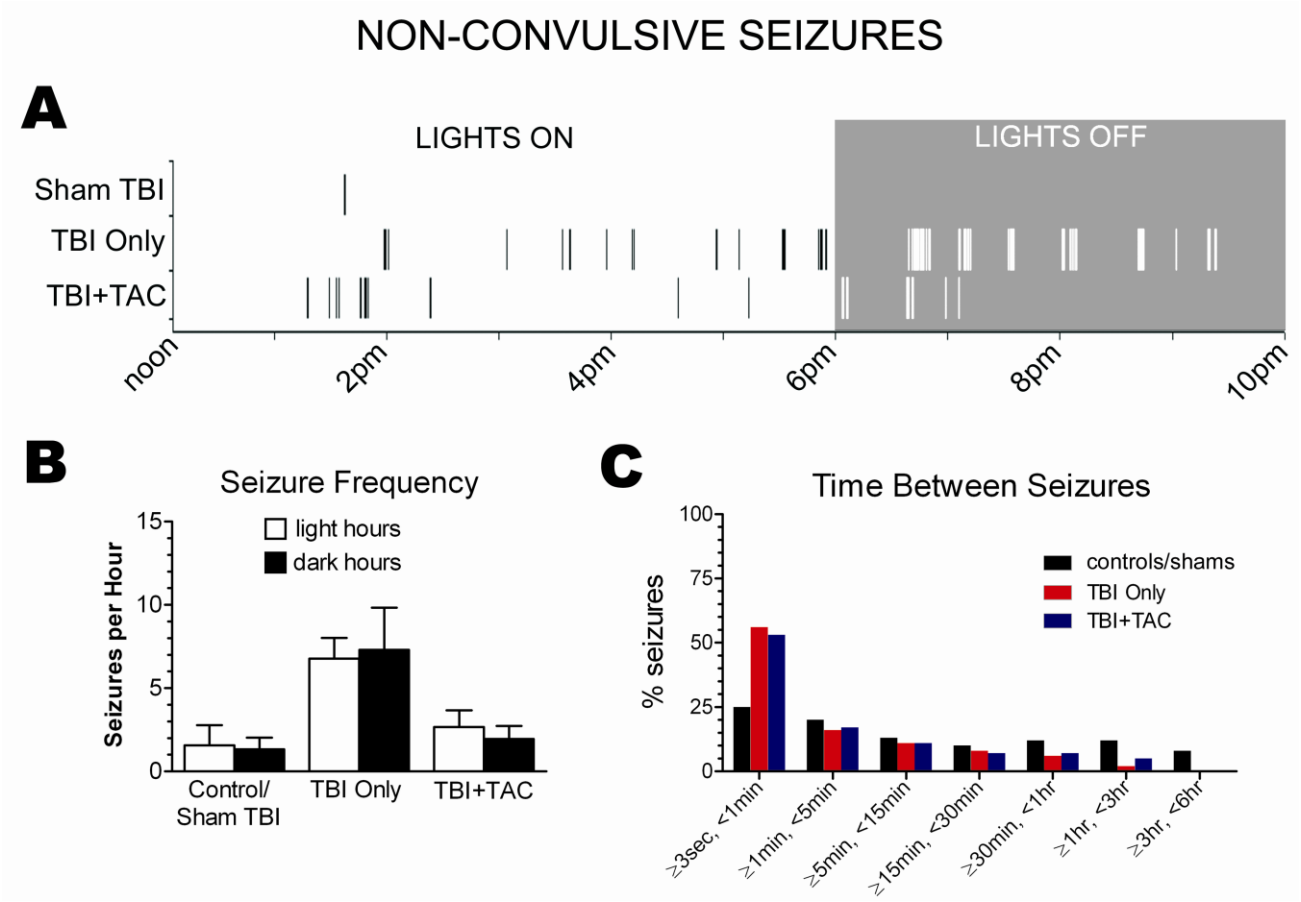

FIGURE 26 – TBI Increased the Clustering of Non-Convulsive Seizures. Adult, male Sprague-Dawley rats were administered lateral fluid percussion TBI followed by Tacrolimus ("TBI+TAC") or no injection ("TBI Only"), and then were monitored for spontaneous seizure activity months later, along with age-matched uninjured ("Controls") and Sham TBI rats. **A**) Raster plot with hashes (|) marking the onset times of spontaneous non-convulsive seizures during typical 10 hour video-ECoG recordings of Sham TBI, TBI Only, and TBI+TAC rats. **B**) Seizure frequency did not differ significantly between light and dark phases (paired Student's t tests). **C**) Binned analysis revealed that a majority of non-convulsive seizures occurred within seconds of one another in TBI Only rats and TBI+TAC rats, but not in controls/shams.

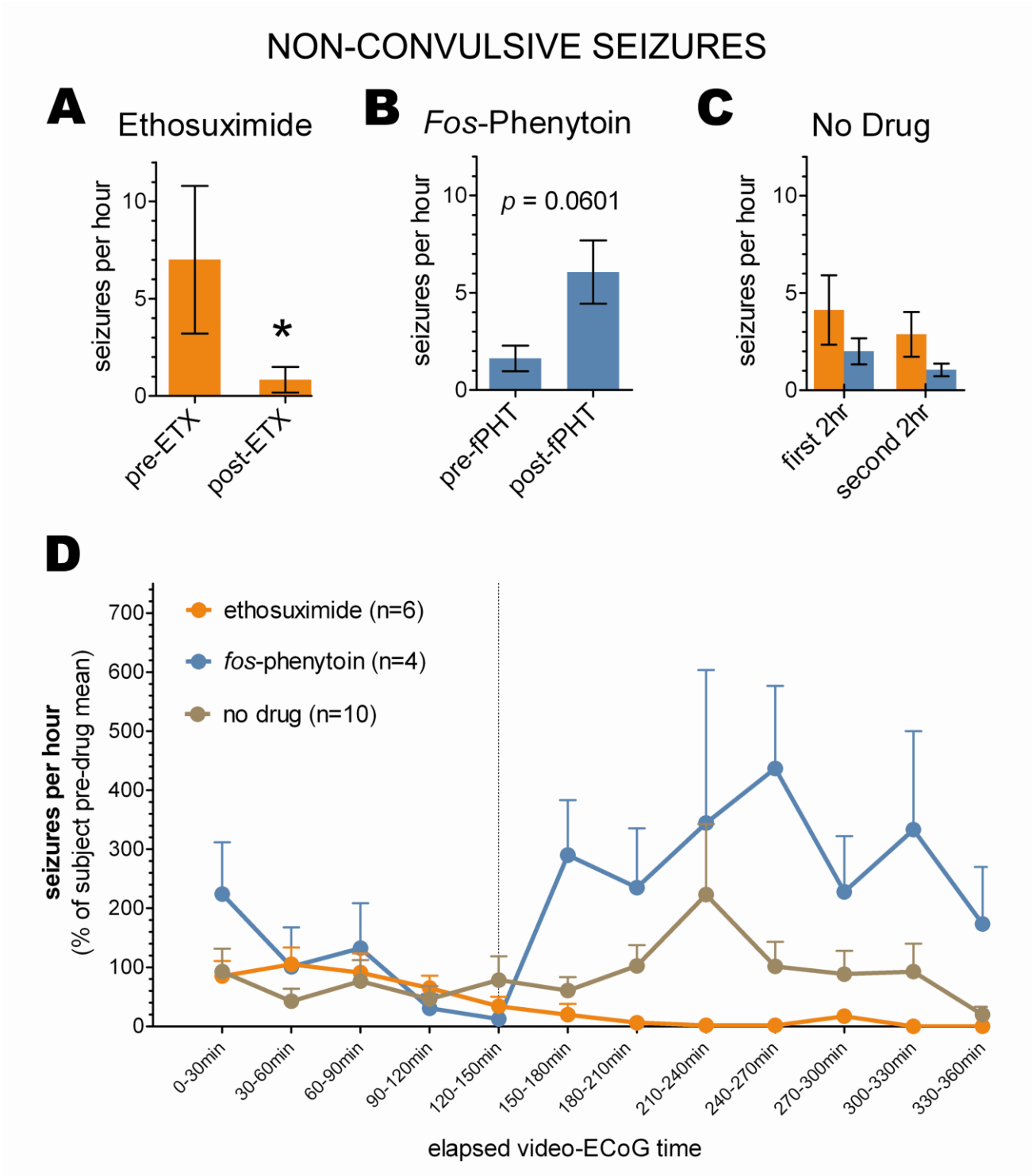
NON-CONVULSIVE SEIZURES
A
Ethosuximide
seizures per hour
10
5
0
*
pre-ETX
post-ETX
B
Fos-Phenytoin
p = 0.0601
pre-fPHT
post-fPHT
C
No Drug
first 2hr
second 2hr
D
ethosuximide (n=6)
fos-phenytoin (n=4)
no drug (n=10)
seizures per hour
(% of subject pre-drug mean)
700
600
500
400
300
200
100
0
0-30min
30-60min
60-90min
90-120min
120-150min
150-180min
180-210min
210-240min
240-270min
270-300min
300-330min
330-360min
elapsed video-ECoG time

FIGURE 27 – Ethosuximide and *fos*-Phenytoin Differentially Affected the Frequency of Non-Convulsive Seizures. Non-convulsive seizures were pharmacologically characterized by administering conventional anti-seizure medications to epileptic rats during video-ECoG recording. Rats exhibiting a high frequency of non-convulsive seizures (≥5/hr; n=6) were administered a single dose of ethosuximide ("ETX," 50mg/kg, i.p), whereas rats exhibiting a moderate seizure frequency (≈2/hr; n=4) were administered *fos*-phenytoin ("fPHT," 40mg phenytoin equivalents/kg, i.p.). **A**) ETX treatment was associated with a significant decrease in the frequency of non-convulsive seizures. **B**) fPHT treatment appeared to increase the frequency of non-convulsive seizures, but not to a statistically significant extent. **C**) Changes in seizure frequency after ETX or fPHT treatment likely represent drug effects, since seizure frequency did not fluctuate significantly in previously-recorded, drug-free recordings of the same rats (rats later administered ETX, orange; rats later administered fPHT, blue). **D**) Temporal profile showing changes in seizure frequency which began soon after drug administration (vertical dotted line) and which were not observed when no drug was administered. ETX data compared by Wilcoxon matched-pairs signed rank test. fPHT data compared by paired Student's t-tests. All data presented as mean ± standard error of the mean (S.E.M.). * $p<0.05$

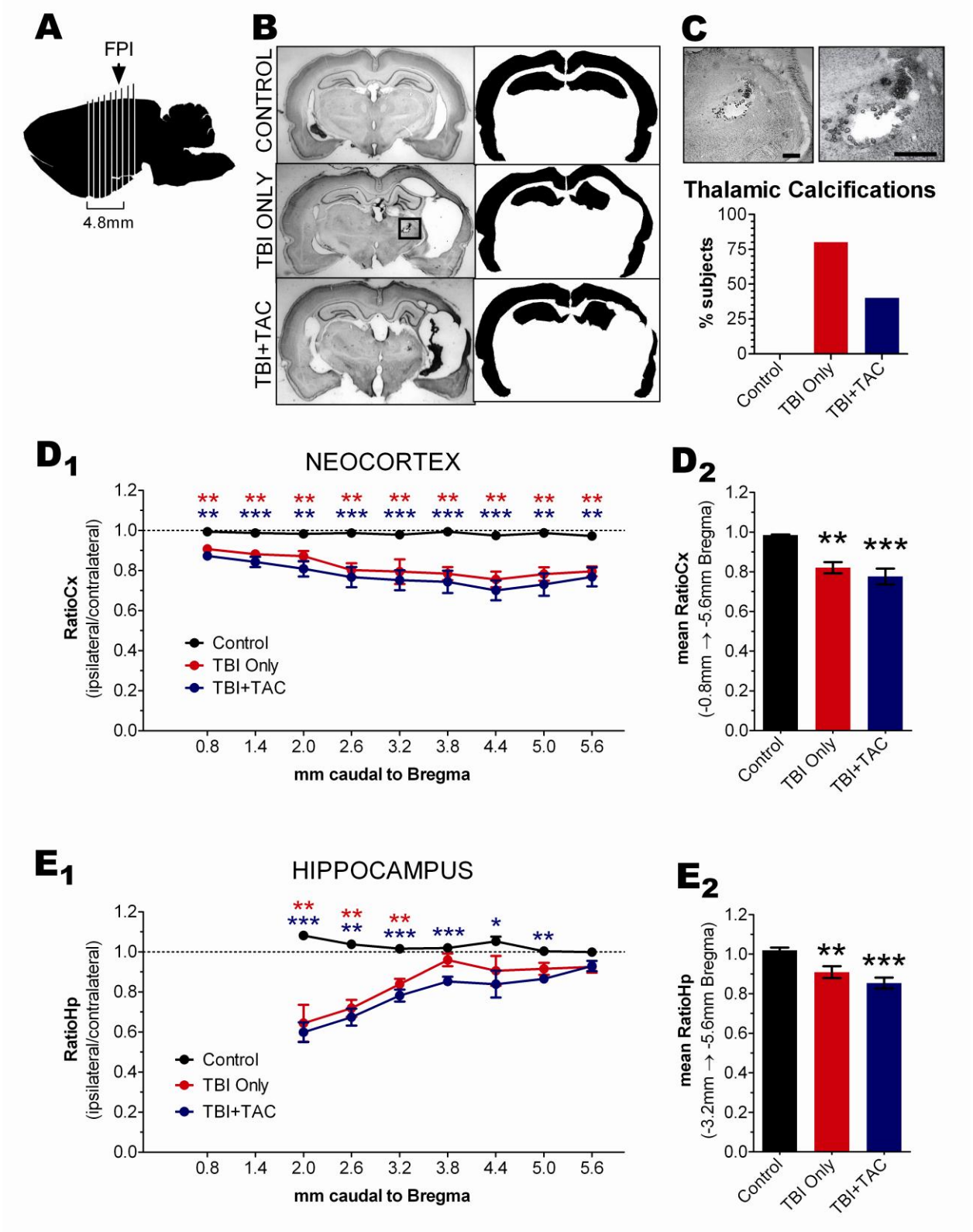
A
FPI
4.8mm
B
CONTROL
TBI ONLY
TBI+TAC
C
Thalamic Calcifications
% subjects
100
75
50
25
0
Control
TBI Only
TBI+TAC
D1
NEOCORTEX
RatioCx
(ipsilateral/contralateral)
Control
TBI Only
TBI+TAC
mm caudal to Bregma
D2
mean RatioCx
(-0.8mm → -5.6mm Bregma)
E1
HIPPOCAMPUS
RatioHp
(ipsilateral/contralateral)
E2
mean RatioHp
(-3.2mm → -5.6mm Bregma)

FIGURE 28 – TBI Caused Thalamic Calcifications and Cortical Atrophy. Rats were sacrificed and processed for thionine histology after completion of video-ECoG, approximately 42 ± 9 weeks after lateral fluid percussion TBI, or at an equivalent age in uninjured controls. **A**) Illustration indicating where sections were collected relative to the site of fluid percussion impact (FPI). **B**) Low-magnification (0.5x) light micrographs of representative, thionine-stained sections from -3.8mm Bregma, and the corresponding traces of neocortex and hippocampus which were used for measuring area (in black). Inset indicates a thalamic calcification; a smaller calcification can also be seen in the TBI+TAC image. **C**) Thalamic calcification from (B, inset) shown at 5x and 10x magnification, and a graph of the percentage of rats having at least 1 thalamic calcification. **D**) TBI Only and TBI+TAC rats showed significant but comparable decreases in RatioCx when assessed at each Bregma level (D_1) and when averaged across Bregma levels (D_2). **E**) TBI Only and TBI+TAC rats showed significant but comparable decreases in RatioCx when assessed at the rostral Bregma levels (E_1) and when averaged from Bregma -3.2mm to -5.6mm (E_2). The decrease in RatioHp in the rostral sections (Bregma -2.0mm and -2.6mm) appeared to be due to shrinkage of the hippocampus along the rostro-caudal axis; the affected sections were therefore excluded from the mean RatioHp. Means compared by Kruskal-Wallis test with *post hoc* Mann Whitney tests. Scale bar, 0.5mm. *p<0.05 *vs*. control, **p<0.01 *vs*. control, ***p<0.001 *vs*. control

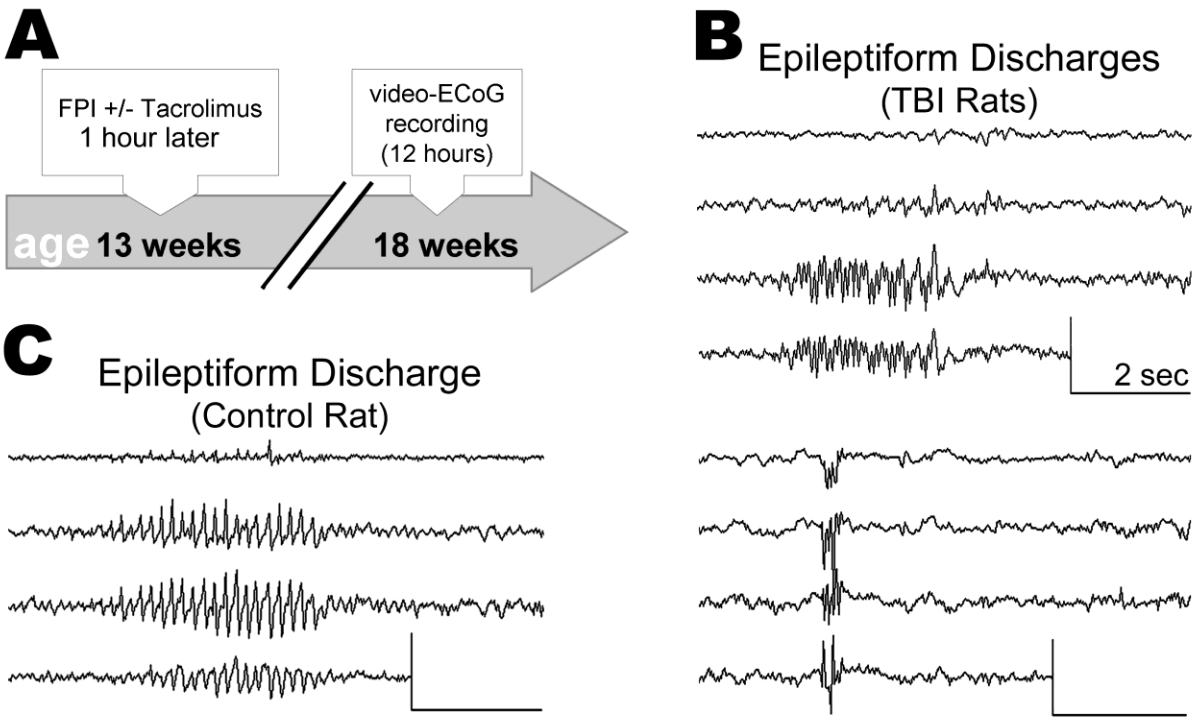

FIGURE 29 – No Seizures Were Observed at 5 Weeks Post-TBI. Adult, male Sprague-Dawley rats were subjected to lateral fluid percussion TBI, followed 1 hour later by administration of Tacrolimus (5mg/kg; i.p.; "TBI+TAC"; n=4) or no injection ("TBI Only"; n=5), and then were video-ECoG monitored at 5 weeks post-TBI along with uninjured littermates ("Control;" n=4). **A**) Timeline of Experiment 2. **B**) Examples of paroxysmal electrographic discharges lasting <5 seconds from two different TBI Only rats. Similar phenomena were observed occasionally (<1/hr) in all TBI rats and were interpreted as epileptiform discharges. **C**) An example of the epileptiform activity exhibited by one control rat. All scale bars, 0.4mV by 3 seconds.

DISCUSSION

The present study characterized the biochemical, histological, and electrographic consequences of lateral traumatic brain injury (TBI) in a rat model. Chapter I demonstrated an acute post-TBI loss of dendritic spines from principal cells of the ipsilateral neocortex and bilateral dentate gyrus. Administering the calcineurin inhibitor, Tacrolimus (FK506), 1 hour after TBI prevented this spine loss. Chapter II then characterized the role of calcineurin in TBI-induced spine loss. Western blots revealed evidence of an acute post-TBI increase in the cortical activity of cofilin, an actin-depolymerizing protein which had been previously implicated in dendritic spine loss [23,211,241]. Administering Tacrolimus 1 hour after TBI prevented the apparent activation of cofilin in the neocortex. In addition, enzymatic assays showed an acute post-TBI increase in calcineurin activity in the hippocampus. Chapter III then assessed the long-term consequences of an acute post-TBI increase in calcineurin activity. Specifically, rats were administered a calcineurin inhibitor, Tacrolimus (FK506), at 1 hour post-TBI and then monitored for spontaneous seizure activity months later. This acute treatment with Tacrolimus reduced the frequency of late non-convulsive seizures months later. The results presented in these chapters together demonstrate that a calcineurin inhibitor, Tacrolimus, can mitigate two significant consequences of lateral TBI, an acute loss of dendritic spines and the delayed development of non-convulsive

seizures. However, It remains unclear whether the spine loss and seizure development are related phenomena. The spine loss and seizure development may be two independent outcomes of a Tacrolimus-sensitive event. Alternatively, spine loss may be an early but critical event in epileptogenesis, as has been hypothesized previously [78]. The remainder of this discussion considers the evidence for a causal relationship between spine loss and epileptogenesis.

Could the spine loss observed in Chapter I somehow give rise to the late spontaneous seizures seen in Chapter III? Evidence for this possibility comes from a different model of epileptogenesis, the “cortical undercut” model. In one version of this model, adult rat neocortex is partially but chronically isolated through mechanical lesions of the cortical white matter [302]. After an electrographically silent period of days to weeks, the undercut cortex begins to show recurrent epileptiform activity [280,303]. Studies of this model have identified potential mechanisms of epileptogenesis. One mechanism may be the formation of new excitatory circuits, as epileptogenesis coincides with axonal sprouting and an increase in connectivity among layer V neurons [304,305]. Furthermore, blocking synaptic activity acutely after cortical undercut can prevent both the axonal sprouting and the development of epileptiform activity [306,307,308]. These studies collectively suggest that an up-regulation of excitatory synapses in the undercut neocortex may give rise to epilepsy.

How could the undercut injury lead to an up-regulation of excitatory synapses? One possibility is that the deafferentation triggers a compensatory increase in the strength or number of excitatory synapses [283]. For example, *de novo* intracortical connections may develop to replace the severed, extracortical ones [305]. However,

replacing extracortical connections with intracortical ones could dramatically alter network dynamics, potentially resulting in hyper-excitable or hyper-synchronous circuits [283]. Deafferentation could also cause hyper-excitability in the absence of synaptogenesis, by triggering a homeostatic increase in the sensitivity of surviving connections [309]. Regardless of the underlying mechanism, these studies show that deafferentation can trigger an up-regulation of excitatory synapses, potentially resulting in epilepsy.

The changes in spine density we observed after lateral TBI may reflect synaptic re-wiring like that observed in the cortical undercut model [305]. In the cortical undercut model, injury causes a deafferentation of neocortical pyramidal cells and a consequent up-regulation of excitatory synapses. In the lateral TBI model, we observed an acute loss and subsequent regrowth of dendritic spines, which could equate to deafferentation and re-afferentation, respectively. Though spine regrowth may signify circuit restoration rather than alteration, we also observed an abnormal increase in spine density in the hippocampus 1 week post-TBI, which suggests *de novo* synaptogenesis. Lateral TBI and cortical undercut therefore may both induce epilepsy through a common mechanism: a compensatory but maladaptive elaboration of excitatory synapses. It is important to note that, in the present study, spine loss and regrowth were observed on layer II/III pyramidal neurons, whereas the cortical undercut studies focused on layer V pyramidals [302,304,305]. Still, deafferentation has been shown to cause an increase in dendritic spine density on layer II/III pyramidals [310], which suggests that connectivity in layer II/III is also subject to homeostatic regulation. A loss of dendritic

spines in layer II/III could therefore trigger compensatory changes in neuronal networks, and so facilitate epileptogenesis in our TBI model.

While our data raise the possibility that spine loss is involved in post-traumatic epileptogenesis, many related questions remain unanswered. For example, do the changes in dendritic spine density we observed after TBI truly represent changes in synaptic circuitry? This question could be answered with combination of anatomical and physiological techniques. Anatomical techniques, such as array tomography and electron microscopy, could be used to correlate spine density with synapse density after TBI. If these methods detect a change in synapse density, the functional consequences could then be assessed by electrophysiology and/or functional imaging. For example, synaptic activity could be measured within fluorescently-labeled neurons showing an increase in spine density. These experiments would reveal whether the spine overgrowth at 1 week post-TBI represents an excess of excitatory synapses. Also, paired intracellular recordings or functional imaging could be used to test whether local connectivity is enhanced after TBI as it is after cortical undercut [305]. An increase in synaptic activity or local connectivity would confirm that TBI alters synaptic circuits, consistent with the changes in dendritic spine density described in Chapter I.

Another important question concerns whether synaptic re-wiring is necessary for post-traumatic epilepsy. Studies of the cortical undercut model suggest that newly-formed excitatory circuits give rise to epileptiform activity [311]. Do similar circuits form after lateral fluid percussion TBI? If so, are these circuits responsible for the late spontaneous seizures described in Chapter III? Excitatory synaptogenesis has been observed after lateral TBI [209], which could explain the regrowth (and overgrowth) of

dendritic spines shown in Chapter I. However, it is unclear whether this synaptogenesis is adaptive or maladaptive (*i.e.,* epileptogenic). To test whether synaptogenesis is epileptogenic, rats could be treated after TBI with an inhibitor of synaptogenesis and then monitored for spontaneous seizures months later. For example, the anti-epileptic drug Gabapentin has been shown to inhibit excitatory synaptogenesis during development [312] and may similarly interfere with reactive synaptogenesis in the adult brain [311]. Interestingly, epileptogenesis in the cortical undercut model is delayed when rats are treated with Gabapentin after the undercut [311]. Another drug, the experimental Rac1 inhibitor NSC23766, may also block excitatory synaptogenesis in the adult brain, as it has been shown to prevent spine overgrowth a mouse model of spinal cord injury [313].

In conclusion, the present study reveals a role for the calcium-sensitive phosphatase, calcineurin, in TBI pathology. Administering a calcineurin inhibitor to rats at 1 hour post-TBI prevented the subsequent loss of dendritic spines from principal cortical cells, likely through downstream inhibition of the actin-depolymerizing protein, cofilin. The same drug treatment also prevented a TBI-induced increase in non-convulsive seizures. These findings further our understanding of the mechanisms by which TBI can alter neural circuitry, and emphasize the potential for calcineurin as a therapeutic target in the treatment of TBI.

LIST OF REFERENCES

LIST OF REFERENCES

1. Hofer SB, Bonhoeffer T (2010) Dendritic spines: the stuff that memories are made of? Curr Biol 20: R157-159.

2. Bailey CH, Kandel ER (1993) Structural changes accompanying memory storage. Annu Rev Physiol 55: 397-426.

3. Ramon y Cajal S (1891) Sur la structure de l'écorce cérébrale de quelques mammifères. La Cellule 7: 125-176.

4. Ramon y Cajal S (1888) Estructura de los centros nerviosos de las aves. Rev Trim Histol Norm Pat 1: 1-10.

5. Nimchinsky EA, Sabatini BL, Svoboda K (2002) Structure and function of dendritic spines. Annu Rev Physiol 64: 313-353.

6. Arellano JI, Espinosa A, Fairen A, Yuste R, DeFelipe J (2007) Non-synaptic dendritic spines in neocortex. Neuroscience 145: 464-469.

7. Kennedy MB, Beale HC, Carlisle HJ, Washburn LR (2005) Integration of biochemical signalling in spines. Nat Rev Neurosci 6: 423-434.

8. Yuste R (2011) Dendritic spines and distributed circuits. Neuron 71: 772-781.

9. Sheng M, Hoogenraad CC (2007) The postsynaptic architecture of excitatory synapses: a more quantitative view. Annu Rev Biochem 76: 823-847.

10. Choi DW (1988) Glutamate neurotoxicity and diseases of the nervous system. Neuron 1: 623-634.

11. Halpain S, Hipolito A, Saffer L (1998) Regulation of F-actin stability in dendritic spines by glutamate receptors and calcineurin. J Neurosci 18: 9835-9844.

12. Pak DT, Sheng M (2003) Targeted protein degradation and synapse remodeling by an inducible protein kinase. Science 302: 1368-1373.

13. Dieterich DC, Karpova A, Mikhaylova M, Zdobnova I, Konig I, et al. (2008) Caldendrin-Jacob: a protein liaison that couples NMDA receptor signalling to the nucleus. PLoS Biol 6: e34.

14. Turrigiano GG, Leslie KR, Desai NS, Rutherford LC, Nelson SB (1998) Activity-dependent scaling of quantal amplitude in neocortical neurons. Nature 391: 892-896.

15. Nakayama K, Kiyosue K, Taguchi T (2005) Diminished neuronal activity increases neuron-neuron connectivity underlying silent synapse formation and the rapid conversion of silent to functional synapses. J Neurosci 25: 4040-4051.

16. Parnavelas JG, Lynch G, Brecha N, Cotman CW, Globus A (1974) Spine loss and regrowth in hippocampus following deafferentation. Nature 248: 71-73.

17. Blinzinger K, Kreutzberg G (1968) Displacement of synaptic terminals from regenerating motoneurons by microglial cells. Z Zellforsch Mikrosk Anat 85: 145-157.

18. Trapp BD, Wujek JR, Criste GA, Jalabi W, Yin X, et al. (2007) Evidence for synaptic stripping by cortical microglia. Glia 55: 360-368.

19. Wake H, Moorhouse AJ, Jinno S, Kohsaka S, Nabekura J (2009) Resting microglia directly monitor the functional state of synapses in vivo and determine the fate of ischemic terminals. J Neurosci 29: 3974-3980.

20. Paolicelli RC, Bolasco G, Pagani F, Maggi L, Scianni M, et al. (2011) Synaptic pruning by microglia is necessary for normal brain development. Science 333: 1456-1458.

21. Beattie EC, Carroll RC, Yu X, Morishita W, Yasuda H, et al. (2000) Regulation of AMPA receptor endocytosis by a signaling mechanism shared with LTD. Nat Neurosci 3: 1291-1300.

22. Shi SH, Hayashi Y, Petralia RS, Zaman SH, Wenthold RJ, et al. (1999) Rapid spine delivery and redistribution of AMPA receptors after synaptic NMDA receptor activation. Science 284: 1811-1816.

23. Zhou Q, Homma KJ, Poo MM (2004) Shrinkage of dendritic spines associated with long-term depression of hippocampal synapses. Neuron 44: 749-757.

24. Lang C, Barco A, Zablow L, Kandel ER, Siegelbaum SA, et al. (2004) Transient expansion of synaptically connected dendritic spines upon induction of hippocampal long-term potentiation. Proc Natl Acad Sci U S A 101: 16665-16670.

25. Biess A, Korkotian E, Holcman D (2007) Diffusion in a dendritic spine: the role of geometry. Phys Rev E Stat Nonlin Soft Matter Phys 76: 021922.

26. Bloodgood BL, Sabatini BL (2005) Neuronal activity regulates diffusion across the neck of dendritic spines. Science 310: 866-869.

27. Bloodgood BL, Giessel AJ, Sabatini BL (2009) Biphasic synaptic Ca influx arising from compartmentalized electrical signals in dendritic spines. PLoS Biol 7: e1000190.

28. Cavazzini M, Bliss T, Emptage N (2005) Ca2+ and synaptic plasticity. Cell Calcium 38: 355-367.

29. Bardo S, Cavazzini MG, Emptage N (2006) The role of the endoplasmic reticulum Ca2+ store in the plasticity of central neurons. Trends Pharmacol Sci 27: 78-84.

30. Bloodgood BL, Sabatini BL (2007) Ca(2+) signaling in dendritic spines. Curr Opin Neurobiol 17: 345-351.

31. Blackstone C, Sheng M (2002) Postsynaptic calcium signaling microdomains in neurons. Front Biosci 7: d872-885.

32. Tymianski M, Tator CH (1996) Normal and abnormal calcium homeostasis in neurons: a basis for the pathophysiology of traumatic and ischemic central nervous system injury. Neurosurgery 38: 1176-1195.

33. Delorenzo RJ, Sun DA, Deshpande LS (2005) Cellular mechanisms underlying acquired epilepsy: the calcium hypothesis of the induction and maintainance of epilepsy. Pharmacol Ther 105: 229-266.

34. Limbrick DD, Jr., Pal S, DeLorenzo RJ (2001) Hippocampal neurons exhibit both persistent Ca2+ influx and impairment of Ca2+ sequestration/extrusion mechanisms following excitotoxic glutamate exposure. Brain Res 894: 56-67.

35. Sun DA, Deshpande LS, Sombati S, Baranova A, Wilson MS, et al. (2008) Traumatic brain injury causes a long-lasting calcium (Ca2+)-plateau of elevated intracellular Ca levels and altered Ca2+ homeostatic mechanisms in hippocampal neurons surviving brain injury. Eur J Neurosci 27: 1659-1672.

36. Takechi H, Eilers J, Konnerth A (1998) A new class of synaptic response involving calcium release in dendritic spines. Nature 396: 757-760.

37. Vanderklish PW, Edelman GM (2002) Dendritic spines elongate after stimulation of group 1 metabotropic glutamate receptors in cultured hippocampal neurons. Proc Natl Acad Sci U S A 99: 1639-1644.

38. Wang SS, Denk W, Hausser M (2000) Coincidence detection in single dendritic spines mediated by calcium release. Nat Neurosci 3: 1266-1273.

39. Nevian T, Sakmann B (2006) Spine Ca2+ signaling in spike-timing-dependent plasticity. J Neurosci 26: 11001-11013.

40. Colwell CS, Levine MS (1999) Metabotropic glutamate receptor modulation of excitotoxicity in the neostriatum: role of calcium channels. Brain Res 833: 234-241.

41. Koh JY, Palmer E, Cotman CW (1991) Activation of the metabotropic glutamate receptor attenuates N-methyl-D-aspartate neurotoxicity in cortical cultures. Proc Natl Acad Sci U S A 88: 9431-9435.

42. Nicoletti F, Bruno V, Catania MV, Battaglia G, Copani A, et al. (1999) Group-I metabotropic glutamate receptors: hypotheses to explain their dual role in neurotoxicity and neuroprotection. Neuropharmacology 38: 1477-1484.

43. Xu W, Wong TP, Chery N, Gaertner T, Wang YT, et al. (2007) Calpain-mediated mGluR1alpha truncation: a key step in excitotoxicity. Neuron 53: 399-412.

44. Kerchner GA, Nicoll RA (2008) Silent synapses and the emergence of a postsynaptic mechanism for LTP. Nat Rev Neurosci 9: 813-825.

45. Kuner T, Beck C, Sakmann B, Seeburg PH (2001) Channel-lining residues of the AMPA receptor M2 segment: structural environment of the Q/R site and identification of the selectivity filter. J Neurosci 21: 4162-4172.

46. Burnashev N, Villarroel A, Sakmann B (1996) Dimensions and ion selectivity of recombinant AMPA and kainate receptor channels and their dependence on Q/R site residues. J Physiol 496 (Pt 1): 165-173.

47. Isaac JT, Ashby M, McBain CJ (2007) The role of the GluR2 subunit in AMPA receptor function and synaptic plasticity. Neuron 54: 859-871.

48. Tanaka H, Grooms SY, Bennett MV, Zukin RS (2000) The AMPAR subunit GluR2: still front and center-stage. Brain Res 886: 190-207.

49. Pollard H, Heron A, Moreau J, Ben-Ari Y, Khrestchatisky M (1993) Alterations of the GluR-B AMPA receptor subunit flip/flop expression in kainate-induced epilepsy and ischemia. Neuroscience 57: 545-554.

50. Noh KM, Yokota H, Mashiko T, Castillo PE, Zukin RS, et al. (2005) Blockade of calcium-permeable AMPA receptors protects hippocampal neurons against global ischemia-induced death. Proc Natl Acad Sci U S A 102: 12230-12235.

51. Sattler R, Tymianski M (2001) Molecular mechanisms of glutamate receptor-mediated excitotoxic neuronal cell death. Mol Neurobiol 24: 107-129.

52. Feldmeyer D, Kask K, Brusa R, Kornau HC, Kolhekar R, et al. (1999) Neurological dysfunctions in mice expressing different levels of the Q/R site-unedited AMPAR subunit GluR-B. Nat Neurosci 2: 57-64.

53. Kask K, Zamanillo D, Rozov A, Burnashev N, Sprengel R, et al. (1998) The AMPA receptor subunit GluR-B in its Q/R site-unedited form is not essential for brain development and function. Proc Natl Acad Sci U S A 95: 13777-13782.

54. Rakhade SN, Zhou C, Aujla PK, Fishman R, Sucher NJ, et al. (2008) Early alterations of AMPA receptors mediate synaptic potentiation induced by neonatal seizures. J Neurosci 28: 7979-7990.

55. Huettner JE (2003) Kainate receptors and synaptic transmission. Prog Neurobiol 70: 387-407.

56. Isaac JT, Mellor J, Hurtado D, Roche KW (2004) Kainate receptor trafficking: physiological roles and molecular mechanisms. Pharmacol Ther 104: 163-172.

57. Amaral DG, Dent JA (1981) Development of the mossy fibers of the dentate gyrus: I. A light and electron microscopic study of the mossy fibers and their expansions. J Comp Neurol 195: 51-86.

58. Bloodgood BL, Sabatini BL (2008) Regulation of synaptic signalling by postsynaptic, non-glutamate receptor ion channels. J Physiol 586: 1475-1480.

59. Jeffs GJ, Meloni BP, Bakker AJ, Knuckey NW (2007) The role of the Na(+)/Ca(2+) exchanger (NCX) in neurons following ischaemia. J Clin Neurosci 14: 507-514.

60. Besancon E, Guo S, Lok J, Tymianski M, Lo EH (2008) Beyond NMDA and AMPA glutamate receptors: emerging mechanisms for ionic imbalance and cell death in stroke. Trends Pharmacol Sci 29: 268-275.

61. Sobczyk A, Scheuss V, Svoboda K (2005) NMDA receptor subunit-dependent [Ca2+] signaling in individual hippocampal dendritic spines. J Neurosci 25: 6037-6046.

62. Garaschuk O, Schneggenburger R, Schirra C, Tempia F, Konnerth A (1996) Fractional Ca2+ currents through somatic and dendritic glutamate receptor channels of rat hippocampal CA1 pyramidal neurones. J Physiol 491 (Pt 3): 757-772.

63. Monyer H, Burnashev N, Laurie DJ, Sakmann B, Seeburg PH (1994) Developmental and regional expression in the rat brain and functional properties of four NMDA receptors. Neuron 12: 529-540.

64. Burnashev N, Schoepfer R, Monyer H, Ruppersberg JP, Gunther W, et al. (1992) Control by asparagine residues of calcium permeability and magnesium blockade in the NMDA receptor. Science 257: 1415-1419.

65. Arundine M, Tymianski M (2003) Molecular mechanisms of calcium-dependent neurodegeneration in excitotoxicity. Cell Calcium 34: 325-337.

66. Choi DW, Koh JY, Peters S (1988) Pharmacology of glutamate neurotoxicity in cortical cell culture: attenuation by NMDA antagonists. J Neurosci 8: 185-196.

67. Simon RP, Swan JH, Griffiths T, Meldrum BS (1984) Blockade of N-methyl-D-aspartate receptors may protect against ischemic damage in the brain. Science 226: 850-852.

68. Faden AI, Demediuk P, Panter SS, Vink R (1989) The role of excitatory amino acids and NMDA receptors in traumatic brain injury. Science 244: 798-800.

69. Tymianski M, Wallace MC, Spigelman I, Uno M, Carlen PL, et al. (1993) Cell-permeant Ca2+ chelators reduce early excitotoxic and ischemic neuronal injury in vitro and in vivo. Neuron 11: 221-235.

70. Choi DW (1988) Calcium-mediated neurotoxicity: relationship to specific channel types and role in ischemic damage. Trends Neurosci 11: 465-469.

71. Tymianski M, Charlton MP, Carlen PL, Tator CH (1993) Source specificity of early calcium neurotoxicity in cultured embryonic spinal neurons. J Neurosci 13: 2085-2104.

72. Sattler R, Xiong Z, Lu WY, MacDonald JF, Tymianski M (2000) Distinct roles of synaptic and extrasynaptic NMDA receptors in excitotoxicity. J Neurosci 20: 22-33.

73. Sheng M, Pak DT (2000) Ligand-gated ion channel interactions with cytoskeletal and signaling proteins. Annu Rev Physiol 62: 755-778.

74. Franks KM, Sejnowski TJ (2002) Complexity of calcium signaling in synaptic spines. Bioessays 24: 1130-1144.

75. Aarts MM, Tymianski M (2004) Molecular mechanisms underlying specificity of excitotoxic signaling in neurons. Curr Mol Med 4: 137-147.

76. Sattler R, Charlton MP, Hafner M, Tymianski M (1998) Distinct influx pathways, not calcium load, determine neuronal vulnerability to calcium neurotoxicity. J Neurochem 71: 2349-2364.

77. Hardingham GE, Bading H (2003) The Yin and Yang of NMDA receptor signalling. Trends Neurosci 26: 81-89.

78. Swann JW, Al-Noori S, Jiang M, Lee CL (2000) Spine loss and other dendritic abnormalities in epilepsy. Hippocampus 10: 617-625.

79. Fiala JC, Spacek J, Harris KM (2002) Dendritic spine pathology: cause or consequence of neurological disorders? Brain Res Brain Res Rev 39: 29-54.

80. Olney JW, Fuller T, de Gubareff T (1979) Acute dendrotoxic changes in the hippocampus of kainate treated rats. Brain Res 176: 91-100.

81. Greenwood SM, Connolly CN (2007) Dendritic and mitochondrial changes during glutamate excitotoxicity. Neuropharmacology 53: 891-898.

82. Olney JW, Collins RC, Sloviter RS (1986) Excitotoxic mechanisms of epileptic brain damage. Adv Neurol 44: 857-877.

83. Hori N, Carpenter DO (1994) Functional and morphological changes induced by transient in vivo ischemia. Exp Neurol 129: 279-289.

84. Park JS, Bateman MC, Goldberg MP (1996) Rapid alterations in dendrite morphology during sublethal hypoxia or glutamate receptor activation. Neurobiol Dis 3: 215-227.

85. Katayama Y, Becker DP, Tamura T, Ikezaki K (1990) Early cellular swelling in experimental traumatic brain injury: a phenomenon mediated by excitatory amino acids. Acta Neurochir Suppl (Wien) 51: 271-273.

86. Folkerts MM, Berman RF, Muizelaar JP, Rafols JA (1998) Disruption of MAP-2 immunostaining in rat hippocampus after traumatic brain injury. J Neurotrauma 15: 349-363.

87. Unterberg AW, Stover J, Kress B, Kiening KL (2004) Edema and brain trauma. Neuroscience 129: 1021-1029.

88. Hasbani MJ, Schlief ML, Fisher DA, Goldberg MP (2001) Dendritic spines lost during glutamate receptor activation reemerge at original sites of synaptic contact. J Neurosci 21: 2393-2403.

89. Hasbani MJ, Hyrc KL, Faddis BT, Romano C, Goldberg MP (1998) Distinct roles for sodium, chloride, and calcium in excitotoxic dendritic injury and recovery. Exp Neurol 154: 241-258.

90. Ikegaya Y, Kim JA, Baba M, Iwatsubo T, Nishiyama N, et al. (2001) Rapid and reversible changes in dendrite morphology and synaptic efficacy following NMDA receptor activation: implication for a cellular defense against excitotoxicity. J Cell Sci 114: 4083-4093.

91. Ikonomidou C, Price MT, Mosinger JL, Frierdich G, Labruyere J, et al. (1989) Hypobaric-ischemic conditions produce glutamate-like cytopathology in infant rat brain. J Neurosci 9: 1693-1700.

92. Zhang S, Boyd J, Delaney K, Murphy TH (2005) Rapid reversible changes in dendritic spine structure in vivo gated by the degree of ischemia. J Neurosci 25: 5333-5338.

93. Andrew RD, Labron MW, Boehnke SE, Carnduff L, Kirov SA (2007) Physiological evidence that pyramidal neurons lack functional water channels. Cereb Cortex 17: 787-802.

94. Hasbani MJ, Viquez NM, Goldberg MP (2001) NMDA receptors mediate hypoxic spine loss in cultured neurons. Neuroreport 12: 2731-2735.

95. Takeuchi H, Mizuno T, Zhang G, Wang J, Kawanokuchi J, et al. (2005) Neuritic beading induced by activated microglia is an early feature of neuronal dysfunction toward neuronal death by inhibition of mitochondrial respiration and axonal transport. J Biol Chem 280: 10444-10454.

96. Emery DG, Lucas JH (1995) Ultrastructural damage and neuritic beading in cold-stressed spinal neurons with comparisons to NMDA and A23187 toxicity. Brain Res 692: 161-173.

97. Kirov SA, Petrak LJ, Fiala JC, Harris KM (2004) Dendritic spines disappear with chilling but proliferate excessively upon rewarming of mature hippocampus. Neuroscience 127: 69-80.

98. Inoue H, Okada Y (2007) Roles of volume-sensitive chloride channel in excitotoxic neuronal injury. J Neurosci 27: 1445-1455.

99. Al-Noori S, Swann JW (2000) A role for sodium and chloride in kainic acid-induced beading of inhibitory interneuron dendrites. Neuroscience 101: 337-348.

100. LoPachin RM, Gaughan CL, Lehning EJ, Weber ML, Taylor CP (2001) Effects of ion channel blockade on the distribution of Na, K, Ca and other elements in oxygen-glucose deprived CA1 hippocampal neurons. Neuroscience 103: 971-983.

101. Oliva AA, Jr., Lam TT, Swann JW (2002) Distally directed dendrotoxicity induced by kainic Acid in hippocampal interneurons of green fluorescent protein-expressing transgenic mice. J Neurosci 22: 8052-8062.

102. Greenwood SM, Mizielinska SM, Frenguelli BG, Harvey J, Connolly CN (2007) Mitochondrial dysfunction and dendritic beading during neuronal toxicity. J Biol Chem 282: 26235-26244.

103. Hoskison MM, Shuttleworth CW (2006) Microtubule disruption, not calpain-dependent loss of MAP2, contributes to enduring NMDA-induced dendritic dysfunction in acute hippocampal slices. Exp Neurol 202: 302-312.

104. Sanchez C, Diaz-Nido J, Avila J (2000) Phosphorylation of microtubule-associated protein 2 (MAP2) and its relevance for the regulation of the neuronal cytoskeleton function. Prog Neurobiol 61: 133-168.

105. Dehmelt L, Halpain S (2005) The MAP2/Tau family of microtubule-associated proteins. Genome Biol 6: 204.

106. Arias C, Arrieta I, Massieu L, Tapia R (1997) Neuronal damage and MAP2 changes induced by the glutamate transport inhibitor dihydrokainate and by kainate in rat hippocampus in vivo. Exp Brain Res 116: 467-476.

107. Hoskison MM, Yanagawa Y, Obata K, Shuttleworth CW (2007) Calcium-dependent NMDA-induced dendritic injury and MAP2 loss in acute hippocampal slices. Neuroscience 145: 66-79.

108. McNeil RS, Swann JW, Brinkley BR, Clark GD (1999) Neuronal cytoskeletal alterations evoked by a platelet-activating factor (PAF) analogue. Cell Motil Cytoskeleton 43: 99-113.

109. Bindokas VP, Miller RJ (1995) Excitotoxic degeneration is initiated at non-random sites in cultured rat cerebellar neurons. J Neurosci 15: 6999-7011.

110. Slemmer JE, De Zeeuw CI, Weber JT (2005) Don't get too excited: mechanisms of glutamate-mediated Purkinje cell death. Prog Brain Res 148: 367-390.

111. Rusnak F, Mertz P (2000) Calcineurin: form and function. Physiol Rev 80: 1483-1521.

112. Aramburu J, Rao A, Klee CB (2000) Calcineurin: from structure to function. Curr Top Cell Regul 36: 237-295.

113. Klee CB, Ren H, Wang X (1998) Regulation of the calmodulin-stimulated protein phosphatase, calcineurin. J Biol Chem 273: 13367-13370.

114. Groth RD, Dunbar RL, Mermelstein PG (2003) Calcineurin regulation of neuronal plasticity. Biochem Biophys Res Commun 311: 1159-1171.

115. Mulkey RM, Herron CE, Malenka RC (1993) An essential role for protein phosphatases in hippocampal long-term depression. Science 261: 1051-1055.

116. Mulkey RM, Endo S, Shenolikar S, Malenka RC (1994) Involvement of a calcineurin/inhibitor-1 phosphatase cascade in hippocampal long-term depression. Nature 369: 486-488.

117. Snyder GL, Galdi S, Fienberg AA, Allen P, Nairn AC, et al. (2003) Regulation of AMPA receptor dephosphorylation by glutamate receptor agonists. Neuropharmacology 45: 703-713.

118. Kurz JE, Moore BJ, Henderson SC, Campbell JN, Churn SB (2008) A cellular mechanism for dendritic spine loss in the pilocarpine model of status epilepticus. Epilepsia 49: 1696-1710.

119. Sarmiere PD, Bamburg JR (2004) Regulation of the neuronal actin cytoskeleton by ADF/cofilin. J Neurobiol 58: 103-117.

120. Fifkova E, Delay RJ (1982) Cytoplasmic actin in neuronal processes as a possible mediator of synaptic plasticity. J Cell Biol 95: 345-350.

121. Cohen RS, Chung SK, Pfaff DW (1985) Immunocytochemical localization of actin in dendritic spines of the cerebral cortex using colloidal gold as a probe. Cell Mol Neurobiol 5: 271-284.

122. Racz B, Weinberg RJ (2006) Spatial organization of cofilin in dendritic spines. Neuroscience 138: 447-456.

123. Honkura N, Matsuzaki M, Noguchi J, Ellis-Davies GC, Kasai H (2008) The subspine organization of actin fibers regulates the structure and plasticity of dendritic spines. Neuron 57: 719-729.

124. Meng Y, Zhang Y, Tregoubov V, Janus C, Cruz L, et al. (2002) Abnormal spine morphology and enhanced LTP in LIMK-1 knockout mice. Neuron 35: 121-133.

125. Meng Y, Zhang Y, Tregoubov V, Falls DL, Jia Z (2003) Regulation of spine morphology and synaptic function by LIMK and the actin cytoskeleton. Rev Neurosci 14: 233-240.

126. Meng Y, Takahashi H, Meng J, Zhang Y, Lu G, et al. (2004) Regulation of ADF/cofilin phosphorylation and synaptic function by LIM-kinase. Neuropharmacology 47: 746-754.

127. Mizuno K, Okano I, Ohashi K, Nunoue K, Kuma K, et al. (1994) Identification of a human cDNA encoding a novel protein kinase with two repeats of the LIM/double zinc finger motif. Oncogene 9: 1605-1612.

128. Ohashi K, Toshima J, Tajinda K, Nakamura T, Mizuno K (1994) Molecular cloning of a chicken lung cDNA encoding a novel protein kinase with N-terminal two LIM/double zinc finger motifs. J Biochem 116: 636-642.

129. Scott RW, Olson MF (2007) LIM kinases: function, regulation and association with human disease. J Mol Med 85: 555-568.

130. Bernard O (2007) Lim kinases, regulators of actin dynamics. Int J Biochem Cell Biol 39: 1071-1076.

131. Wang Y, Shibasaki F, Mizuno K (2005) Calcium signal-induced cofilin dephosphorylation is mediated by Slingshot via calcineurin. J Biol Chem 280: 12683-12689.

132. Niwa R, Nagata-Ohashi K, Takeichi M, Mizuno K, Uemura T (2002) Control of actin reorganization by Slingshot, a family of phosphatases that dephosphorylate ADF/cofilin. Cell 108: 233-246.

133. Kurita S, Watanabe Y, Gunji E, Ohashi K, Mizuno K (2008) Molecular dissection of the mechanisms of substrate recognition and F-actin-mediated activation of cofilin-phosphatase slingshot-1. J Biol Chem.

134. Ohta Y, Kousaka K, Nagata-Ohashi K, Ohashi K, Muramoto A, et al. (2003) Differential activities, subcellular distribution and tissue expression patterns of three members of Slingshot family phosphatases that dephosphorylate cofilin. Genes Cells 8: 811-824.

135. Zhou L, Jones E, Haber M, Murai K Regulation of dendritic spine morphology through slingshot phosphatase signalling. Program 239.13. Society for Neuroscience, 2008. Washington, D.C.: 2008 Neuroscience Meeting Planner.

136. Fukazawa Y, Saitoh Y, Ozawa F, Ohta Y, Mizuno K, et al. (2003) Hippocampal LTP is accompanied by enhanced F-actin content within the dendritic spine that is essential for late LTP maintenance in vivo. Neuron 38: 447-460.

137. Coue M, Brenner SL, Spector I, Korn ED (1987) Inhibition of actin polymerization by latrunculin A. FEBS Lett 213: 316-318.

138. Graber S, Maiti S, Halpain S (2004) Cathepsin B-like proteolysis and MARCKS degradation in sub-lethal NMDA-induced collapse of dendritic spines. Neuropharmacology 47: 706-713.

139. Allison DW, Gelfand VI, Spector I, Craig AM (1998) Role of actin in anchoring postsynaptic receptors in cultured hippocampal neurons: differential attachment of NMDA versus AMPA receptors. J Neurosci 18: 2423-2436.

140. Zhang W, Benson DL (2001) Stages of synapse development defined by dependence on F-actin. J Neurosci 21: 5169-5181.

141. Pak DT, Yang S, Rudolph-Correia S, Kim E, Sheng M (2001) Regulation of dendritic spine morphology by SPAR, a PSD-95-associated RapGAP. Neuron 31: 289-303.

142. Wu LX, Sun CK, Zhang YM, Fan M, Xu J, et al. (2007) Involvement of the Snk-SPAR pathway in glutamate-induced excitotoxicity in cultured hippocampal neurons. Brain Res 1168: 38-45.

143. Fu Z, Lee SH, Simonetta A, Hansen J, Sheng M, et al. (2007) Differential roles of Rap1 and Rap2 small GTPases in neurite retraction and synapse elimination in hippocampal spiny neurons. J Neurochem 100: 118-131.

144. Ponimaskin E, Voyno-Yasenetskaya T, Richter DW, Schachner M, Dityatev A (2007) Morphogenic signaling in neurons via neurotransmitter receptors and small GTPases. Mol Neurobiol 35: 278-287.

145. Seeburg DP, Feliu-Mojer M, Gaiottino J, Pak DT, Sheng M (2008) Critical role of CDK5 and Polo-like kinase 2 in homeostatic synaptic plasticity during elevated activity. Neuron 58: 571-583.

146. Ang XL, Seeburg DP, Sheng M, Harper JW (2008) Regulation of Postsynaptic RapGAP SPAR by Polo-like Kinase 2 and the SCF{beta}-TRCP Ubiquitin Ligase in Hippocampal Neurons. J Biol Chem 283: 29424-29432.

147. Bingol B, Schuman EM (2006) Activity-dependent dynamics and sequestration of proteasomes in dendritic spines. Nature 441: 1144-1148.

148. Turrigiano GG (2008) The self-tuning neuron: synaptic scaling of excitatory synapses. Cell 135: 422-435.

149. Ouimet CC, Wang JK, Walaas SI, Albert KA, Greengard P (1990) Localization of the MARCKS (87 kDa) protein, a major specific substrate for protein kinase C, in rat brain. J Neurosci 10: 1683-1698.

150. Calabrese B, Halpain S (2005) Essential role for the PKC target MARCKS in maintaining dendritic spine morphology. Neuron 48: 77-90.

151. Meller R, Thompson SJ, Lusardi TA, Ordonez AN, Ashley MD, et al. (2008) Ubiquitin proteasome-mediated synaptic reorganization: a novel mechanism underlying rapid ischemic tolerance. J Neurosci 28: 50-59.

152. Solomonia RO, Apkhazava D, Nozadze M, Jackson AP, McCabe BJ, et al. (2008) Different forms of MARCKS protein are involved in memory formation in the learning process of imprinting. Exp Brain Res 188: 323-330.

153. Hussain RJ, Stumpo DJ, Blackshear PJ, Lenox RH, Abel T, et al. (2006) Myristoylated alanine rich C kinase substrate (MARCKS) heterozygous mutant mice exhibit deficits in hippocampal mossy fiber-CA3 long-term potentiation. Hippocampus 16: 495-503.

154. Chakravarthy B, Morley P, Whitfield J (1999) Ca2+-calmodulin and protein kinase Cs: a hypothetical synthesis of their conflicting convergences on shared substrate domains. Trends Neurosci 22: 12-16.

155. Arbuzova A, Schmitz AA, Vergeres G (2002) Cross-talk unfolded: MARCKS proteins. Biochem J 362: 1-12.

156. Hartwig JH, Thelen M, Rosen A, Janmey PA, Nairn AC, et al. (1992) MARCKS is an actin filament crosslinking protein regulated by protein kinase C and calcium-calmodulin. Nature 356: 618-622.

157. Wagey R, Hu J, Pelech SL, Raymond LA, Krieger C (2001) Modulation of NMDA-mediated excitotoxicity by protein kinase C. J Neurochem 78: 715-726.

158. Koponen S, Kurkinen K, Akerman KE, Mochly-Rosen D, Chan PH, et al. (2003) Prevention of NMDA-induced death of cortical neurons by inhibition of protein kinase Czeta. J Neurochem 86: 442-450.

159. Spizz G, Blackshear PJ (1997) Identification and characterization of cathepsin B as the cellular MARCKS cleaving enzyme. J Biol Chem 272: 23833-23842.

160. Faul M, Xu L, Wald MM, Coronado VG (2010) Traumatic brain injury in the United States: emergency department visits, hospitalizations, and deaths. In: Control NCfIPa, editor. Atlanta (GA).

161. Masel BE, DeWitt DS (2010) Traumatic brain injury: a disease process, not an event. J Neurotrauma 27: 1529-1540.

162. Finkelstein E, Corso PS, Miller TR (2006) The incidence and economic burden of injuries in the United States. Oxford ; New York: Oxford University Press. xiii, 187 p. p.

163. Garga N, Lowenstein DH (2006) Posttraumatic epilepsy: a major problem in desperate need of major advances. Epilepsy Curr 6: 1-5.

164. Lowenstein DH (2009) Epilepsy after head injury: an overview. Epilepsia 50 Suppl 2: 4-9.

165. Hauser WA, Annegers JF, Kurland LT (1991) Prevalence of epilepsy in Rochester, Minnesota: 1940-1980. Epilepsia 32: 429-445.

166. Hudak AM, Trivedi K, Harper CR, Booker K, Caesar RR, et al. (2004) Evaluation of seizure-like episodes in survivors of moderate and severe traumatic brain injury. J Head Trauma Rehabil 19: 290-295.

167. Diaz-Arrastia R, Agostini MA, Frol AB, Mickey B, Fleckenstein J, et al. (2000) Neurophysiologic and neuroradiologic features of intractable epilepsy after traumatic brain injury in adults. Arch Neurol 57: 1611-1616.

168. Marks DA, Kim J, Spencer DD, Spencer SS (1995) Seizure localization and pathology following head injury in patients with uncontrolled epilepsy. Neurology 45: 2051-2057.

169. Semah F, Picot MC, Adam C, Broglin D, Arzimanoglou A, et al. (1998) Is the underlying cause of epilepsy a major prognostic factor for recurrence? Neurology 51: 1256-1262.

170. Temkin NR (2009) Preventing and treating posttraumatic seizures: the human experience. Epilepsia 50 Suppl 2: 10-13.

171. Pitkanen A (2010) Therapeutic approaches to epileptogenesis--hope on the horizon. Epilepsia 51 Suppl 3: 2-17.

172. D'Ambrosio R, Fairbanks JP, Fender JS, Born DE, Doyle DL, et al. (2004) Post-traumatic epilepsy following fluid percussion injury in the rat. Brain 127: 304-314.

173. Kharatishvili I, Nissinen JP, McIntosh TK, Pitkanen A (2006) A model of posttraumatic epilepsy induced by lateral fluid-percussion brain injury in rats. Neuroscience 140: 685-697.

174. Hunt RF, Scheff SW, Smith BN (2009) Posttraumatic epilepsy after controlled cortical impact injury in mice. Exp Neurol 215: 243-252.

175. Bolkvadze T, Pitkanen A (2011) Development of Post-Traumatic Epilepsy after Controlled Cortical Impact and Lateral Fluid-Percussion Induced Brain Injury in the Mouse. J Neurotrauma.

176. Benardo LS (2003) Prevention of epilepsy after head trauma: do we need new drugs or a new approach? Epilepsia 44 Suppl 10: 27-33.

177. Echegoyen J, Armstrong C, Morgan RJ, Soltesz I (2009) Single application of a CB1 receptor antagonist rapidly following head injury prevents long-term hyperexcitability in a rat model. Epilepsy Res 85: 123-127.

178. Zipfel GJ, Babcock DJ, Lee JM, Choi DW (2000) Neuronal apoptosis after CNS injury: the roles of glutamate and calcium. J Neurotrauma 17: 857-869.

179. Lenzlinger PM, Morganti-Kossmann MC, Laurer HL, McIntosh TK (2001) The duality of the inflammatory response to traumatic brain injury. Mol Neurobiol 24: 169-181.

180. Lyeth BG, Jenkins LW, Hamm RJ, Dixon CE, Phillips LL, et al. (1990) Prolonged memory impairment in the absence of hippocampal cell death following traumatic brain injury in the rat. Brain Res 526: 249-258.

181. Pitkanen A, McIntosh TK (2006) Animal models of post-traumatic epilepsy. J Neurotrauma 23: 241-261.

182. McKinney RA, Capogna M, Durr R, Gahwiler BH, Thompson SM (1999) Miniature synaptic events maintain dendritic spines via AMPA receptor activation. Nat Neurosci 2: 44-49.

183. Campbell JN, Kurz JE, Churn SB (2009) Pathological Remodeling of Dendritic Spines. In: Baylog LR, editor. Dendritic Spines: Biochemistry, Modeling and Properties. New York: Nova Science Publishers. pp. 45-66.

184. Halpain S, Girault JA, Greengard P (1990) Activation of NMDA receptors induces dephosphorylation of DARPP-32 in rat striatal slices. Nature 343: 369-372.

185. Choi DW (1992) Excitotoxic cell death. J Neurobiol 23: 1261-1276.

186. Campbell JN, Low B, Kurz JE, Patel SS, Young MT, et al. (2011) Mechanisms of Dendritic Spine Remodeling in a Rat Model of Traumatic Brain Injury. J Neurotrauma epub Aug 16.

187. Dixon CE, Lyeth BG, Povlishock JT, Findling RL, Hamm RJ, et al. (1987) A fluid percussion model of experimental brain injury in the rat. J Neurosurg 67: 110-119.

188. Paxinos G, Watson C (1998) The rat brain in stereotaxic coordinates. San Diego: Academic Press. 1 v. (unpaged) p.

189. Fiala JC, Spacek J, Harris KM (2008) Dendrite Structure. In: Stuart G, Spruston N, Häusser M, editors. Dendrites. 2nd ed. Oxford: Oxford University Press. pp. 1-41.

190. Jones EG, Powell TP (1969) Morphological variations in the dendritic spines of the neocortex. J Cell Sci 5: 509-529.

191. Thompson HJ, Lifshitz J, Marklund N, Grady MS, Graham DI, et al. (2005) Lateral fluid percussion brain injury: a 15-year review and evaluation. J Neurotrauma 22: 42-75.

192. Monfils MH, Teskey GC (2004) Induction of long-term depression is associated with decreased dendritic length and spine density in layers III and V of sensorimotor neocortex. Synapse 53: 114-121.

193. Bourne J, Harris KM (2007) Do thin spines learn to be mushroom spines that remember? Curr Opin Neurobiol 17: 381-386.

194. Spruston N, McBain C (2007) Structural and Functional Properties of Hippocampal Neurons. In: Andersen P, editor. The Hippocampus Book. New York: Oxford University Press. pp. 133-202.

195. Schwarzbach E, Bonislawski DP, Xiong G, Cohen AS (2006) Mechanisms underlying the inability to induce area CA1 LTP in the mouse after traumatic brain injury. Hippocampus 16: 541-550.

196. Ruan YW, Lei Z, Fan Y, Zou B, Xu ZC (2009) Diversity and fluctuation of spine morphology in CA1 pyramidal neurons after transient global ischemia. J Neurosci Res 87: 61-68.

197. Anderson KJ, Scheff SW, DeKosky ST (1986) Reactive synaptogenesis in hippocampal area CA1 of aged and young adult rats. J Comp Neurol 252: 374-384.

198. Esclapez M, Hirsch JC, Ben-Ari Y, Bernard C (1999) Newly formed excitatory pathways provide a substrate for hyperexcitability in experimental temporal lobe epilepsy. J Comp Neurol 408: 449-460.

199. Isokawa M (2000) Remodeling dendritic spines of dentate granule cells in temporal lobe epilepsy patients and the rat pilocarpine model. Epilepsia 41 Suppl 6: S14-17.

200. Grutzendler J, Kasthuri N, Gan WB (2002) Long-term dendritic spine stability in the adult cortex. Nature 420: 812-816.

201. Xu HT, Pan F, Yang G, Gan WB (2007) Choice of cranial window type for in vivo imaging affects dendritic spine turnover in the cortex. Nat Neurosci 10: 549-551.

202. Spires-Jones TL, Kay K, Matsouka R, Rozkalne A, Betensky RA, et al. (2011) Calcineurin inhibition with systemic FK506 treatment increases dendritic branching and dendritic spine density in healthy adult mouse brain. Neurosci Lett 487: 260-263.

203. Schwartz N, Schohl A, Ruthazer ES (2009) Neural activity regulates synaptic properties and dendritic structure in vivo through calcineurin/NFAT signaling. Neuron 62: 655-669.

204. Zeng LH, Xu L, Rensing NR, Sinatra PM, Rothman SM, et al. (2007) Kainate seizures cause acute dendritic injury and actin depolymerization in vivo. J Neurosci 27: 11604-11613.

205. Hoskison MM, Moore AN, Hu B, Orsi S, Kobori N, et al. (2009) Persistent working memory dysfunction following traumatic brain injury: Evidence for a time-dependent mechanism. Neuroscience 159: 483-491.

206. Wu GY, Zou DJ, Rajan I, Cline H (1999) Dendritic dynamics in vivo change during neuronal maturation. J Neurosci 19: 4472-4483.

207. Ansari MA, Roberts KN, Scheff SW (2008) A time course of contusion-induced oxidative stress and synaptic proteins in cortex in a rat model of TBI. J Neurotrauma 25: 513-526.

208. Petrak LJ, Harris KM, Kirov SA (2005) Synaptogenesis on mature hippocampal dendrites occurs via filopodia and immature spines during blocked synaptic transmission. J Comp Neurol 484: 183-190.

209. Scheff SW, Price DA, Hicks RR, Baldwin SA, Robinson S, et al. (2005) Synaptogenesis in the hippocampal CA1 field following traumatic brain injury. J Neurotrauma 22: 719-732.

210. Seeburg DP, Sheng M (2008) Activity-induced Polo-like kinase 2 is required for homeostatic plasticity of hippocampal neurons during epileptiform activity. J Neurosci 28: 6583-6591.

211. Shankar GM, Bloodgood BL, Townsend M, Walsh DM, Selkoe DJ, et al. (2007) Natural oligomers of the Alzheimer amyloid-beta protein induce reversible synapse loss by modulating an NMDA-type glutamate receptor-dependent signaling pathway. J Neurosci 27: 2866-2875.

212. Megias M, Emri Z, Freund TF, Gulyas AI (2001) Total number and distribution of inhibitory and excitatory synapses on hippocampal CA1 pyramidal cells. Neuroscience 102: 527-540.

213. Norris CM, Scheff S (2009) Recovery of afferent function and synaptic strength in hippocampal CA1 following traumatic brain injury. J Neurotrauma 26: 2269-2278.

214. Cesa R, Morando L, Strata P (2005) Purkinje cell spinogenesis during architectural rewiring in the mature cerebellum. Eur J Neurosci 22: 579-586.

215. Corbett D, Giles T, Evans S, McLean J, Biernaskie J (2006) Dynamic changes in CA1 dendritic spines associated with ischemic tolerance. Exp Neurol 202: 133-138.

216. Dietrich WD, Alonso O, Busto R, Prado R, Zhao W, et al. (1998) Posttraumatic cerebral ischemia after fluid percussion brain injury: an autoradiographic and histopathological study in rats. Neurosurgery 43: 585-593; discussion 593-584.

217. Akasu T, Muraoka N, Hasuo H (2002) Hyperexcitability of hippocampal CA1 neurons after fluid percussion injury of the rat cerebral cortex. Neurosci Lett 329: 305-308.

218. Shao LR, Dudek FE (2005) Electrophysiological evidence using focal flash photolysis of caged glutamate that CA1 pyramidal cells receive excitatory synaptic input from the subiculum. J Neurophysiol 93: 3007-3011.

219. Faul M, Xu L, Wald M, Coronado V (2010) Traumatic brain injury in the United States: emergency department visits, hospitalizations, and deaths.

220. Ghajar J (2000) Traumatic brain injury. Lancet 356: 923-929.

221. Siesjo BK, Siesjo P (1996) Mechanisms of secondary brain injury. Eur J Anaesthesiol 13: 247-268.

222. Deshpande LS, Sun DA, Sombati S, Baranova A, Wilson MS, et al. (2008) Alterations in neuronal calcium levels are associated with cognitive deficits after traumatic brain injury. Neurosci Lett 441: 115-119.

223. Pallen CJ, Wang JH (1985) A multifunctional calmodulin-stimulated phosphatase. Arch Biochem Biophys 237: 281-291.

224. Kurz JE, Parsons JT, Rana A, Gibson CJ, Hamm RJ, et al. (2005) A significant increase in both basal and maximal calcineurin activity following fluid percussion injury in the rat. J Neurotrauma 22: 476-490.

225. Kurz JE, Hamm RJ, Singleton RH, Povlishock JT, Churn SB (2005) A persistent change in subcellular distribution of calcineurin following fluid percussion injury in the rat. Brain Res.

226. Fernandez AM, Fernandez S, Carrero P, Garcia-Garcia M, Torres-Aleman I (2007) Calcineurin in reactive astrocytes plays a key role in the interplay between proinflammatory and anti-inflammatory signals. J Neurosci 27: 8745-8756.

227. Dawson TM, Steiner JP, Dawson VL, Dinerman JL, Uhl GR, et al. (1993) Immunosuppressant FK506 enhances phosphorylation of nitric oxide synthase and protects against glutamate neurotoxicity. Proc Natl Acad Sci U S A 90: 9808-9812.

228. Szydlowska K, Zawadzka M, Kaminska B (2006) Neuroprotectant FK506 inhibits glutamate-induced apoptosis of astrocytes in vitro and in vivo. J Neurochem 99: 965-975.

229. Norris CM, Kadish I, Blalock EM, Chen KC, Thibault V, et al. (2005) Calcineurin triggers reactive/inflammatory processes in astrocytes and is upregulated in aging and Alzheimer's models. J Neurosci 25: 4649-4658.

230. Park KS, Mohapatra DP, Misonou H, Trimmer JS (2006) Graded regulation of the Kv2.1 potassium channel by variable phosphorylation. Science 313: 976-979.

231. Wu HY, Hudry E, Hashimoto T, Kuchibhotla K, Rozkalne A, et al. (2010) Amyloid beta induces the morphological neurodegenerative triad of spine loss, dendritic simplification, and neuritic dystrophies through calcineurin activation. J Neurosci 30: 2636-2649.

232. Kurz JE, Hamm RJ, Singleton RH, Povlishock JT, Churn SB (2005) A persistent change in subcellular distribution of calcineurin following fluid percussion injury in the rat. Brain Res 1048: 153-160.

233. Campbell JN, Churn SB, Register D (2011) Traumatic Brain Injury Causes an FK506-Sensitive Loss and an Overgrowth of Dendritic Spines in Rat Forebrain. J Neurotrauma epub April 27.

234. Pallen CJ, Wang JH (1983) Calmodulin-stimulated dephosphorylation of p-nitrophenyl phosphate and free phosphotyrosine by calcineurin. J Biol Chem 258: 8550-8553.

235. Kurz JE, Sheets D, Parsons JT, Rana A, Delorenzo RJ, et al. (2001) A significant increase in both basal and maximal calcineurin activity in the rat pilocarpine model of status epilepticus. J Neurochem 78: 304-315.

236. Bradford MM (1976) A rapid and sensitive method for the quantitation of microgram quantities of protein utilizing the principle of protein-dye binding. Anal Biochem 72: 248-254.

237. Churn SB, Taft WC, Billingsley MS, Sankaran B, DeLorenzo RJ (1992) Global forebrain ischemia induces a posttranslational modification of multifunctional calcium- and calmodulin-dependent kinase II. J Neurochem 59: 1221-1232.

238. Romero-Calvo I, Ocon B, Martinez-Moya P, Suarez MD, Zarzuelo A, et al. (2010) Reversible Ponceau staining as a loading control alternative to actin in Western blots. Anal Biochem 401: 318-320.

239. Hallam TM, Floyd CL, Folkerts MM, Lee LL, Gong QZ, et al. (2004) Comparison of behavioral deficits and acute neuronal degeneration in rat lateral fluid percussion and weight-drop brain injury models. J Neurotrauma 21: 521-539.

240. Kurz JE, Rana A, Parsons JT, Churn SB (2003) Status epilepticus-induced changes in the subcellular distribution and activity of calcineurin in rat forebrain. Neurobiol Dis 14: 483-493.

241. Meberg PJ, Ono S, Minamide LS, Takahashi M, Bamburg JR (1998) Actin depolymerizing factor and cofilin phosphorylation dynamics: response to signals that regulate neurite extension. Cell Motil Cytoskeleton 39: 172-190.

242. Morishita W, Marie H, Malenka RC (2005) Distinct triggering and expression mechanisms underlie LTD of AMPA and NMDA synaptic responses. Nat Neurosci 8: 1043-1050.

243. Bales JW, Ma X, Yan HQ, Jenkins LW, Dixon CE (2010) Regional calcineurin subunit B isoform expression in rat hippocampus following a traumatic brain injury. Brain Res 1358: 211-220.

244. Manalan AS, Klee CB (1983) Activation of calcineurin by limited proteolysis. Proc Natl Acad Sci U S A 80: 4291-4295.

245. D'Amelio M, Cavallucci V, Middei S, Marchetti C, Pacioni S, et al. (2010) Caspase-3 triggers early synaptic dysfunction in a mouse model of Alzheimer's disease. Nat Neurosci.

246. Moriyama K, Iida K, Yahara I (1996) Phosphorylation of Ser-3 of cofilin regulates its essential function on actin. Genes to Cells 1: 73-86.

247. Bernstein BW, Bamburg JR (2010) ADF/cofilin: a functional node in cell biology. Trends Cell Biol 20: 187-195.

248. Ansari MA, Roberts KN, Scheff SW (2008) Oxidative stress and modification of synaptic proteins in hippocampus after traumatic brain injury. Free Radic Biol Med 45: 443-452.

249. Kay JE, Doe SE, Benzie CR (1989) The mechanism of action of the immunosuppressive drug FK-506. Cell Immunol 124: 175-181.

250. Kato H, Oikawa T, Otsuka K, Takahashi A, Itoyama Y (2000) Postischemic changes in the immunophilin FKBP12 in the rat brain. Brain Res Mol Brain Res 84: 58-66.

251. McNamara JO, Huang YZ, Leonard AS (2006) Molecular signaling mechanisms underlying epileptogenesis. Sci STKE 2006: re12.

252. Moia LJ, Matsui H, de Barros GA, Tomizawa K, Miyamoto K, et al. (1994) Immunosuppressants and calcineurin inhibitors, cyclosporin A and FK506, reversibly inhibit epileptogenesis in amygdaloid kindled rat. Brain Res 648: 337-341.

253. Moriwaki A, Lu YF, Hayashi Y, Tomizawa K, Tokuda M, et al. (1996) Immunosuppressant FK506 prevents mossy fiber sprouting induced by kindling stimulation. Neurosci Res 25: 191-194.

254. Jung S, Bullis JB, Lau IH, Jones TD, Warner LN, et al. (2010) Downregulation of dendritic HCN channel gating in epilepsy is mediated by altered phosphorylation signaling. J Neurosci 30: 6678-6688.

255. Curia G, Levitt M, Fender JS, Miller JW, Ojemann J, et al. (2011) Impact of injury location and severity on posttraumatic epilepsy in the rat: role of frontal neocortex. Cereb Cortex 21: 1574-1592.

256. Misonou H, Mohapatra DP, Park EW, Leung V, Zhen D, et al. (2004) Regulation of ion channel localization and phosphorylation by neuronal activity. Nat Neurosci 7: 711-718.

257. Racine RJ (1972) Modification of seizure activity by electrical stimulation. II. Motor seizure. Electroencephalogr Clin Neurophysiol 32: 281-294.

258. Rasband WS (1997-2011) ImageJ. Bethesda, Maryland, USA: U. S. National Institutes of Health.

259. Kharatishvili I, Pitkanen A (2010) Association of the severity of cortical damage with the occurrence of spontaneous seizures and hyperexcitability in an animal model of posttraumatic epilepsy. Epilepsy Res 90: 47-59.

260. D'Ambrosio R, Fender JS, Fairbanks JP, Simon EA, Born DE, et al. (2005) Progression from frontal-parietal to mesial-temporal epilepsy after fluid percussion injury in the rat. Brain 128: 174-188.

261. Rakhade SN, Klein PM, Huynh T, Hilario-Gomez C, Kosaras B, et al. (2011) Development of later life spontaneous seizures in a rodent model of hypoxia-induced neonatal seizures. Epilepsia 52: 753-765.

262. Polack PO, Charpier S (2009) Ethosuximide converts ictogenic neurons initiating absence seizures into normal neurons in a genetic model. Epilepsia 50: 1816-1820.

263. Sharma V, Babu PP, Singh A, Singh S, Singh R (2007) Iron-induced experimental cortical seizures: electroencephalographic mapping of seizure spread in the subcortical brain areas. Seizure 16: 680-690.

264. Gurbanova AA, Aker R, Berkman K, Onat FY, van Rijn CM, et al. (2006) Effect of systemic and intracortical administration of phenytoin in two genetic models of absence epilepsy. Br J Pharmacol 148: 1076-1082.

265. Micheletti G, Vergnes M, Marescaux C, Reis J, Depaulis A, et al. (1985) Antiepileptic drug evaluation in a new animal model: spontaneous petit mal epilepsy in the rat. Arzneimittelforschung 35: 483-485.

266. Rundfeldt C, Honack D, Loscher W (1990) Phenytoin potently increases the threshold for focal seizures in amygdala-kindled rats. Neuropharmacology 29: 845-851.

267. Bernaskova K, Mares P (2010) Similar effects of lamotrigine and phenytoin against cortical epileptic foci in immature rats. Physiol Res 59: 113-119.

268. Loscher W, Reissmuller E, Ebert U (1998) Anticonvulsant effect of fosphenytoin in amygdala-kindled rats: comparison with phenytoin. Epilepsy Res 30: 69-76.

269. Pierce JE, Smith DH, Trojanowski JQ, McIntosh TK (1998) Enduring cognitive, neurobehavioral and histopathological changes persist for up to one year following severe experimental brain injury in rats. Neuroscience 87: 359-369.

270. Thomale UW, Bender M, Casalis P, Rupprecht S, Griebenow M, et al. (2007) Tacrolimus depresses local immune cell infiltration but fails to reduce cortical contusion volume in brain-injured rats. Immunobiology 212: 567-576.

271. Scheff SW, Sullivan PG (1999) Cyclosporin A significantly ameliorates cortical damage following experimental traumatic brain injury in rodents. J Neurotrauma 16: 783-792.

272. Butcher SP, Henshall DC, Teramura Y, Iwasaki K, Sharkey J (1997) Neuroprotective actions of FK506 in experimental stroke: in vivo evidence against an antiexcitotoxic mechanism. J Neurosci 17: 6939-6946.

273. Jung S, Jones TD, Lugo JN, Jr., Sheerin AH, Miller JW, et al. (2007) Progressive dendritic HCN channelopathy during epileptogenesis in the rat pilocarpine model of epilepsy. J Neurosci 27: 13012-13021.

274. Jung S, Warner LN, Pitsch J, Becker AJ, Poolos NP (2011) Rapid Loss of Dendritic HCN Channel Expression in Hippocampal Pyramidal Neurons following Status Epilepticus. J Neurosci 31: 14291-14295.

275. Kase D, Inoue T, Imoto K (2011) Roles of the subthalamic nucleus and subthalamic HCN channels in absence seizures. J Neurophysiol.

276. Ludwig A, Budde T, Stieber J, Moosmang S, Wahl C, et al. (2003) Absence epilepsy and sinus dysrhythmia in mice lacking the pacemaker channel HCN2. EMBO J 22: 216-224.

277. Sama MA, Mathis DM, Furman JL, Abdul HM, Artiushin IA, et al. (2008) Interleukin-1beta-dependent signaling between astrocytes and neurons depends critically on astrocytic calcineurin/NFAT activity. J Biol Chem 283: 21953-21964.

278. Canellada A, Cano E, Sanchez-Ruiloba L, Zafra F, Redondo JM (2006) Calcium-dependent expression of TNF-alpha in neural cells is mediated by the calcineurin/NFAT pathway. Mol Cell Neurosci 31: 692-701.

279. Friedman A, Dingledine R (2011) Molecular cascades that mediate the influence of inflammation on epilepsy. Epilepsia 52 Suppl 3: 33-39.

280. Echlin FA, Battista A (1963) Epileptiform Seizures from Chronic Isolated Cortex. Arch Neurol 9: 154-170.

281. Prince DA (1999) Epileptogenic neurons and circuits. Adv Neurol 79: 665-684.

282. Volman V, Bazhenov M, Sejnowski TJ (2011) Pattern of trauma determines the threshold for epileptic activity in a model of cortical deafferentation. Proc Natl Acad Sci U S A 108: 15402-15407.

283. Houweling AR, Bazhenov M, Timofeev I, Steriade M, Sejnowski TJ (2005) Homeostatic synaptic plasticity can explain post-traumatic epileptogenesis in chronically isolated neocortex. Cereb Cortex 15: 834-845.

284. Isokawa M, Levesque MF (1991) Increased NMDA responses and dendritic degeneration in human epileptic hippocampal neurons in slices. Neurosci Lett 132: 212-216.

285. Isokawa M, Levesque M, Fried I, Engel J, Jr. (1997) Glutamate currents in morphologically identified human dentate granule cells in temporal lobe epilepsy. J Neurophysiol 77: 3355-3369.

286. Sankar R, Shin D, Mazarati AM, Liu H, Katsumori H, et al. (2000) Epileptogenesis after status epilepticus reflects age- and model-dependent plasticity. Ann Neurol 48: 580-589.

287. Priel MR, dos Santos NF, Cavalheiro EA (1996) Developmental aspects of the pilocarpine model of epilepsy. Epilepsy Res 26: 115-121.

288. D'Ambrosio R, Miller JW (2010) Point. Epilepsy Curr 10: 90.

289. Dudek FE, Bertram EH (2010) Counterpoint to "what is an epileptic seizure?" by D'Ambrosio and Miller. Epilepsy Curr 10: 91-94.

290. Kelly KM (2004) Modeling traumatic brain injury and posttraumatic epilepsy. Epilepsy Curr 4: 160-161.

291. Eastman CL, Verley DR, Fender JS, Stewart TH, Nov E, et al. (2011) Antiepileptic and antiepileptogenic performance of carisbamate after head injury in the rat: blind and randomized studies. J Pharmacol Exp Ther 336: 779-790.

292. Francois J, Boehrer A, Nehlig A (2008) Effects of carisbamate (RWJ-333369) in two models of genetically determined generalized epilepsy, the GAERS and the audiogenic Wistar AS. Epilepsia 49: 393-399.

293. Kochen S, Giagante B, Oddo S (2002) Spike-and-wave complexes and seizure exacerbation caused by carbamazepine. Eur J Neurol 9: 41-47.

294. Sitnikova E (2010) Thalamo-cortical mechanisms of sleep spindles and spike-wave discharges in rat model of absence epilepsy (a review). Epilepsy Res 89: 17-26.

295. Rajna P, Lona C (1989) Sensory stimulation for inhibition of epileptic seizures. Epilepsia 30: 168-174.

296. Valentine PA, Fremit SL, Teskey GC (2005) Sensory stimulation reduces seizure severity but not afterdischarge duration of partial seizures kindled in the hippocampus at threshold intensities. Neurosci Lett 388: 33-38.

297. Shuper A, Vining EP (1991) Photosensitive complex partial seizures aggravated by phenytoin. Pediatr Neurol 7: 471-472.

298. Paz JT, Christian CA, Parada I, Prince DA, Huguenard JR (2010) Focal cortical infarcts alter intrinsic excitability and synaptic excitation in the reticular thalamic nucleus. J Neurosci 30: 5465-5479.

299. van Luijtelaar G, Sitnikova E (2006) Global and focal aspects of absence epilepsy: the contribution of genetic models. Neurosci Biobehav Rev 30: 983-1003.

300. Francois J, Germe K, Ferrandon A, Koning E, Nehlig A (2011) Carisbamate has powerful disease-modifying effects in the lithium-pilocarpine model of temporal lobe epilepsy. Neuropharmacology 61: 313-328.

301. Ferreira BL, Valle AC, Cavalheiro EA, Timo-Iaria C (2003) Absence-like seizures in adult rats following pilocarpine-induced status epilepticus early in life. Braz J Med Biol Res 36: 1685-1694.

302. Hoffman SN, Salin PA, Prince DA (1994) Chronic neocortical epileptogenesis in vitro. J Neurophysiol 71: 1762-1773.

303. Prince DA, Tseng GF (1993) Epileptogenesis in chronically injured cortex: in vitro studies. J Neurophysiol 69: 1276-1291.

304. Salin P, Tseng GF, Hoffman S, Parada I, Prince DA (1995) Axonal sprouting in layer V pyramidal neurons of chronically injured cerebral cortex. J Neurosci 15: 8234-8245.

305. Jin X, Prince DA, Huguenard JR (2006) Enhanced excitatory synaptic connectivity in layer v pyramidal neurons of chronically injured epileptogenic neocortex in rats. J Neurosci 26: 4891-4900.

306. Graber KD, Prince DA (1999) Tetrodotoxin prevents posttraumatic epileptogenesis in rats. Ann Neurol 46: 234-242.

307. Graber KD, Prince DA (2004) A critical period for prevention of posttraumatic neocortical hyperexcitability in rats. Ann Neurol 55: 860-870.

308. Prince DA, Parada I, Scalise K, Graber K, Jin X, et al. (2009) Epilepsy following cortical injury: cellular and molecular mechanisms as targets for potential prophylaxis. Epilepsia 50 Suppl 2: 30-40.

309. Volman V, Sejnowski TJ, Bazhenov M (2011) Topological basis of epileptogenesis in a model of severe cortical trauma. J Neurophysiol 106: 1933-1942.

310. Harmon KM, Wellman CL (2003) Differential effects of cholinergic lesions on dendritic spines in frontal cortex of young adult and aging rats. Brain Res 992: 60-68.

311. Li H, McDonald W, Parada I, Faria L, Graber K, et al. (2011) Targets for preventing epilepsy following cortical injury. Neurosci Lett 497: 172-176.

312. Eroglu C, Allen NJ, Susman MW, O'Rourke NA, Park CY, et al. (2009) Gabapentin receptor alpha2delta-1 is a neuronal thrombospondin receptor responsible for excitatory CNS synaptogenesis. Cell 139: 380-392.

313. Tan AM, Stamboulian S, Chang YW, Zhao P, Hains AB, et al. (2008) Neuropathic pain memory is maintained by Rac1-regulated dendritic spine remodeling after spinal cord injury. J Neurosci 28: 13173-13183.

VITA

John Nelson Campbell was born on April 2, 1978, in Richmond, Virginia, and is an American citizen. He graduated from Huguenot Academy in 1996, and received a Bachelor of Science in Interdisciplinary Studies: Biological Psychology from The College of William & Mary in 2002.

Awards

2011 Society for Neuroscience international travel award to the World Congress of the International Brain Research Organization (IBRO), Florence, Italy

2010 inductee in the Phi Kappa Phi honor society

2010 Robert F. Spencer Neuroscience Award from the Virginia Commonwealth University Department of Anatomy and Neurobiology

2009 top abstract/poster in the Central Virginia Society for Neuroscience poster session

2009 student travel award for the Joint Symposium of the International and National Neurotrauma Societies, Santa Barbara, CA

Publications

Campbell, J.N., Low, B., Kurz, J.E., Patel, S.S., Young, M.T., & Churn, S.B., *Mechanisms of dendritic spine remodeling in a rat model of traumatic brain injury*. J Neurotrauma (in press; epub on August 12, 2011)

Campbell, J.N., Low, B., Register, D.R., & Churn, S.B., *Traumatic Brain Injury Causes an FK506-Sensitive Loss and an Overgrowth of Dendritic Spines in Rat Forebrain*. J Neurotrauma (in press; epub on April 25, 2011)

Campbell, J.N., Kurz, J.E., & Churn, S.B., *Pathological Remodeling of Dendritic Spines.* In Louis R. Baylog (Ed.), Dendritic Spines: Biochemistry, Modeling, & Properties (2009). Hauppage, New York: Nova Science Publishers.

Kurz, J.E., Moore, B.J., Henderson, S.C., Campbell, J.N., & Churn, S.B., *A cellular mechanism for dendritic spine loss in the pilocarpine model of status epilepticus*. Epilepsia, 2008. 49(10)